NOTICE

The quality of this microform is heavily dependent upon the quality of the original thesis submitted for microfilming. Every effort has been made to ensure the highest quality of reproduction possible.

If pages are missing, contact the university which granted the degree.

Some pages may have indistinct print especially if the original pages were typed with a poor typewriter ribbon or if the university sent us an inferior photocopy.

Reproduction in full or in part of this microform is governed by the Canadian Copyright Act, R.S.C. 1970, c. C-30, and subsequent amendments.

AVIS

La qualité de cette microforme dépend grandement de la qualité de la thèse soumise au microfilmage. Nous avons tout fait pour assurer une qualité supérieure de reproduction.

S'il manque des pages, veuillez communiquer avec l'université qui a conféré le grade.

La qualité d'impression de certaines pages peut laisser à désirer, surtout si les pages originales ont été dactylographiées à l'aide d'un ruban usé ou si l'université nous a fait parvenir une photocopie de qualité inférieure.

La reproduction, même partielle, de cette microforme est soumise à la Loi canadienne sur le droit d'auteur, SRC 1970, c. C-30, et ses amendements subséquents.

Subcarrier Multiplexing for Fiber-Based Video Distribution: A Performance Study

by

Philippe Claude Neusy, B.A.Sc.

A thesis submitted to the
School of Graduate Studies and Research
in partial fulfillment of the requirements
for the degree

Master of Applied Science

Ottawa-Carleton Institute for Electrical Engineering
Department of Electrical Engineering
Faculty of Engineering
University of Ottawa

NOTICE

The quality of this microform is heavily dependent upon the quality of the original thesis submitted for microfilming. Every effort has been made to ensure the highest quality of reproduction possible.

If pages are missing, contact the university which granted the degree.

Some pages may have indistinct print especially if the original pages were typed with a poor typewriter ribbon or if the university sent us an inferior photocopy.

Reproduction in full or in part of this microform is governed by the Canadian Copyright Act, R.S.C. 1970, c. C-30, and subsequent amendments.

AVIS

La qualité de cette microforme dépend grandement de la qualité de la thèse soumise au microfilmage. Nous avons tout fait pour assurer une qualité supérieure de reproduction.

S'il manque des pages, veuillez communiquer avec l'université qui a conféré le grade.

La qualité d'impression de certaines pages peut laisser à désirer, surtout si les pages originales ont été dactylographiées à l'aide d'un ruban usé ou si l'université nous a fait parvenir une photocopie de qualité inférieure.

La reproduction, même partielle, de cette microforme est soumise à la Loi canadienne sur le droit d'auteur, SRC 1970, c. C-30, et ses amendements subséquents.

ISBN 0-315-60568-5

UNIVERSITÉ D'OTTAWA
UNIVERSITY OF OTTAWA

Abstract

Subcarrier transmission of multi-channel video signals over optical fibers may find widespread application in video distribution systems. This thesis details a comparative study that has been conducted for subcarrier multiplexing systems using various video signal modulation formats. In particular, we have investigated: AM-VSB (NTSC), high-index FM, 4-level QAM, and HDTV (Zenith). For each modulation scheme, a minimum CNR must be achieved to meet the required SNR. For analog fiber optic systems, system degradation results from laser intrinsic nonlinearities and clipping at threshold, and from noise sources (laser RIN (relative intensity noise), signal shot noise and preamplifier thermal noise at the receiver). We have also considered the possibility of using laser optical amplifiers to increase the system margin. Again, device nonlinearities must be considered, as well as further degradation from signal-spontaneous beat noise.

A communication system simulator software package BOSS (Block Oriented Systems Simulator) was used to develop a laser model based on the classic laser rate equations to predict nonlinear distortion. Adding Langevin noise terms to the rate equations, BOSS was also used to obtain the RIN spectrum. A similar model was developed for the optical amplifier based on the rate equation and wave equation of the optical amplifier. Results of the comparative study are given.

0.1 Acknowledgements

I would like to thank my thesis supervisor Dr. W. F. McGee, for his help and encouragement over the course of the research and the writing of the thesis.

Methi Methiwalla, Jung Kim, Peter Chow, and Jan Glinski of BNR have been very helpful in this project.

Dr. P. Galko is gratefully acknowledged for his help with Latex.

Thanks to M. Sablatash of CRC for providing us with his report on HDTV (Zenith).

The SUN workstation used to run the simulations is used for the Photonic Networks project of Prof. M. Kavehrad of our University.

This work was supported by a Natural Sciences and Engineering Research Council (NSERC) PostGraduate Scholarship, by BNR and NSERC through the Industrial Research Chair program and the Telecommunications Research Institute of Ontario by the Photonics Network project (M. Kavehrad).

Contents

0.1 Acknowledgements 1

1 Introduction **7**

1.1 Introduction 7

1.2 Organization of this Thesis 11

1.3 Review of Related Work 12

2 Issues in Computer Simulation **15**

2.1 Stability of Simulation 15

2.2 Noise Modeling 19

2.3 Evaluation of Distortion using Monte Carlo Method 19

2.4 A Carrier Frequency Assignment for Nonlinear Distortion 21

3 Laser **23**

3.1 Linearized Rate Equations 23

3.2 Phase Plane Analysis 27

3.3 Nonlinear Distortion 33

3.4 Clipping 40

3.5 Relative Intensity Noise 43

4 Optical Amplifier **51**

4.1 Introduction 51

4.2 Nonlinear Model 51

4.3 Amplifier Noise 55

5 System Design **57**

5.1 CNR Requirement 57

5.2 CNR Calculation 59

5.3 Nonlinear Distortion 61

5.4 System Design 63

6 Summary and Research Suggestions **72**

6.1 Summary 72

6.2 Suggestions for Further Research 73

A A Carrier Frequency Assignment for Nonlinear Distortion **75**

B Traveling Wave Equation for Optical Amplifier **79**

C BOSS Modules **81**

Bibliography 101

List of Figures

1 Fiber-based Subcarrier Multiplexed System 8
2 Frequency Division Multiplexing of N video channels with N carriers 9
3 S-plane with poles S1, S2 and S3. 16
4 Z-plane with poles Z1, Z2 and Z3. 16
5 Response for $\|z_p\| = 0.59$. 18
6 Response for $\|z_p\| = 0.997$. 18
7 Response for $\|z_p\| = 1.0048$. 18
8 Distortion Spectrum for NTSC spectrum 20
9 Total Distortion vs Distortion greater than third order 22
10 Transfer Function for the Laser biased at 50 mA 26
11 Transfer Function for the Laser biased at 75 mA 26
12 Phase Plane for laser biased at 50 mA 28
13 Phase Plane for laser biased at 75 mA 29
14 Phase Plane for laser biased at 50 mA 30
15 Phase Plane for laser with $\epsilon = 7.83E - 23$. 31
16 Initial points for Phase Plane. 32
17 Second Harmonic Distortion for a 50 mA bias 35
18 Second Harmonic Distortion for a 75 mA bias 35
19 Second Harmonic Levels at 1 GHz. 36
20 Total Distortion Spectrum with BOSS for a bias of 50 mA. 37
21 Total Distortion Spectrum with BOSS for a bias of 75 mA. 38
22 Total Distortion vs second harmonic for 50 mA 39
23 Total Distortion vs second harmonic for 75 mA 39
24 Clipping due to laser threshold 41

25 Clipping Spectrum from BOSS. 42
26 Shot Noise processes that give rise to RIN. 44
27 Calculated RIN for 50 mA bias. 47
28 Calculated RIN for 75 mA bias. 47
29 RIN for 50 mA bias from BOSS. 48
30 RIN for 75 mA bias from BOSS 49
31 Comparison of RIN levels for a 75 mA bias. 50
32 The TW semiconductor optical amplifier structure. 52
33 The nonlinear distortion level for the optical amplifier with the NTSC spectrum. 54
34 Simulation Results averaged over 8 points, for NTSC 62
35 Simulation Results averaged over 8 points, for FM 62
36 Assumptions for CNR calculations 64
37 Signal and noise level for FM system, m=0.0089. 65
38 Λ-curve for AM-VSB sytem 67
39 Λ-curve for a 20 channel system, NTSC 68
40 Λ-curve for a 6.5 dB system margin, NTSC 68
41 Λ-curve for FM system 69
42 Λ-curve for 4-level QAM system 70
43 Λ-curve for HDTV system 71

List of Tables

3.1 Laser Parameters 25

5.1 System Requirement 59
5.2 Summary 66
5.3 System Parameters for NTSC 67
5.4 System Parameters for FM 69
5.5 System Parameters for 4-level QAM 70
5.6 System Parameters for HDTV (Zenith) 71

Chapter 1

Introduction

1.1 Introduction

One application of the terahertz bandwidth of the optical fiber is the distribution of multi-channel video signals to the home. Though optical fiber systems have been in use for video transmission, it has been essentially for trunks, which are point-to-point links, where there is no splitting loss and where expensive end-terminals are not a major drawback. In the case of video distribution, which is a widespread application, a low cost solution is highly desirable. Certainly, the most desirable scheme would be to use the NTSC signal format, which would imply that upon detection of the optical signal, it could be fed directly into existing television sets. However, the AM-VSB NTSC signal has a relatively high CNR requirement. Also, little of the fiber bandwidth, laser bandwidth, and detector bandwidth is being exploited. Less stringent CNR requirements can be set if high-index FM modulation or QAM digital modulation schemes are used, which use more of the readily available bandwidth. Another interesting modulation scheme is the HDTV format proposed by Zenith, which also results in a lower CNR requirement. The drawback of such systems is the conversion required at each end-terminal.

In this thesis, we perform a comparative study of optical subcarrier multiplexed video systems. This was achieved by developing a computer model of the laser, which can be used to predict laser nonlinear distortion as well as laser noise. We also developed a similar model for the semiconductor optical amplifier to determine nonlinear distortion.

This approach is necessary because the intermodulation distortion level in a multi-channel system is dependent on the phases of all the carriers. Since these phases are

assumed to be independent, the resultant distortion level is random. It is practically not feasible to determine the distortion level analytically. Therefore, it is necessary to approach the problem by first obtaining a computer model of the laser and optical amplifier and then running Monte Carlo computer simulations to obtain the intermodulation distortion[1].

Subcarrier multiplexed systems can be represented as given in Figure 1. The N video channels are multiplexed in the frequency domain (see Figure 2). Each video signal modulates carriers spaced equally in the signal band. These modulated carriers are then added together along with a d.c. bias to form the electrical drive current that then directly modulates the laser. The subcarriers refer to the electrical carriers as opposed to the single optical carrier that is intensity modulated by the multiplexed current. The optical signal from the laser is then coupled into a fiber that acts as a waveguide. At the other end of the fiber, a p.i.n. diode converts the received optical signal back into an electrical current. The electrical signal is de-multiplexed and the separate channels can then be demodulated and the video signal recovered.

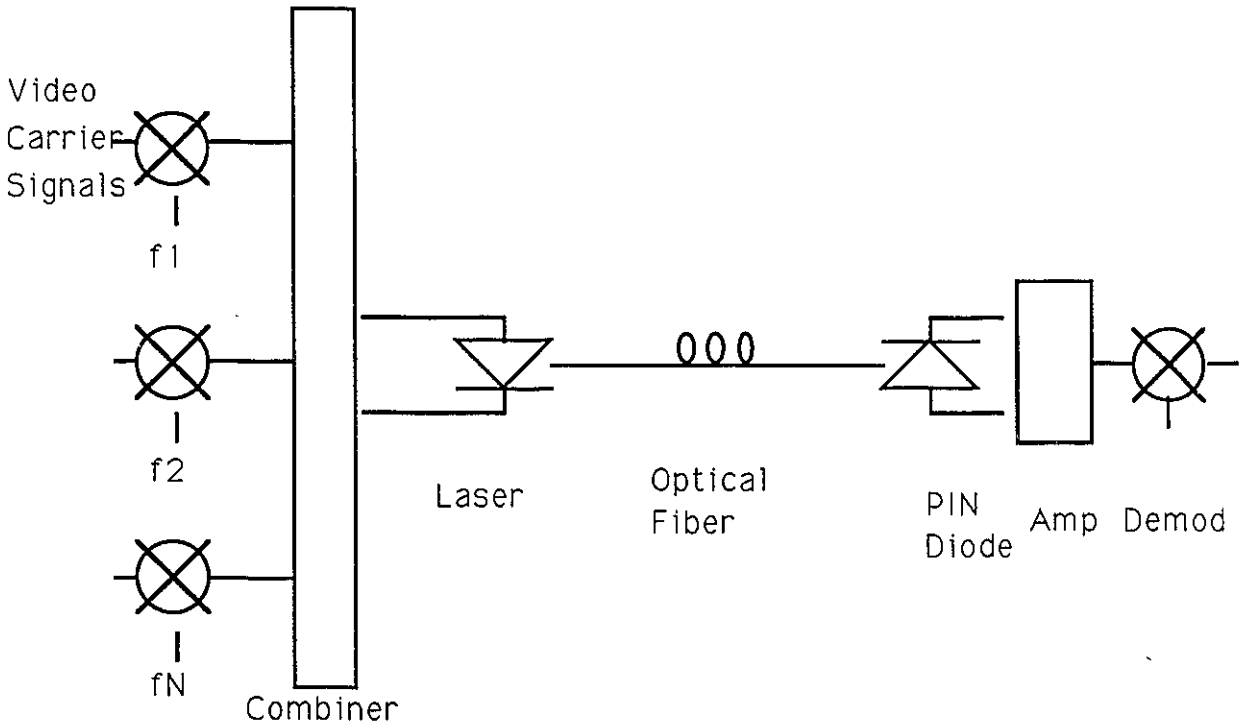

Fig. 1. Fiber-based Subcarrier Multiplexed System

To increase the system power margin, it is useful to consider the possibility of using optical amplifiers. Such a device amplifies the signal in the optical domain. Semiconductor optical amplifiers have the same essential structure as lasers, except that there is no feedback loop in the active region and therefore, the signal is amplified only for a single pass through the gain medium. Optical amplifiers are attractive in video distribution systems because in increasing the system margin, they allow for further splitting before detection.

Subcarrier systems offer a lot of flexibility, since the modulation scheme used to encode the video signal may itself be analog (e.g. AM-VSB or FM) or digital (e.g. 4-level QAM). In deciding which modulation technique to use, one must weigh improvements in CNR requirements against increased receiver complexity.

With respect to digital modulation of video signals, one can argue that subcarrier multiplexing has advantages over a purely digital signal, where the video channels are time-multiplexed. In the latter case, the multiplexing and de-multiplexing digital circuitry must operate at the bit rate of the aggregate video signal, whereas, with subcarrier multiplexing, the digital circuitry can operate at a lower bit rate, i.e. at the rate of a single digital video signal.

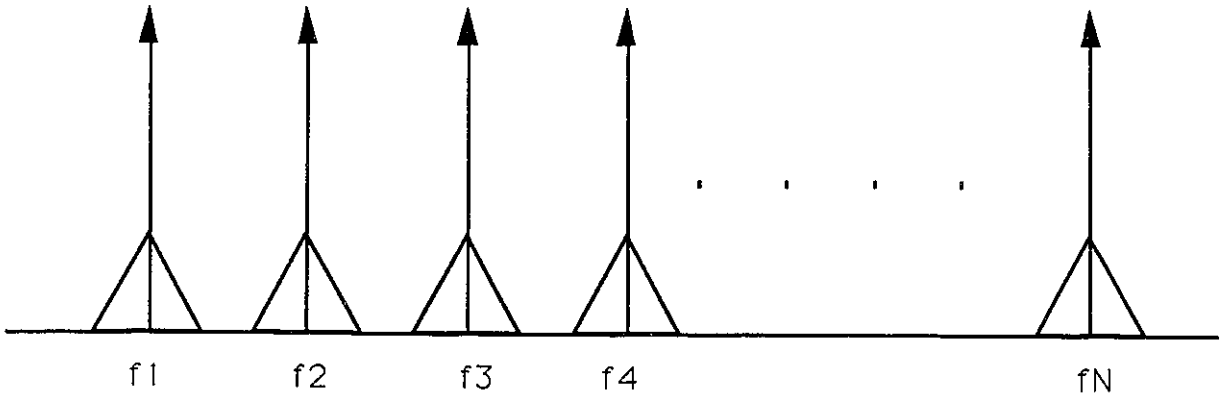

Fig. 2. Frequency Division Multiplexing of N video channels with N carriers

The problem that we attempt to resolve in this thesis can be stated as being one of determining which system is best suited for video distribution. Once that has been determined, we can establish the optimal setting for the system parameters, e.g. the operating point for the laser and the optical modulation index. The primary objective is to meet the system CNR requirements. One must consider all degradation sources. The

three major components of a fiber-based system are: the laser, which is the source; the fiber, which is the transmission medium; and the photodetector, which is the receiver. The single-mode glass fiber is considered to be ideal, i.e. linear and nondispersive (since it is single-mode, and we assume an operating wavelength in the low dispersion region for the fiber). Our only consideration for the fiber will be its attenuation and the laser-fiber coupling loss. The optical detector is also assumed to be ideal, apart from the thermal noise associated with the detector circuit and the shot noise due to the random nature of the optical signal.

The laser represents the main source of degradation. It is both nonlinear and noisy. The nonlinearity is from two sources: clipping at threshold and intrinsic dynamic nonlinearities, as described by the classic laser rate equations. Since laser rate equations are very important in this work, we will give them here and describe them briefly, as follows:

$$\frac{dN(t)}{dt} = \frac{I_A}{V'} - \frac{N}{\tau_n} - g_0(N - N_{om})[1 - \epsilon S]S \tag{1.1}$$

$$\frac{dS(t)}{dt} = \Gamma g_0(N - N_{om})[1 - \epsilon S]S - \frac{S}{\tau_p} + \Gamma\beta\frac{N}{\tau_n} \tag{1.2}$$

where N is the carrier density, N_{om} is the carrier density for transparency, I_A is the injected current, V' is the volume of the active region multiplied by the electronic charge, S is the photon density, Γ is the optical confinement factor, g_0 is the optical gain coefficient, τ_n is the electron lifetime, τ_p is the photon lifetime, ϵ is the gain compression, and β is the spontaneous emission factor.

We will now describe each term in the rate equation. In equation (1.1), the first term is the rate at which electrons are being pumped into the active region. The second term is the loss of electrons due to spontaneous emission. The last term is the net stimulated emission, where N_{om} is the electron density at which the stimulated emission is equal to stimulated absorption. Thus we have net stimulated emission only for $N > N_{om}$. The quantity ϵ is the gain compression which damps the laser transient response. Physically, this damping is due to many factors as given in [2].

As for equation (1.2), Γ is the optical confinement, which is due to the difference in volume of the optical and electrical active regions. That is, some of the emitted photons are not in the optical confinement region and hence are lost. The second term is the loss of photons out of the cavity, i.e. light output from the laser. The last term in the second

equation represents a small fraction of the photons from the spontaneous emission that are coherent with the stimulated emission.

The nonlinearity of the laser comes from the stimulated emission term, which is formed by the product of the photon and electron densities.

In the above rate equations, although they appear to be deterministic, each term is the average of a stochastic process that can be modeled as shot noise. As we shall see in Chapter 3, Langevin noise terms can be added to the rate equations in order to include the random behavior of the laser.

We can therefore notice that the laser gives rise to significant signal degradation and this is the main discussion of the thesis.

For the semiconductor optical amplifier, we have a similar set of equations. Equation (1.1) is essentially the same for the amplifier. Equation (1.2), which can be derived from Maxwell's equations, is averaged over the entire active region volume. In the case of the amplifier, we average over time and keep the dependence on the spatial coordinate z, and obtain a so-called traveling-wave equation.

1.2 Organization of this Thesis

In Chapter 2, we discuss various topics in computer simulation. We have grouped various issues that are used in the remainder of the work. They include: stability of computer simulation, noise modeling, evaluation of distortion using the Monte Carlo method, and a carrier frequency assignment for nonlinear distortion.

In Chapter 3, we shall cover the laser model, discussing how a computer-based module was developed, using a communication simulator software package, BOSS (Block Oriented System Simulator). We first linearize the rate equations so that we can apply linear system theory to consider the laser bandwidth, stability and the transient response. We then apply phase plane analysis to help visualize the transient behavior of the laser. Applying perturbation analysis to the laser rate equations, we then compare simulation results from BOSS with results from such analytical techniques. Clipping is then considered. We verify with BOSS assumptions made to obtain a CNR penalty due to clipping. Finally, we validate computer modeling of laser RIN with well-known analytical techniques.

In Chapter 4, we consider a similar model that has been developed for the optical amplifier, based on the rate and wave equation of the optical amplifier. It is also useful in determining the nonlinear distortion from the amplifier. Noise sources of the amplifier will also be discussed.

In Chapter 5, we use the computer modules to perform system studies. In particular, we will consider AM-VSB (NTSC), high index FM, 4-level QAM, and HDTV (Zenith). We first discuss the CNR requirement for each modulation format. We then determine the total system CNR by considering the degradation from each noise source and nonlinear distortion from the laser and optical amplifier using the computer modules. We will essentially conclude that a commercially available laser has sufficient linearity and an acceptable noise level to transmit up to 75 channels, using FM or digital QAM schemes. However, for AM-VSB, the laser does not meet the requirements. Optical amplifiers are shown to be readily applicable to systems that operate in the microwave range. They can therefore be applied to FM and digital schemes but not to those systems that use the NTSC spectrum. Such results agree with the experimental results reported in the literature.

In Chapter 6, we summarize the results and give suggestions for further research.

In Appendix A, we give the computer code developed to obtain a carrier frequency assignment for nonlinear distortion. In Appendix B, we derive the traveling-wave equation for the optical amplifier starting from Maxwell's equations. Finally, in Appendix C, we give the BOSS modules used for the simulations.

1.3 Review of Related Work

To analyze nonlinear distortion, the simplest and most straightforward approach is the Taylor series expansion. This assumes, however, a memoryless system, i.e. one with a flat spectrum. However, the laser, when treated as a memoryless system, is linear. This will be seen in Chapter 3, where we develop an expression for the second harmonic distortion spectrum, which vanishes at d.c. Therefore, the Taylor series cannot be applied to the laser for nonlinear analysis.

There is therefore the need for an expansion that includes both system nonlinearity

and its spectral properties. Such an expansion exists, which is called the Volterra series. However, attempts have been made by our colleague T.K. Biswas to apply this expansion to the laser rate equation, but there are difficulties because of the form of the rate equations.

However, perturbation analysis[3] has been successfully applied to the laser rate equations, which we shall outline in Chapter 3. Essentially, we derive a set of linearized differential equations by ignoring higher order distortion terms. We then apply the Fourier Transform and obtain the distortion spectrum. This analysis is readily applicable, but its drawbacks are that it becomes very tedious for higher order distortions. Also, even though it allows us to derive the individual distortion spectrums, we cannot easily extend this to system design because to do so, we must know how all the distortion terms from the subcarriers will add up to give the total distortion. Nonetheless, we will use this technique to compare with the results from the simulations with BOSS.

Here, we use direct time-domain simulation with BOSS[4]. It was first proposed by Way[5], where he used the software package SPICE. He was required to force the rate equations into an equivalent circuit model, but was successful in getting results for nonlinear distortion that compare well with the measured results. He did not extend his work to analog system design.

In this thesis we show how BOSS can be used to obtain results similar to those obtained by Way. We extend the simulation to analog system design. There were many advantages to using BOSS. The laser module was created with primitive modules available in BOSS. Therefore, the actual code generation for the simulation was completely transparent since the modules were created using a block diagram editor. With the editor, blocks were retrieved from the data base and connected together to form the modules. If one does not have the required block in BOSS for a particular application, FORTRAN code can be written to create the module, which can then be integrated into the other modules.

Designing with BOSS has many advantages, as it encourages good design practices, such as modular design and good documentation, since all variables, modules and edits must be documented. Also, BOSS makes available many options for post-processing. Various signal plots can be made, including spectral analysis, time-domain plots and arbitrary x-y plots, which we use for phase plane analysis.

In subcarrier multiplexed systems, intermodulation distortion is dependent on the phases of the carriers. A similar problem has already been considered by Medhurst[1] for the case of multi-channel FM trunk radio systems. We will make use of his work in dealing with the probability distribution of the distortion level.

As for laser RIN, Yamamoto[6] has shown how analytical results compare well with measured results. Langevin noise terms are introduced into the linearized rate equations to obtain the noise spectrum. We extend this analysis to include the gain compression term in the rate equations. We also show how the laser module developed with BOSS can be extended to include noise sources. With this approach, we obtain results similar to those obtained in previous work. Simulation results have not been previously reported in the literature for the RIN spectrum.

For semiconductor optical amplifiers, most of the work that has been done is with respect to nonlinear distortion for multi-channel optical carriers, where four-wave mixing causes interchannel interference[7]. For subcarrier multiplexing, which uses a single optical carrier, work has been done by Saleh[8], who gives a reduced form for the electrical field and rate equation that are amenable to direct computer simulation. With these equations, Saleh suggest further reduction for a communication system model. Here, we propose again direct time-domain simulation using BOSS and again apply it to perform subcarrier system simulation.

For system design, there have been experimental systems reported in the literature, for AM-VSB[9], FM[10] and the QAM[11] digital scheme. Here, for the first time, we give a comprehensive comparison through computer simulation. For systems with optical amplifiers, there is essentially the work by Way[12], who applied them to FM video distribution. Here, we consider their application to all the proposed modulation schemes.

In this thesis, we also make frequent use of a carrier frequency assignment scheme for nonlinear distortion. Previously reported by Atkinson[13] is an assignment for nonlinear distortion where the carriers are confined to an octave, in which case we do not have second order distortion in the signal band. We extend this to a set of frequencies without this constraint. A program has been written to generate a set of integers (frequencies) which, when passed through a nonlinear system, give rise to second order and third order distortion components that do not occur at any of the original frequencies.

Chapter 2

Issues in Computer Simulation

2.1 Stability of Simulation

Since the laser is a stable physical system, it would seem reasonable to expect a discrete-time domain simulation to be stable. However, in the course of running the simulations, it was discovered that if the time step used for the simulation was too large, the simulation diverged. This was further investigated and we present here the analysis that accounts for this behavior. Note that in this Section, we consider the laser to be linear. This can be achieved by linearizing the rate equations, as will be discussed in Chapter 3.

In our simulation of the laser, we make the following approximation of the first derivative:

$$\frac{dN(t)}{dt} \approx \frac{N(t+T) - N(t)}{T} \tag{2.1}$$

where T is the simulation time step.

Substituting this into the rate equations, we obtain the following form for our discrete time simulation:

$$N(t+T) = N(t) + Tf[I(t), N(t), S(t)] \tag{2.2}$$

Such an approximation of a continuous system with a discrete system is an example of Euler forward integration, which is of the following general form[14]:

$$x_i(nT) = x_i(nT - T) + Tg_i(nT - T) \tag{2.3}$$

This mapping, from continuous to discrete, is stable so long as the poles of the z-transform are within the unit circle as indicated in the Figures 3 and 4. In Figure 4

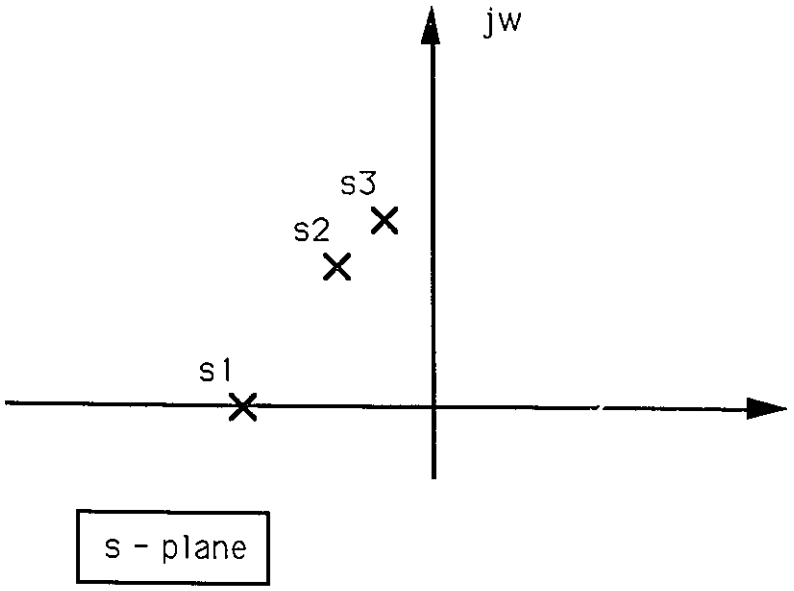

Fig. 3. S-plane with poles S1, S2 and S3.[14]

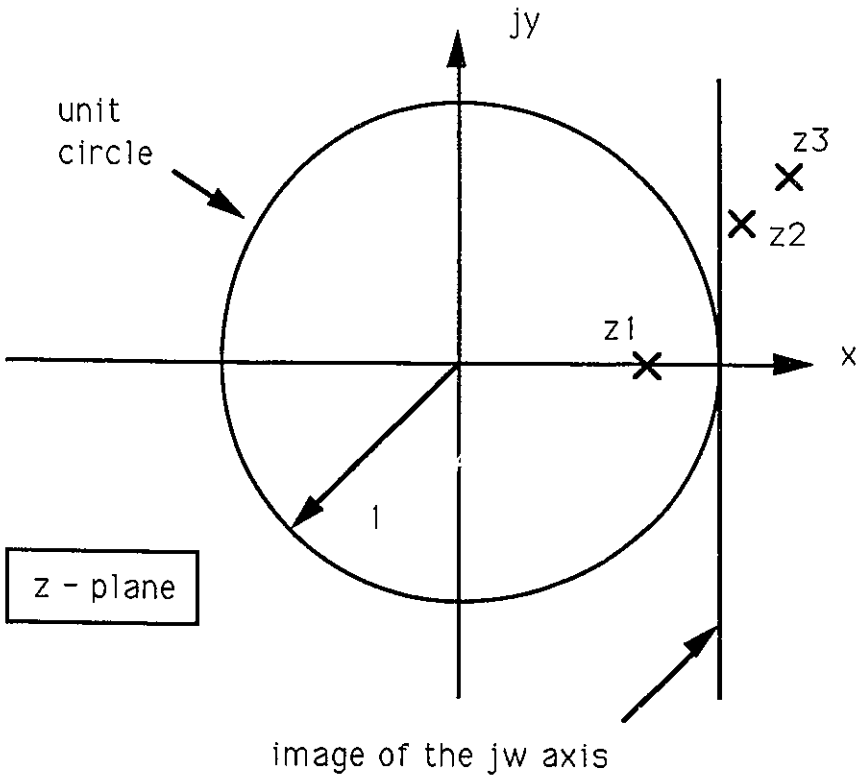

Fig. 4. Z-plane with poles Z1, Z2 and Z3.[14]

we see that the imaginary axis is mapped to an axis that is tangential to the unit circle. The transformation from the s-plane to the z-plane is as follows[14]:

$$z = sT + 1 \tag{2.4}$$

As for any discrete system, we have stability if the poles are within the unit circle. Therefore, for stability $\|z_p\| < 1$, i.e. for $\|sT + 1\| < 1$. With poles at $s = \alpha + j\omega$, we can solve for T at which we are on the verge of instability, and we obtain:

$$T = \frac{2\alpha}{\alpha^2 + \omega^2} \tag{2.5}$$

In Chapter 3, we show that for the laser biased at 75 mA, we have $\alpha = 3.82E10$ and $\omega = 2.589E10$ giving us a critical T of $3.587E - 11$. We have run simulations for $\|z_p\| = 0.59$, $\|z_p\| = 0.997$ and $\|z_p\| = 1.0048$ and give the results in Figures 5, 6, and 7. Going from some initial approximate steady state value, we see that the simulation converges in the first case to a more accurate steady state value. In the second case, as we are on the verge of instability, we have continuous oscillations and, in the last case, we have a divergent solution.

In Figure 4, we have also shown that the imaginary axis in the s-plane is mapped onto a line tangential to the unit circle in the z-domain. This implies that for a good representation of the frequency characteristics of the laser, we must choose a small enough T such that $\|\omega T\| \ll 1$. In our simulations, the largest T that we will use is T=$2.54E-12$ giving us $\|\omega T\| = 0.066$.

Can we do better? Can we find a mapping into the discrete domain that will maintain the stability of the physical system? Backward Euler integration conserves stability of a system, but the transformation is of the following form[14]:

$$x_i(nT) = x_i(nT - T) + Tg_i(nT) \tag{2.6}$$

In our case, since g_i is a function of x_i, we cannot make this substitution. We conclude then that by choosing a sufficiently small T, which is nothing more than the time-step for our simulation, we will have a stable simulation and accurate results.

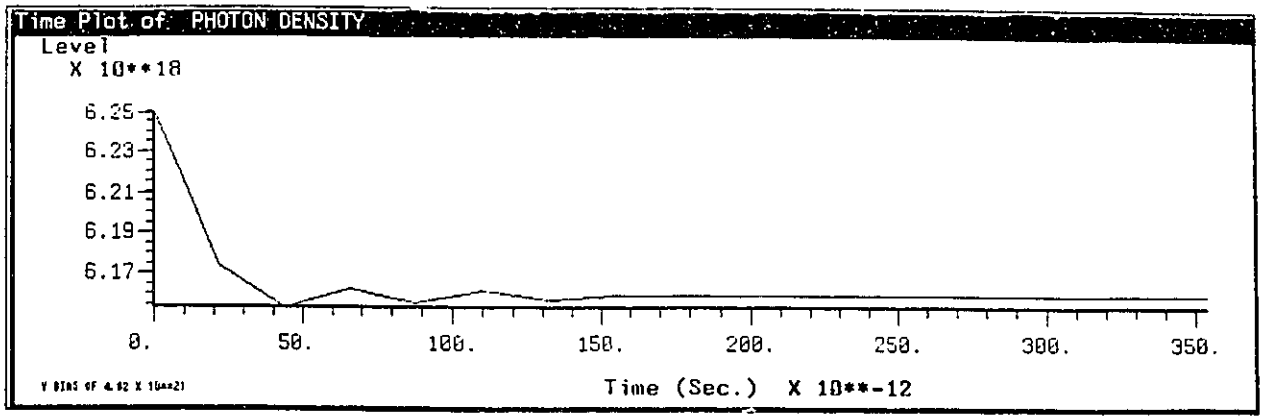

Fig. 5. Response for $\|z_p\| = 0.59$.

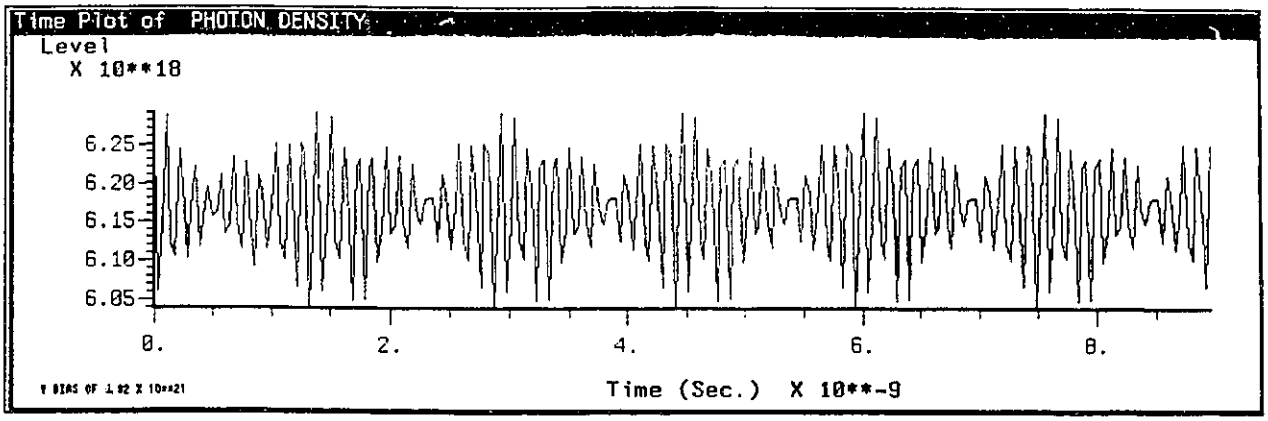

Fig. 6. Response for $\|z_p\| = 0.997$.

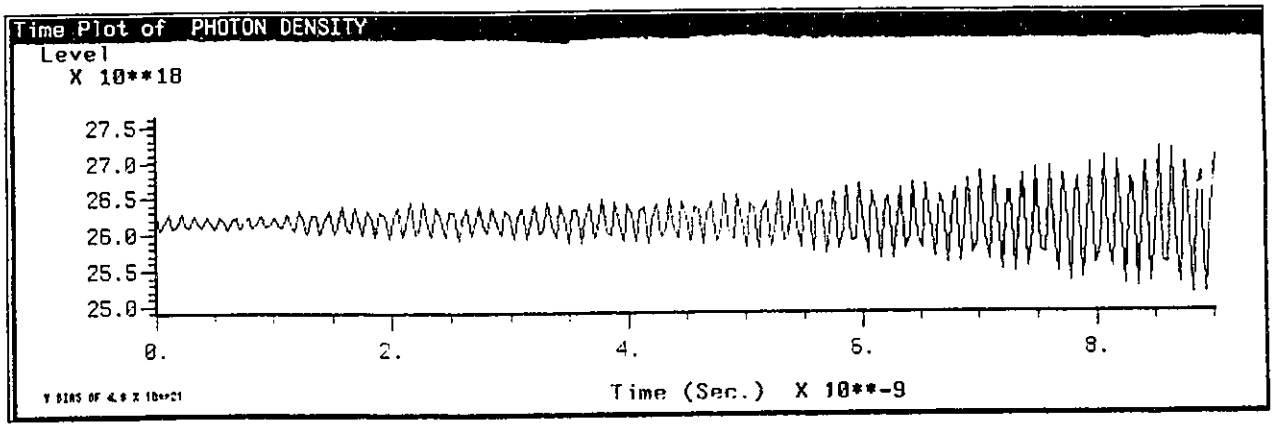

Fig. 7. Response for $\|z_p\| = 1.0048$.

2.2 Noise Modeling

Each term in the laser rate equations represents a stochastic process that can be modeled as shot noise. The spectrum is taken to be white and the power level is taken to be equal to the average of the process. The question that then arises is whether we can modify our laser model by adding noise terms and obtain the laser noise spectrum.

Earlier work has been done by Marcuse to model the laser RIN. In this case, he assumed the noise to be a Gaussian random variable[15]. He gives results in terms of the time domain random fluctuations of the laser output[16].

Since we are primarily interested in the noise power spectral density, i.e. second order statistics, we are not concerned with the probability density function of the random variable. The simplest random variable to generate with a computer is from a uniform distribution, as it is simply a pseudo random number generator. If we use the uniform random variable, we must scale the result such that we get the required level for the power spectrum. With respect to any random number, BOSS scales the spectral height to keep a constant overall power. This scaling is required since the spectral height will vary with the simulation time step because the noise spectrum is distributed over the Nyquist bandwidth for the simulation. Therefore, we must normalize by the time step to keep a constant spectrum. Also, we must include a factor for the variance of a uniform distribution, which is 1/12. The required block was constructed with BOSS and used for each random process.

In Chapter 3, we give the simulation results for laser RIN and compare them with well-known analytical techniques. Both results are in close agreement.

2.3 Evaluation of Distortion using Monte Carlo Method

The intermodulation distortion level in a multi-channel system is dependent on the phases of all the carriers. In a video transmission system, we assume that the phases of the carriers are independent. The intermodulation distortion level is therefore random. An exhaustive approach to determine the distortion level would be to average over all possible phase combinations. Instead, we will use a Monte Carlo computer simulation method. This approach was first suggested by Medhurst[1] to deal with a similar problem for FM

trunk radio systems. The total distortion will be due to many components, whose phases are assumed to be independent. With a sufficient number of carriers, the distortion can be approximated to have a Gaussian distribution. The expected error of the distortion level averaged over a number of simulation runs can then be determined by integrating the Gaussian probability distribution function. This was done by Medhurst. We are given that if we average over 8 simulation runs, we are accurate within 3 dB, 94 times out of a 100.

To determine the intermodulation distortion, we can run a simulation with some carriers removed. The resulting signal in those channels are due to nonlinear distortion from carriers in the other channels. Instead of removing only one carrier and running 8

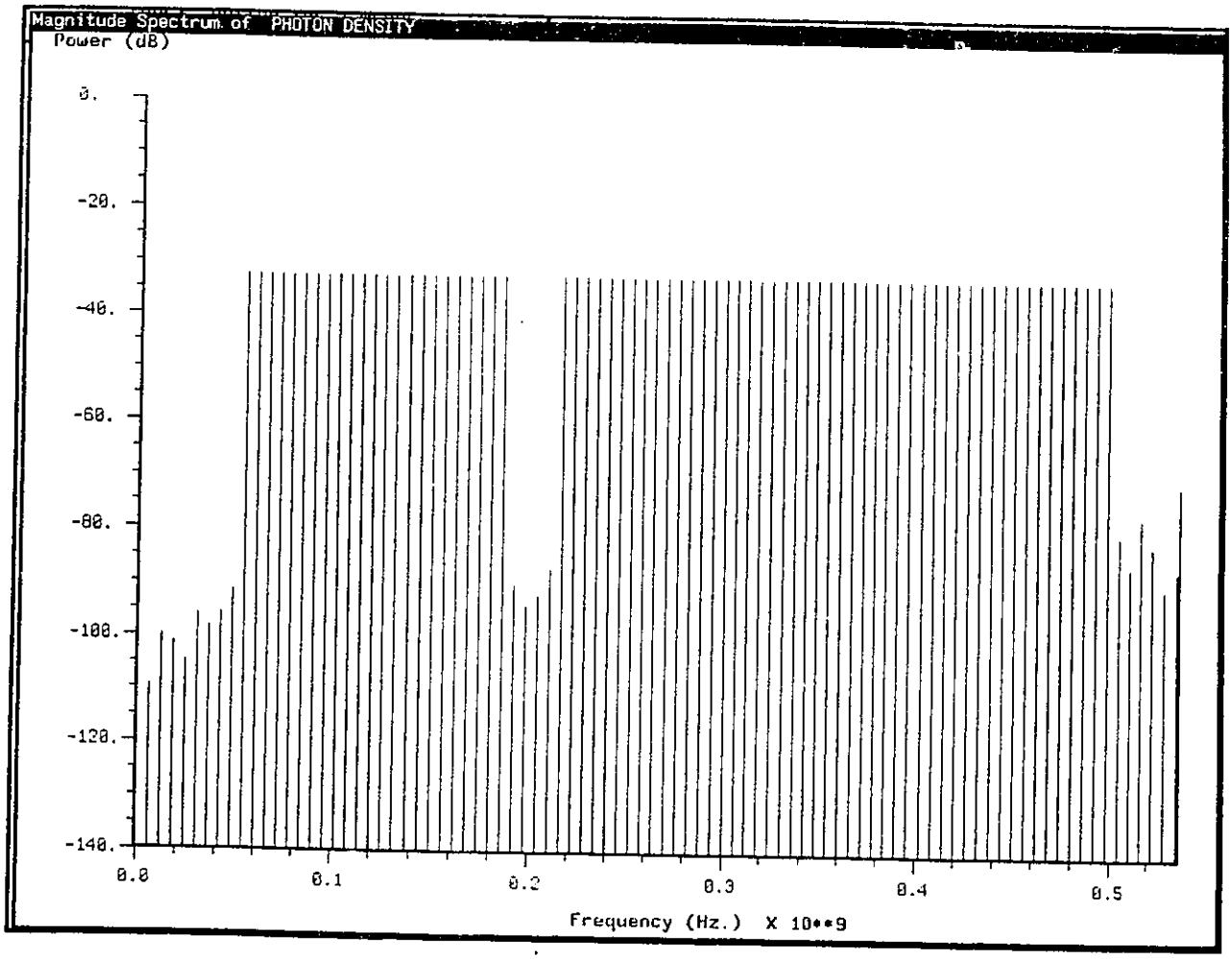

Fig. 8. Distortion Spectrum for NTSC spectrum

simulations, which would be expensive, we will remove 4 adjacent carriers and average over 2 simulation runs. In this case, we are assuming that over 4 adjacent channels, the distortion level is constant. In Figure 8, we give a typical simulation result for the NTSC spectrum, where we have removed the carriers at 192MHz, 198MHz, 204MHz, and 210MHz to determine the average distortion level at 200MHz.

2.4 A Carrier Frequency Assignment for Nonlinear Distortion

We will now discuss a carrier frequency assignment for nonlinear distortion. We will use these frequencies throughout the thesis.

The problem can be stated as being one of choosing a set of integers (frequencies) which, when passed through a nonlinear system, give rise to second and third order distortion components, which do not occur at any of the original frequencies.

This problem has been formulated previously in the case where the carriers are confined to an octave, in which case, the only significant distortion is third order distortion. This was true for some radio systems. In this case, the problem can be defined as obtaining a set of integers with distinct differences[13]. That is, taking any two integers from that set, their differences must be unique. Atkinson has given a table with the first 100 sets of DDS's (distinct difference set)[17]. Better yet, though, for our application, would be to eliminate second order distortion as well. A computer program has been written to generate such a set. The code, as well as a further description is given in Appendix A. We also give the set of the first 35 integers that satisfy this property.

We will now describe an application of this set of numbers. The first 20 integers of the set range from 1 to 903. We can set carriers from 10 MHz to 9.03 GHz. and investigate the distortion spectrum in this bandwidth. If we remove some of the carriers, the distortion at those frequencies will be at least fourth order. This has been done and the results are given in Figure 9. We have indicated the total distortion to be the distortion at any frequency other than those where the carriers have been removed. From this plot, we can conclude that over most of the spectrum, the distortion resulting from orders greater than three are at least 10 dB below the overall distortion. If analytical work is done, it is useful to know that if we consider only second and third order distortion, the results will

have satisfactory accuracy.

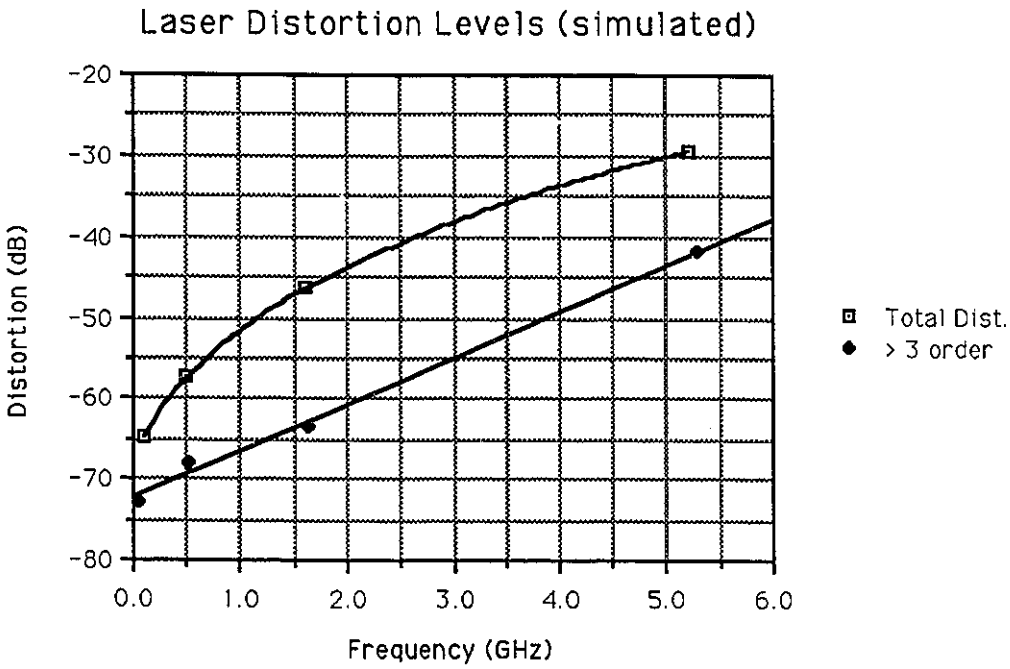

Fig. 9. Total Distortion vs Distortion greater than third order

Chapter 3

Laser

3.1 Linearized Rate Equations

The laser can represent the major source of degradation in a fiber-based system. It is both nonlinear and noisy. We will therefore consider its nonlinearity. However, it is useful to first linearize the laser rate equations so that we can then apply linear system theory to consider its bandwidth, stability and the transient response of the resulting second order system. Bandwidth is clearly important, as we are using frequency multiplexing. As for stability, although lasers are inherently stable physical systems, when we approximate the laser as a discrete system we must be certain that the simulation remains stable. As for response type, as we shall see, the linear transfer functions appears in the expressions for the nonlinear distortion spectrum. We will now linearize the following laser rate equations:

$$\frac{dN(t)}{dt} = \frac{I_A}{V'} - \frac{N}{\tau_n} - g_0(N - N_{om})[1 - \epsilon S]S \tag{3.1}$$

$$\frac{dS(t)}{dt} = \Gamma g_0(N - N_{om})[1 - \epsilon S]S - \frac{S}{\tau_p} + \Gamma\beta\frac{N}{\tau_n} \tag{3.2}$$

In perturbation analysis, as given by Lau[3], one writes down the current as a sum of a steady state and a term for small signal fluctuations from the steady state, and likewise for the photon and electron densities, as follows:

$$\begin{aligned} N(t) &= \overline{N} + \Delta N \\ S(t) &= \overline{S} + \Delta S \\ I(t) &= \overline{I} + \Delta I \end{aligned} \tag{3.3}$$

Substituting (3.3) into the rate equations and using the fact that $\frac{\overline{I}}{V'} - g_0(\overline{N} - N_{om})[1 - \epsilon\overline{S}]\overline{S} - \frac{\overline{N}}{\tau_n} = 0$ and $\Gamma g_0(\overline{N} - N_{om})[1 - \epsilon\overline{S}]\overline{S} - \frac{\overline{S}}{\tau_p} + \Gamma\beta\frac{\overline{N}}{\tau_n} = 0$ we can reduce the rate equations to the following second order set of differential equations:

$$\frac{d\Delta N}{dt} = A_1\Delta N + A_2\Delta S + \frac{\Delta I}{V'} \tag{3.4}$$

$$\frac{d\Delta S}{dt} = A_3\Delta N + A_4\Delta S \tag{3.5}$$

where:

$$\begin{aligned} A_1 &= -g_0[1 - \epsilon\overline{S}]\overline{S} - \frac{1}{\tau_n} \\ A_2 &= -g_0(\overline{N} - N_{om})[1 - 2\epsilon\overline{S}] \\ A_3 &= \Gamma g_0[1 - \epsilon\overline{S}]\overline{S} + \Gamma\beta\frac{1}{\tau_n} \\ A_4 &= \Gamma g_0(\overline{N} - N_{om})[1 - 2\epsilon\overline{S}] - \frac{1}{\tau_p} \end{aligned} \tag{3.6}$$

Since we now have a linear system, we can apply linear system theory for second order systems. Applying the Fourier Transform to (3.4) and (3.5), one can obtain the following expression for the laser transfer function:

$$\frac{\Delta S}{\Delta I} = \frac{A3}{V'}\frac{1}{-\omega^2 + A_4A_1 - A_2A_3 + j\omega(-A_1 - A_4)} \tag{3.7}$$

This second order transfer function has two poles. From the location of these poles, we can say something about stability, bandwidth and response type. For any linear second order system[18] we define ω_n to be the natural undamped frequency and ξ as the damping ratio. In terms of the coefficients of the transfer function, they are given by:

$$\omega_n^2 = A_1A_4 - A_2A_3 \tag{3.8}$$

$$\xi = \frac{(-A_1 - A_4)}{2\sqrt{A_1A_4 - A_2A_3}} \tag{3.9}$$

Poles will be given by $-\alpha \pm j\omega$ where $\alpha = \xi\omega_n$ and $\omega = \omega_n\sqrt{1 - \xi^2}$. The significance of ω_n, the natural undamped frequency, is that it gives us the distance of the poles from the origin. The damping ratio, ξ, will tell us what type of transient response we will have. For $\xi < 0$, we have an unstable system. For $0 < \xi < 1$, we have an underdamped system with some overshoot in the transient response, and for $\xi > 1$ we have an overdamped

Parameter	Description	Values	Units
I_{th}	threshold current	21	mA
V'	volume of active region times electron charge	1.44E-35	m^3 -coulombs
τ_p	photon lifetime	2	ps
τ_n	electron lifetime	3.72	ns
N_{om}	transparent carrier density	4.6E24	m^{-3}
g_o	optical gain constant	1E-12	$s^{-1}m^3$
Γ	optical confinement factor	0.646	-
β	spontaneous emission factor	0.001	-
ϵ	gain compression factor	2.6E-23	m^3

Table 3.1: Laser Parameters

system with no overshoot in the transient response. It will also tell us something about the frequency response of the system, i.e. for $\xi < .707$, we will have resonance at $\omega_p = \omega_n\sqrt{1-2\xi^2}$. If we have resonance in the linear transfer function, we will also have some in the distortion spectrum. This resonance may appear in the signal band and severely affect the CNR.

From the expressions for the A_i's we see that the response is dependent on the intrinsic laser parameters, such as ϵ, β, Γ and g_0. It is also dependent on the steady state values of electron and photon densities, $\overline{N}$ and $\overline{S}$. This is heavily related to the current bias, especially for the photon density, which is essentially proportional to the bias current minus the threshold. Therefore, the bias current will affect the transfer function and, as we shall see later, also the nonlinear distortion spectrum and the RIN spectrum. We will perform our simulation with the laser parameters as given by Way[5]. These parameters are given in Table 3.1. They are for a high-speed GaAlAS single-mode laser diode (Ortel LS-620). We have, however, modified one parameter, ϵ, the gain compression from $3.8E-23$ to $2.6E-23$. With $\epsilon = 3.8E-23$, the laser does not have a bandwidth of 6 GHz. With the modification, the laser does have a 6GHz bandwidth, which is common for a high-speed laser.

To obtain the transfer function of our laser, we take the magnitude of equation (3.7). We have plotted the response for two bias currents, a 50 mA bias and a 75 mA bias, as given in Figures 10 and 11.

How do we obtain the transfer function with a computer simulation? One approach

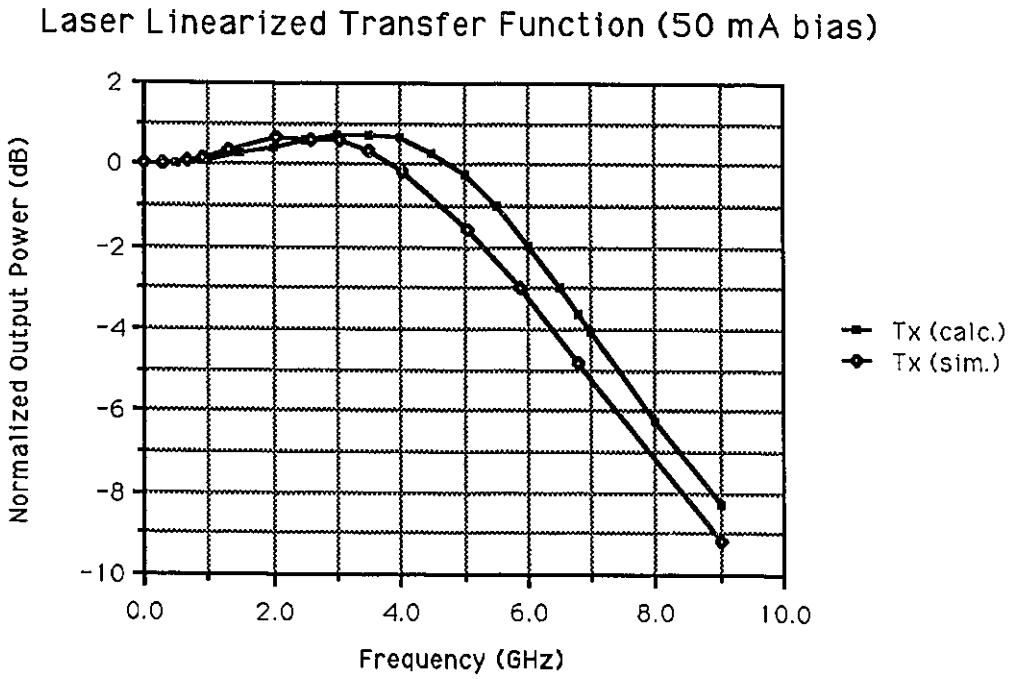

Fig. 10. Transfer Function for the Laser biased at 50 mA

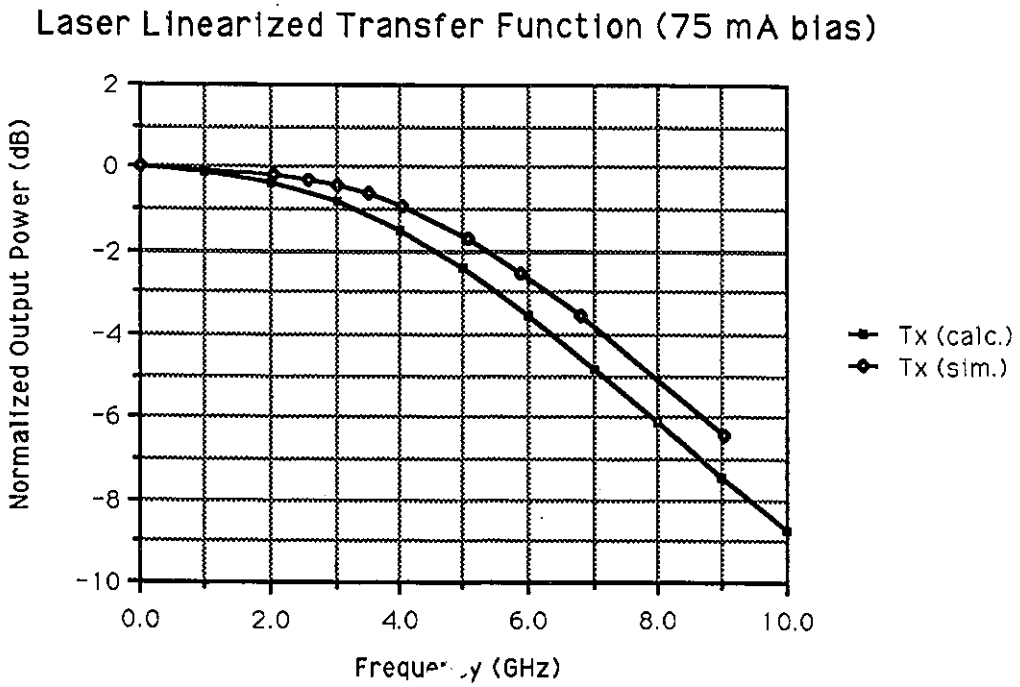

Fig. 11. Transfer Function for the Laser biased at 75 mA

would be to input a single carrier at each frequency, and record the response at each frequency. Alternatively, we could input a number of carriers at many frequencies and obtain the response in one simulation. The problem, however, is that the laser is not linear, and what we get at the output of the laser is from both the nonlinear distortion as well as the linear response. However, if we choose our carriers in a clever way, such that the significant distortion does not fall on our linear response, we can obtain the transfer function of the laser in a single simulation. This is precisely the constraint on the set of carriers that we discussed in Chapter 2. Recall that the first 20 integers from the set range from 1 to 903. We can set carriers from 10 MHz to 9.03 GHz and find the transfer curve in one simulation run.

This was performed with the laser biased at 50mA and 75mA. In figures 10 and 11 we present both simulated and calculated results. We can observe that we do have the required bandwidth of 6GHz. We see that for 50mA we have resonance. For a 50 mA bias, $\xi = 0.5623$, whereas for a 75 mA bias, $\xi = 0.8278$. Therefore, for a 50 mA bias, since $\xi < 0.707$, we have resonance in the frequency domain.

We will now discuss the stability of the laser. With respect to a linear system, we have a stable system if the real part of the poles are negative i.e. we must have $\xi > 0$. Recalling our definition for ξ we see that it is true for $-A_1 > A_4$ which implies that we must have $g_0[1-\epsilon\overline{S}]\overline{S}+\frac{1}{\tau_n}+\frac{1}{\tau_p}-\Gamma g_0(\overline{N}-N_{om})[1-2\epsilon\overline{S}] > 0$. The last two terms relate to the rate of photons leaving and entering the active region. For any physical laser, $\xi > 0$ and therefore lasers are stable.

3.2 Phase Plane Analysis

The phase plane analysis technique can be applied to certain second-order differential equations[19]. The independent variable is eliminated. Notice that the rate equations have the independent variable t and two dependent variables N and S. If we divide one equation by the other, we eliminate the dependent variable t and obtain the following equation:

$$\frac{dN}{dS} = \frac{\frac{I_A}{V} - \frac{N}{\tau_n} - g_0(N-N_{om})[1-\epsilon S]S}{\Gamma g_0(N-N_{om})[1-\epsilon S]S - \frac{S}{\tau_p} + \Gamma\beta\frac{N}{\tau_n}} \tag{3.10}$$

The phase plane is formed by plotting the slopes of the electron density against the

photon density. An infinite slope occurs when the denominator is zero, i.e. when the photon density changes are zero, $dS = 0$ and likewise the line for zero slope occurs when the numerator is zero, i.e. $dN = 0$. We have plotted the phase plane for our particular laser for a bias of 50 mA. In Figure 12, where the lines for zero slope and infinite slope intersect, we have the steady state point (photon and electron changes are zero, $dS = dN = 0$). We have also plotted the turn on trajectory and turn-off trajectory.

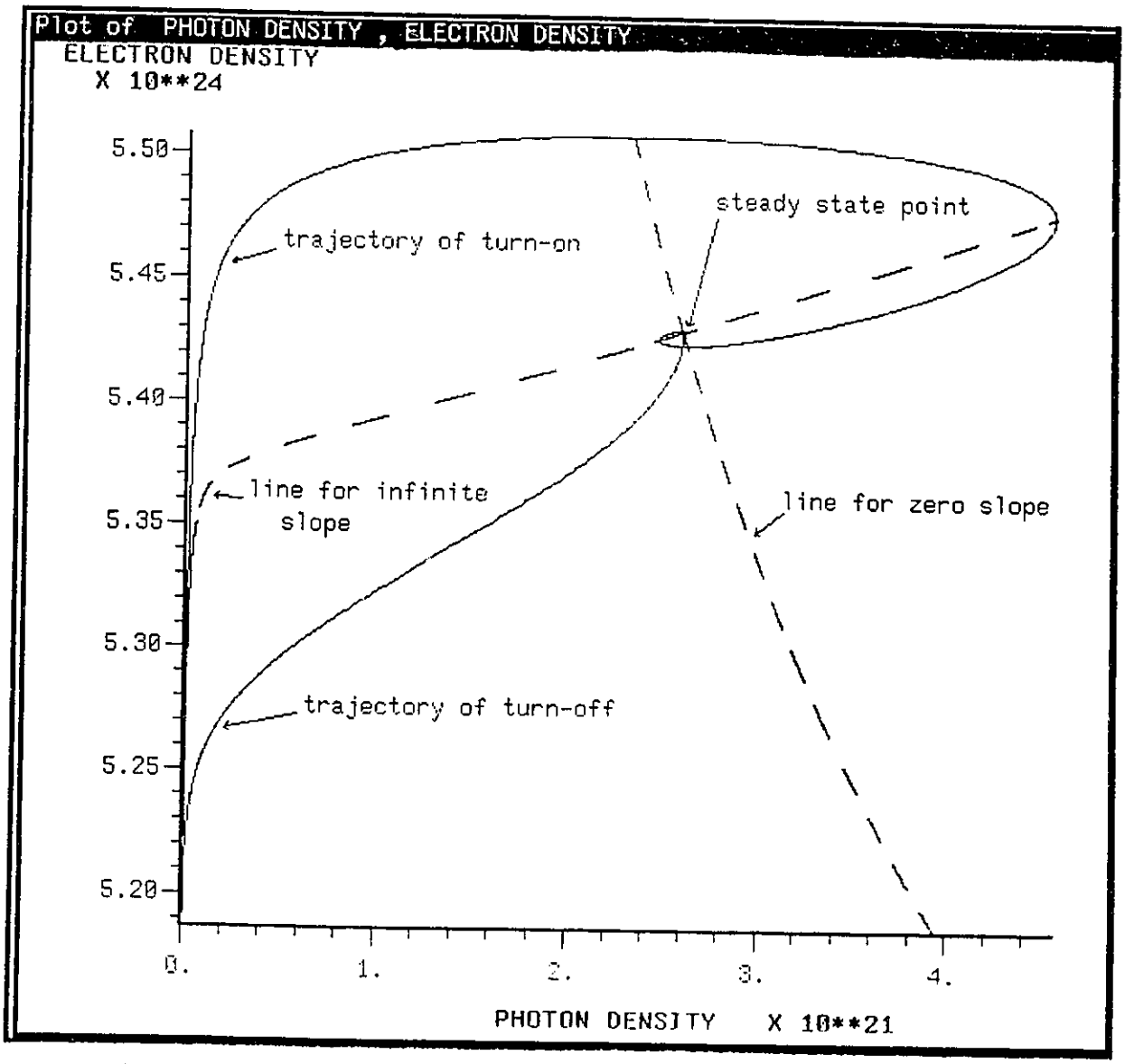

Fig. 12. Phase Plane for laser biased at 50 mA

We can see that at turn-on, the trajectory is somewhat circular, which implies that in the time domain response, the light output will overshoot before reaching a steady state value. At turn-off, the photon density decreases steadily, thus we can expect no overshoot.

The phase plane is a convenient way of visualizing transient behavior with respect to a particular parameter of the laser. In Figures 13, 14, and 15, we show the tail end of a turn-on trajectory for the laser. In Figure 13, $\epsilon = 2.6E - 23$ and the laser is biased at 75mA. We notice that we have overshoot. We can decrease the bias to 50mA, and then

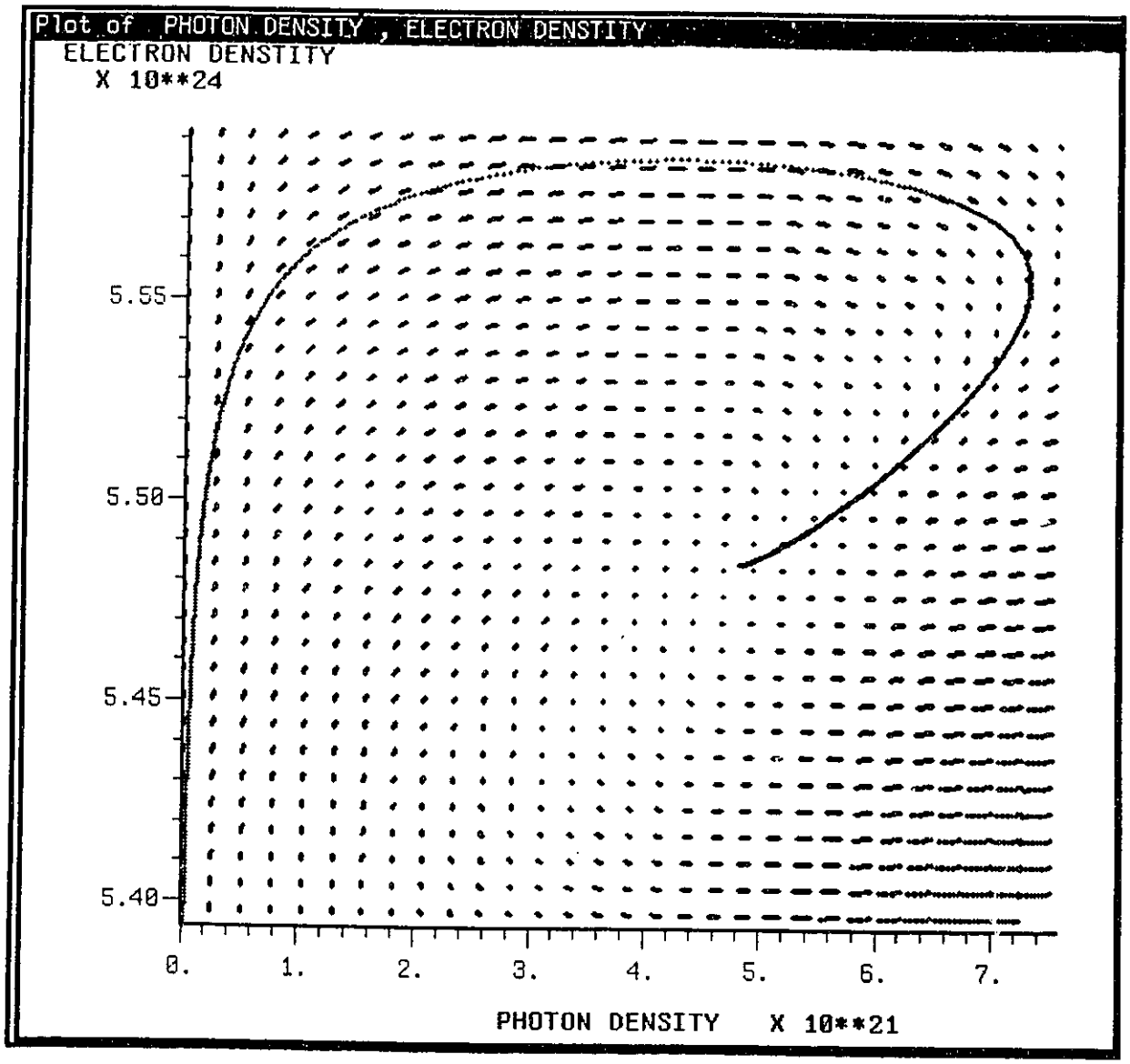

Fig. 13. Phase Plane for laser biased at 75 mA

we have the trajectory in Figure 14. We notice that we have a more circular trajectory which implies more oscillations in the time domain. We can also change the trajectory by changing the intrinsic parameters of the laser, notably, the gain compression ϵ. In Figure 15, keeping the bias at 75mA, we have increased ϵ to $7.83E-23$. In this case, we have no overshoot and we therefore have an overdamped system.

As already stated, ξ, the damping ratio, affects the type of response we have and for Figures 13, 14 and 15 we have for ξ the values of 0.8278, 0.5623 and 3.7322 respectively.

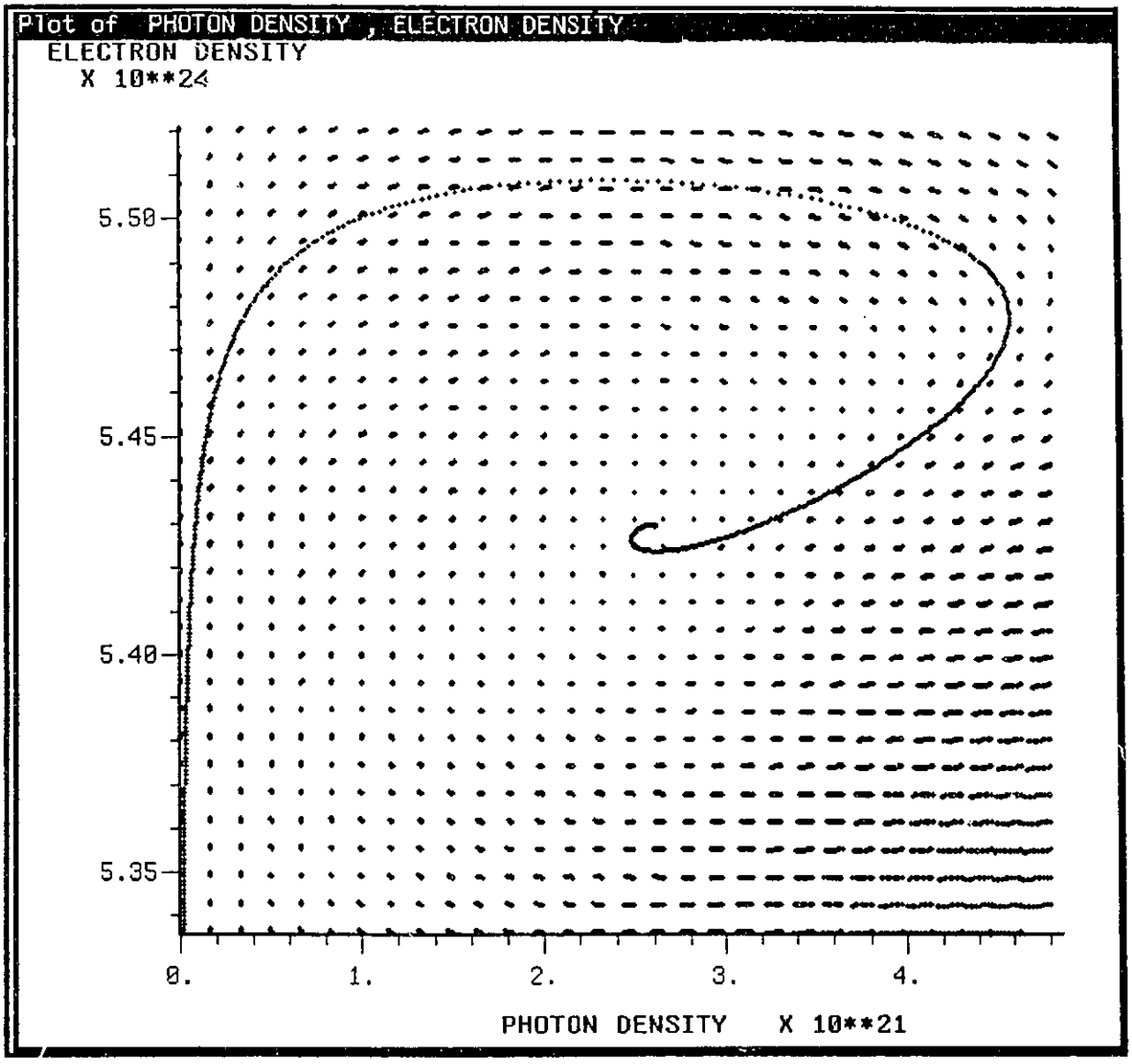

Fig. 14. Phase Plane for laser biased at 50 mA

For $\xi > 1$, we have an overdamped system. Also, in these figures, we show the intermediate trajectory from 900 initial values of photon and electron densities. These initial values are given in Figure 16. What we have then plotted are the next ten simulation values from these initial points. We obtain some valuable insight with respect to the transient behavior of the laser. The slopes of the lines tell us the direction of the trajectory and the lengths of the trajectories tell us how quickly the changes are occurring (in time). We see that the slopes are circular around the steady state points as the solutions

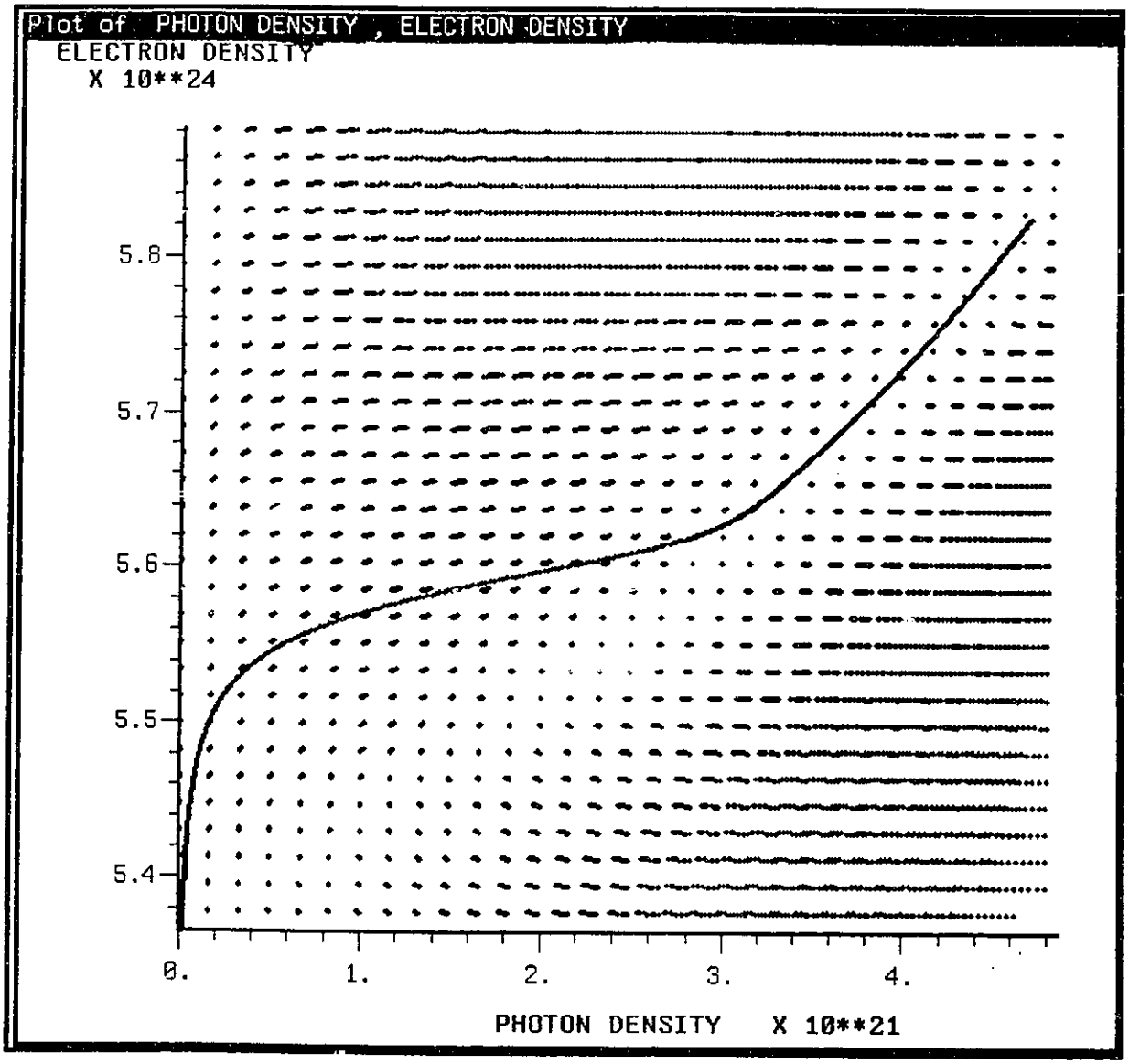

Fig. 15. Phase Plane for laser with $\epsilon = 7.83E - 23$.

converge from everywhere to this point. Also the lengths of the lines close to the steady state value are shorter, since the laser reaches the steady state value very gradually, asymptotically.

The phase plane is helpful for transient analysis, but it cannot be applied to nonlinear distortion prediction, in which case we must consider the spectral properties of the system.

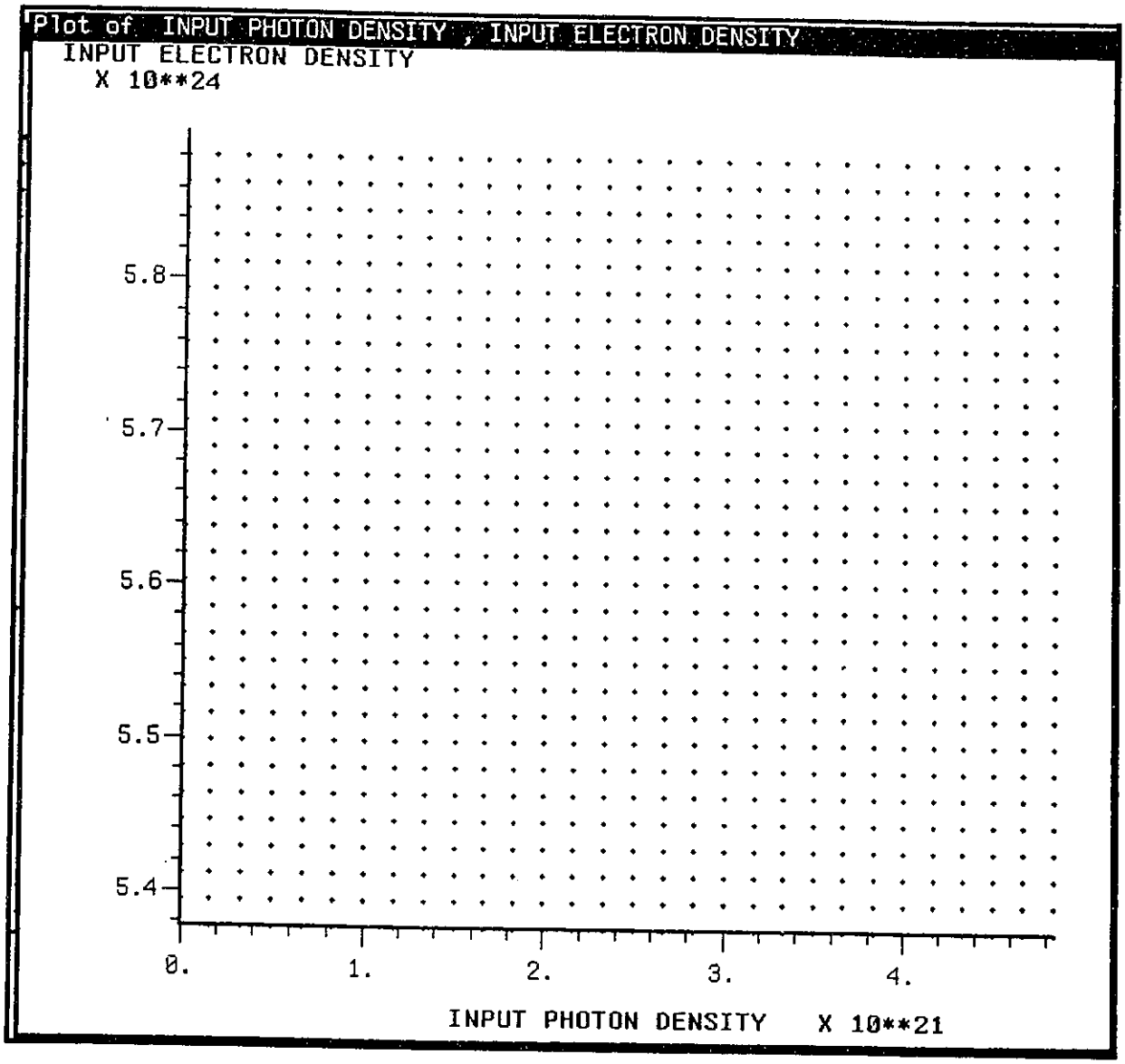

Fig. 16. Initial points for Phase Plane.

3.3 Nonlinear Distortion

In Section 1, we treated the laser as being linear, but as we know, it is not, due to the nonlinear coupling of the photon and electron densities in the stimulated emission term of the rate equations. The distortion spectrum can be obtained analytically, through perturbation analysis, in much the same way as the linear transfer function was obtained. With this technique, every type of distortion can be determined with respect to the linear term e.g. $S^{2\omega_1}/S^{\omega_1}$, $S^{\omega_1-\omega_2}/S^{\omega_1}$. The drawback of this method is that it becomes very tedious, due to the complexity of the rate equations, for higher order terms. Also, having generated expressions for the various distortion terms, how do we find the total distortion from all distortion terms and deal with the multi-carrier case? Nonetheless, it is instructive to see, for example, how the second order distortion spectrum varies with bias current and laser parameters.

We will now proceed with perturbation analysis[3]. The general approach is to write down for the current, and electron and photon densities a series with components at all the original signal frequencies as well as at the beat frequencies generated by the laser nonlinearities. We substitute these expressions into the rate equations, apply trigonometric identities to deal with the products of sinusoids, and disregard all higher order terms with respect to lower order terms. Generally, what we find is that lower order distortion terms drive the higher order terms. We proceed as follows:

$$\begin{aligned} N(t) &= N^0 + \Re(N^{\omega_1} e^{j\omega_1 t}) + \Re(N^{2\omega_1} e^{j2\omega_1 t}) \\ S(t) &= S^0 + \Re(S^{\omega_1} e^{j\omega_1 t}) + \Re(S^{2\omega_1} e^{j2\omega_1 t}) \\ I(t) &= I^0 + \Re(I^{\omega_1} e^{j\omega_1 t}) \end{aligned} \tag{3.11}$$

Substituting into the rate equations, we obtain the following pair of second order differential equations:

$$\frac{dN^{2\omega_1}}{dt} = B_1 N^{2\omega_1} + B_2 S^{2\omega_1} + B_3 N^{\omega_1} S^{\omega_1} + B_4 S^{\omega_1} S^{\omega_1} \tag{3.12}$$

$$\frac{dS^{2\omega_1}}{dt} = B_5 N^{2\omega_1} + B_6 S^{2\omega_1} + B_7 N^{\omega_1} S^{\omega_1} + B_8 S^{\omega_1} S^{\omega_1} \tag{3.13}$$

where:

$$B_1 = -g_0[1 - \epsilon\overline{S}]\overline{S} - \frac{1}{\tau_n}$$

$$
\begin{aligned}
B_2 &= -g_0(\overline{N} - N_{om})[1 - 2\epsilon\overline{S}] \\
B_3 &= -\frac{1}{2}g_0[1 - 2\epsilon\overline{S}] \\
B_4 &= \frac{1}{2}g_0(\overline{N} - N_{om})\epsilon \\
B_5 &= \Gamma g_0[1 - \epsilon\overline{S}]\overline{S} + \Gamma\beta\frac{1}{\tau_n} \\
B_6 &= \Gamma g_0(\overline{N} - N_{om})[1 - 2\epsilon\overline{S}] - \frac{1}{\tau_p} \\
B_7 &= \frac{1}{2}\Gamma g_0[1 - 2\epsilon\overline{S}] \\
B_8 &= -\frac{1}{2}\Gamma g_0(\overline{N} - N_{om})\epsilon
\end{aligned} \tag{3.14}
$$

All terms in the differential equations have frequency $2\omega_1$. The coefficients B_3, B_4, B_7 and B_8 refer to the components resulting from the products $S^{\omega_1} \cdot S^{\omega_1}$ and $S^{\omega_1} \cdot N^{\omega_1}$ that occur at $2\omega_1$ and the components at d.c. have been ignored. Note that in these equations, it is the linear terms, $S^{\omega_1}S^{\omega_1}$ and $S^{\omega_1}N^{\omega_1}$ that drive these second order distortions. Since we have linear differential equations, we can take the Fourier Transform and obtain the spectrum. This has been performed by Darcie[20] for this set of rate equations, which is an extension of earlier work[3] as it includes the gain compression term ϵ. The following expression is given:

$$
\frac{S^{2\omega_1}}{S^{\omega_1}} = m\frac{\omega^2}{\omega_n^2 g(2\omega)} \tag{3.15}
$$

where m is the optical modulation index, $g(\omega)$ is the small signal frequency response that we derived earlier, and is given by:

$$
g(w) = \frac{\omega_n^2}{-\omega^2 + 2j\xi\omega_n + \omega_n^2} \tag{3.16}
$$

We have plotted this function for our laser for two bias currents, in Figures 17 and 18, for a 50 mA bias and a 75 mA bias, which clearly illustrates the effect of bias current and its relation to the small signal response. With the 50mA bias, distortion peaks at approximately 3 GHz, whereas, for the 75mA bias, it reaches a maximum at 8GHz. Since our signal band is up to 6GHz, to avoid excessive intermodulation distortion, we should bias at 75mA. This analysis has been extended by Darcie[20] and he gives results for third order distortion. Each component has a different spectrum. Nonetheless, the small-signal response appears in all these expressions. These results help us in studying the laser

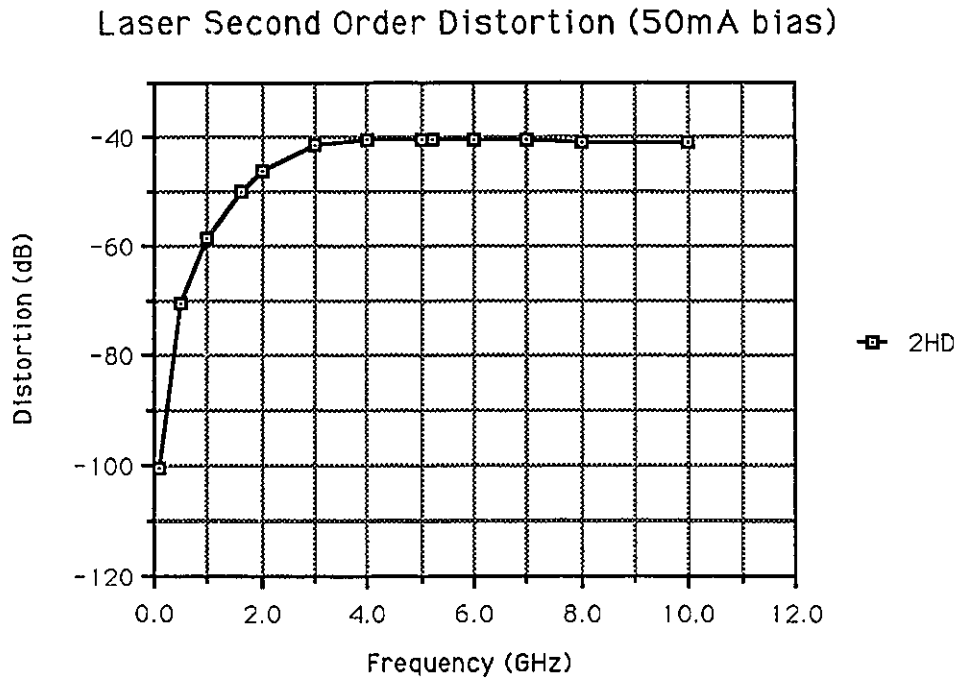

Fig. 17. Second Harmonic Distortion for a 50 mA bias

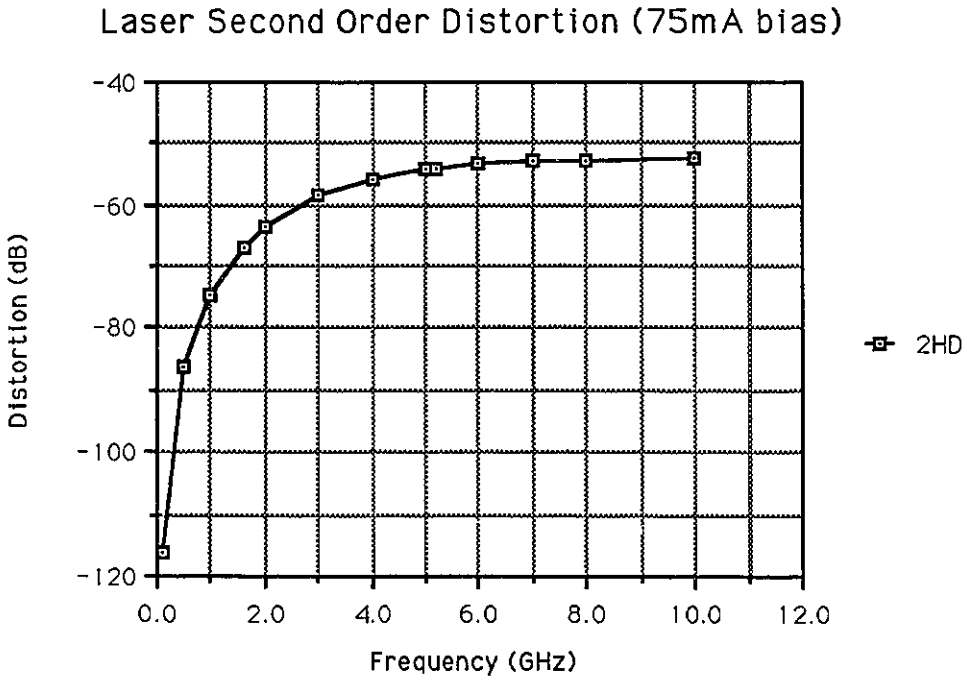

Fig. 18. Second Harmonic Distortion for a 75 mA bias

as a device, but how do we extend this to the design of a multi-channel system? In this case, we must consider all distortion components and their contribution to the total distortion. This will depend on the phases of the carriers and this is too tedious to do in practice.

An alternative is to use the model developed in BOSS. To determine the distortion spectrum, we can place as input to the laser module a d.c. bias plus a carrier and, upon performing the simulation, take the FFT of the output to obtain the distortion level. The simplest case is to place a single carrier and record the second harmonic. Using the unmodified laser parameters given by Way[5], the second harmonic was simulated at 1 GHz for various bias currents. Results are given in Figure 19. The simulation results obtained with BOSS are very similar to those obtained by Way and compare well with his results of second order harmonics measured in the laboratory[5].

In Section 1, we had shown how to obtain the linear transfer function of the laser with a single simulation. The idea was to prevent second and third order distortion from interfering with the linear portion of the laser response. Just as the distortion does not affect the signal carriers, the signal carriers do not conceal the distortion spectrum. It

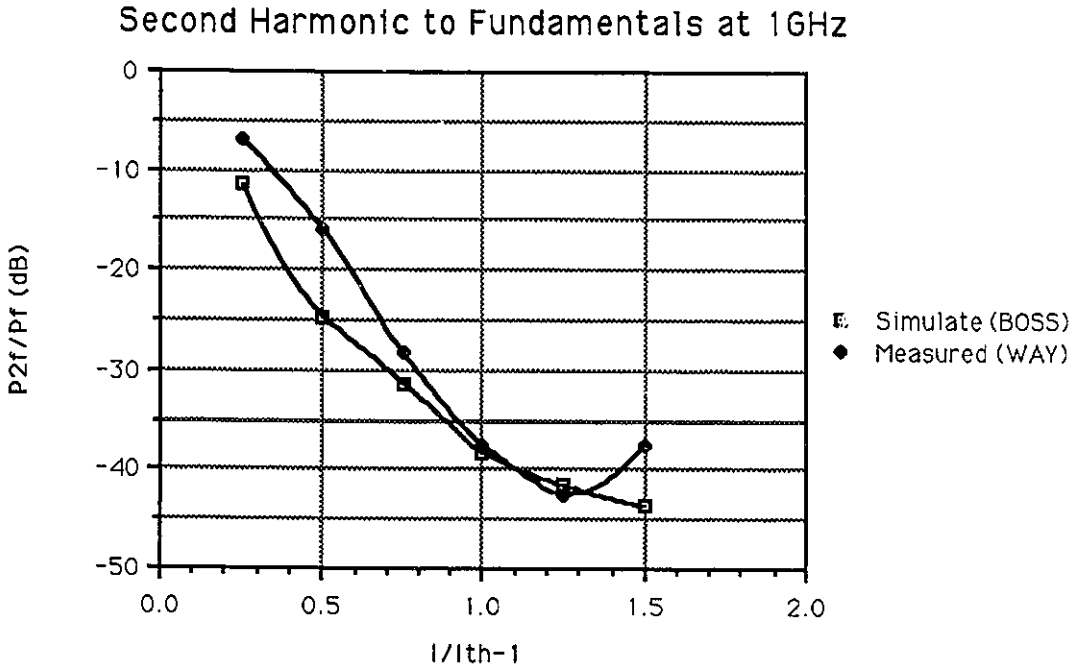

Fig. 19. Second Harmonic Levels at 1 GHz.

will be composed of many distortion components, and by averaging over a few simulation runs, we can compare our simulation results with Darcie's analytical results. The spectrum from BOSS is given in Figures 20 and 21. For a 50 mA bias, the spectrum peaks at 3 GHz and for 75 mA, it reaches a maximum value at 8 GHz. We average over a few simulation runs and plot them with calculated results in Figures 22 and 23. The general frequency dependence is the same. To understand the difference in distortion level, we

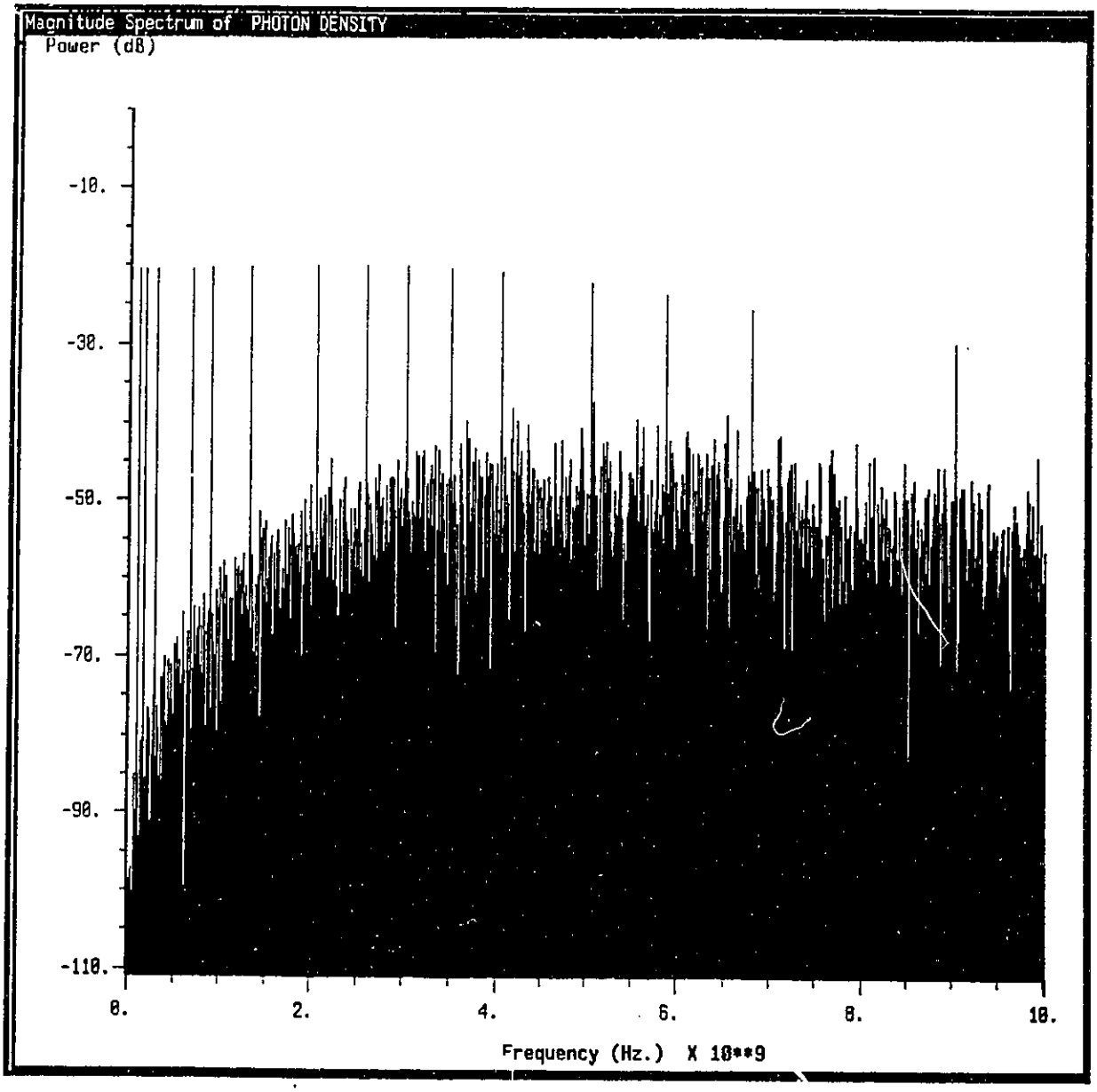

Fig. 20. Total Distortion Spectrum with BOSS for a bias of 50 mA.

recall that in the case of the simulation, we have the total distortion, whereas, for the expression from Darcie, it is the second harmonic from a single carrier. We can conclude that, since the total distortion spectrum has the same shape as the second harmonic spectrum, the most significant distortion is second order.

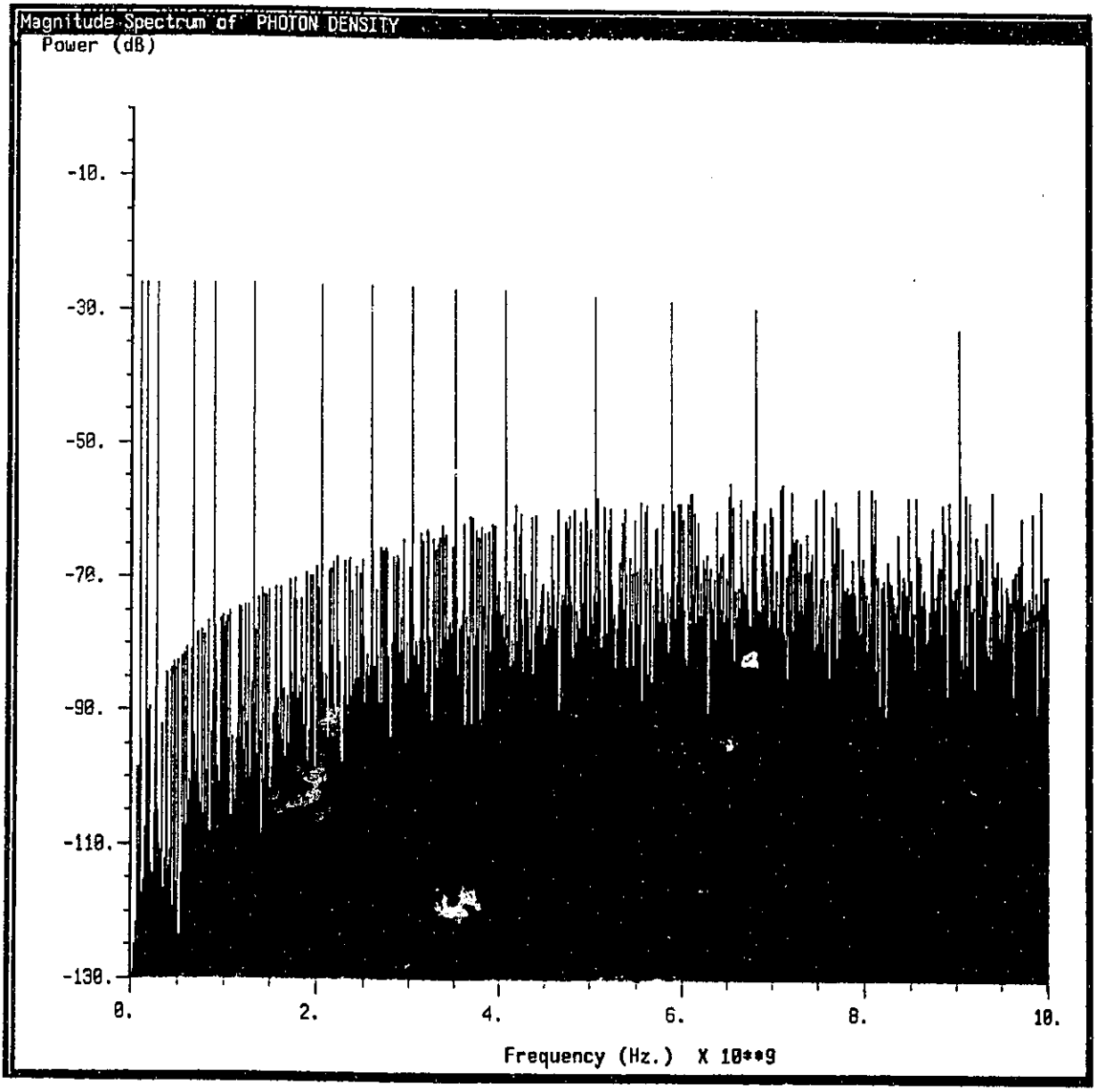

Fig. 21. Total Distortion Spectrum with BOSS for a bias of 75 mA.

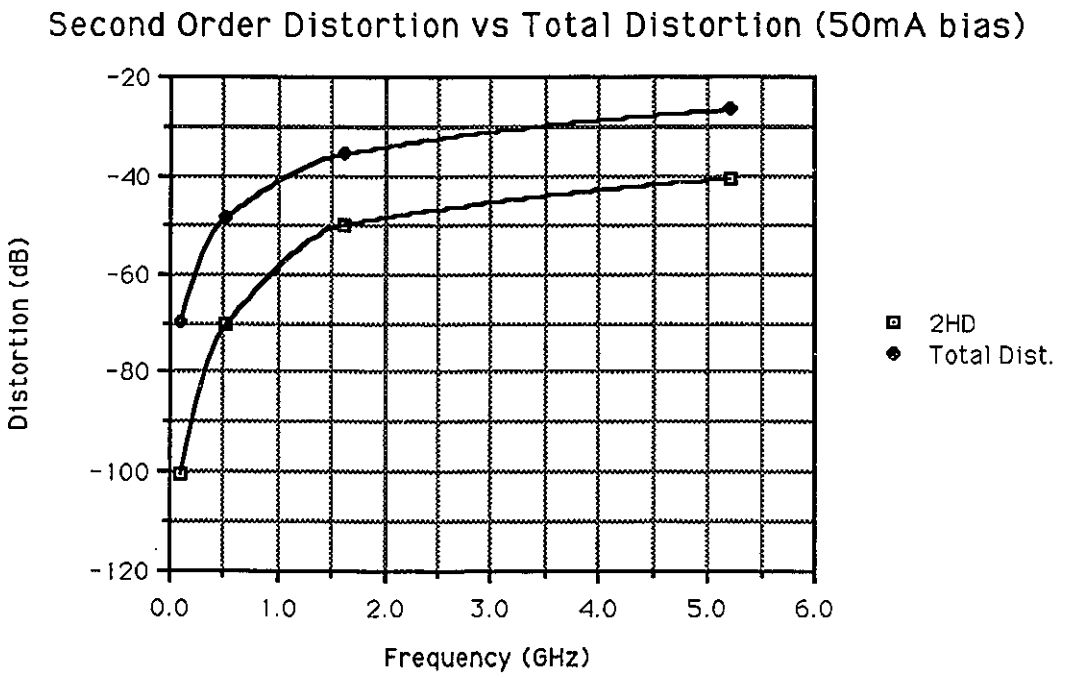

Fig. 22. Total Distortion vs second harmonic for 50 mA

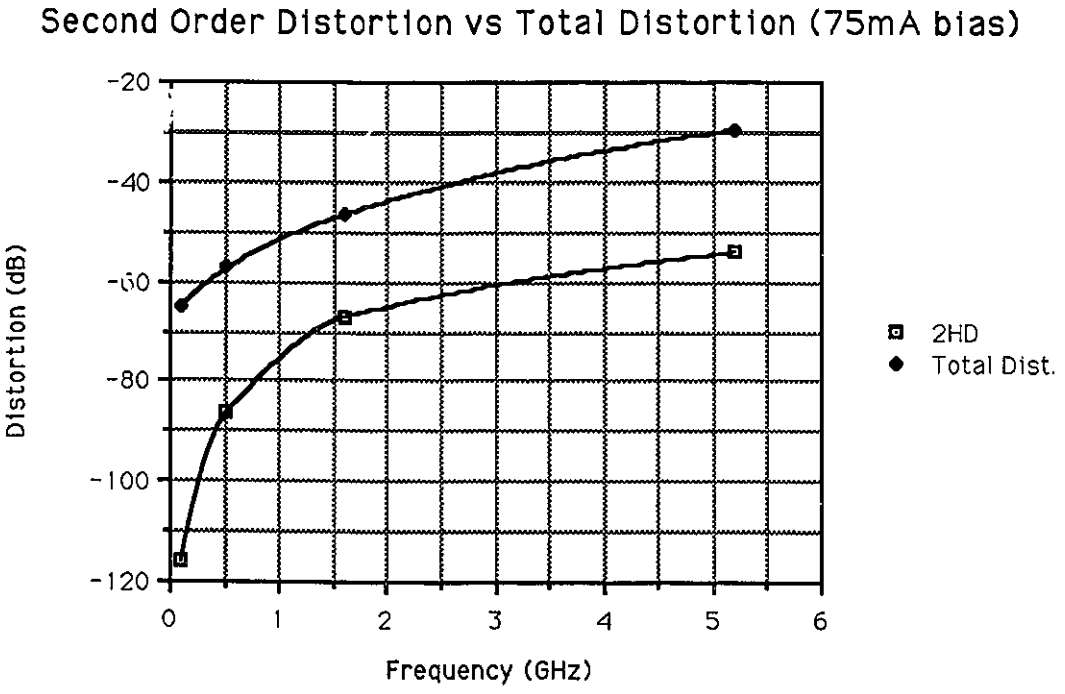

Fig. 23. Total Distortion vs second harmonic for 75 mA

3.4 Clipping

If one looks at the turn-on trajectory in the phase plane, one can see that the photon output is essentially zero until a large value of electron density has been reached. This is because until a large level of electron density has been reached, we have primarily spontaneous emission, due to the N/τ_n term in the rate equation. It is only with a large electron density that stimulated emission does take place and only then do we have a large photon output. This is referred to as the threshold of the laser. For our particular laser, the threshold of the laser is 21 mA.

The laser must therefore be biased above 21 mA to obtain a non-zero output and if we do go below threshold, our output waveform will be clipped. This is illustrated in Figure 24. If we have a small number of carriers, we can assure ourselves that we will not go below threshold by biasing the laser high enough. However, if the number of channels is high, for example 75 channels, we cannot assure that clipping will not take place, because, to do so, we would have to operate it at a very high bias. We must therefore cope with some clipping from the laser.

Clipping has been identified by Saleh[21] as a fundamental limit of system performance of a fiber subcarrier system. Subcarrier systems have a large number of carriers, and even if we can develop a truly linear laser, we will always have to contend with clipping.

In the laser simulations, we assume that we have a second or third order system, depending on whether or not the signal bandwidth is confined to an octave. Therefore, if we double the signal level, we expect the CNR to degrade by the same factor for a second order system, or by twice that for a third order system. Therefore, with one simulation, we can predict the distortion level at any other signal level. However, clipping has a highly nonlinear dependence on optical modulation index and thus on signal level. Therefore, what we choose to do in our simulations is to use a low optical modulation index such that we do not have to concern ourselves with clipping, and then we can treat the laser as a second or third order system. We then deal with clipping separately. In some systems, such as 4-level QAM, where we can have a high tolerance on CNR, we could use a high optical modulation index without laser intrinsic nonlinearities becoming too severe. Clipping then becomes the major source of nonlinear distortion. We will therefore

develop an expression to set a CNR penalty due to clipping.

This work is from Saleh[21], who makes two assumptions, which we can verify with BOSS. The first assumption is that the sum of a large number of carriers with random phase can be approximated by a Gaussian random variable. This is due to the Central Limit Theorem. This is a good approximation for at least 10 carriers[21]. In our system, we use 75 carriers. The second assumption from Saleh is that the distortion power spectrum from the clipped portion of the signal is primarily in the signal band.

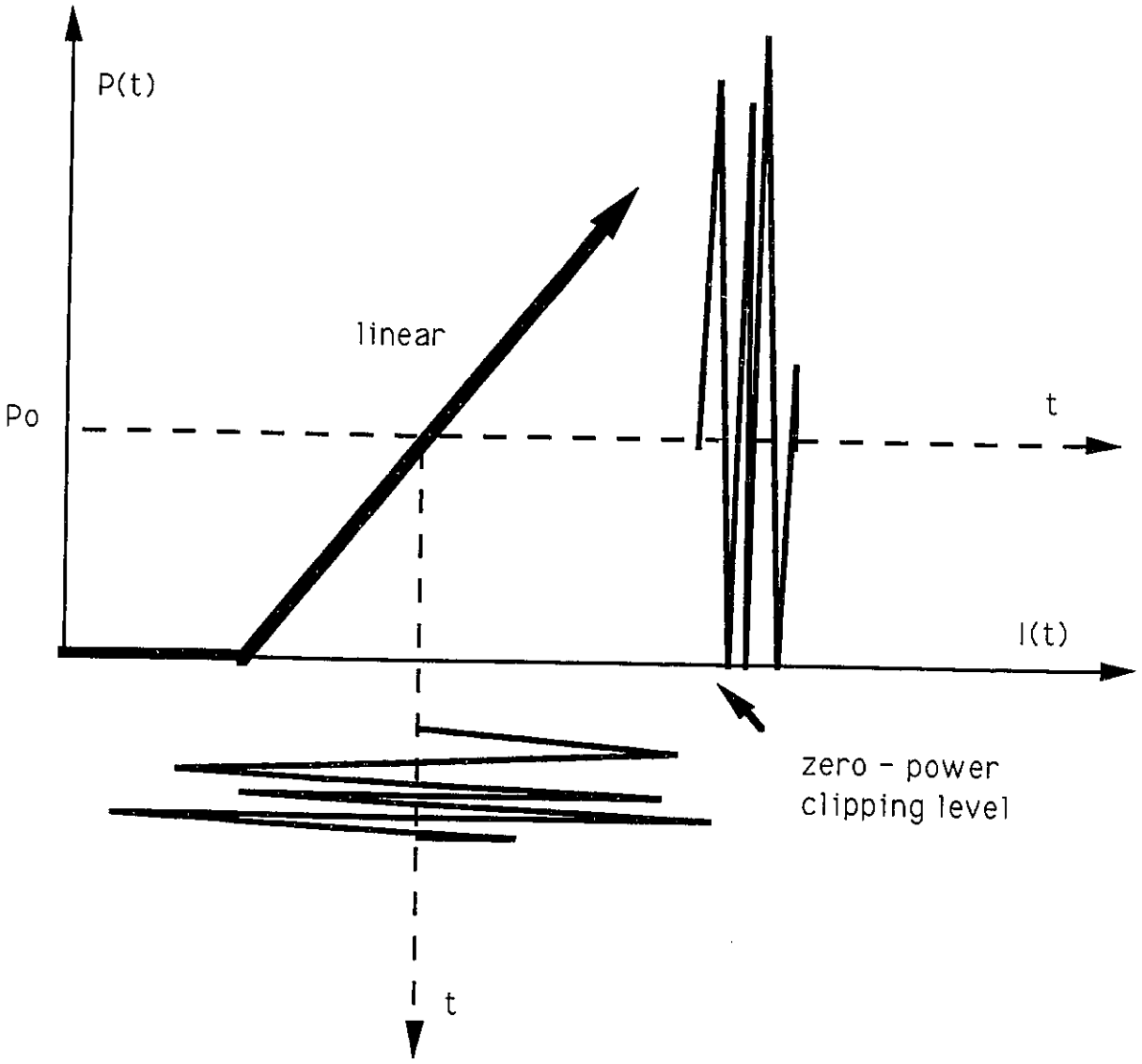

Fig. 24. Clipping due to laser threshold.[21]

It is also assumed to be flat and can therefore be considered to be evenly distributed over all the channels. We can verify this assumption with BOSS. We do so by assuming a 75 channel system with carriers spaced between 1.5GHz and 6.0GHz, which is the signal spectrum for a 4-level QAM system with a channel spacing of 60MHz. The laser bias is 75mA, threshold is 21mA, and the modulation index used is 0.091. In this case, we assume that the laser is perfectly linear, but with clipping at threshold, which is easy to model with BOSS. In Figure 25, we give the distortion spectrum, and upon averaging over a few points, we get a 12 dB CNR. A few comments are in order. From Figure 25, we see that the distorted spectrum is quite flat, and thus can be assumed to be distributed evenly over all channels. From the displayed information with respect to total average

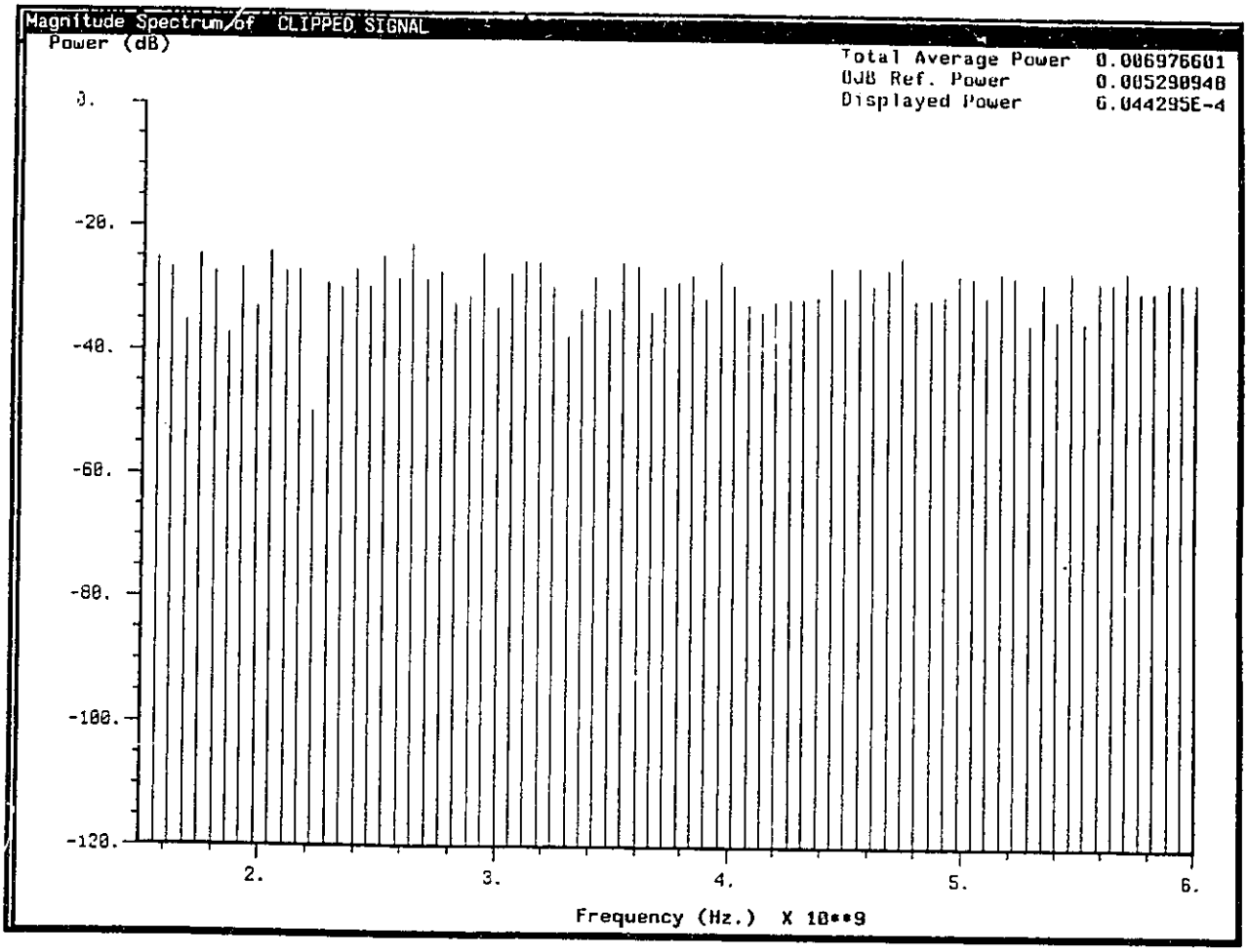

Fig. 25. Clipping Spectrum from BOSS.

power, after removing the 0dB reference power, which is due to the d.c. bias, and accounting for the double-sided spectrum, we see that 72% of the noise power is within the signal bandwidth, which is from 1.5-6.0GHz. We have therefore found Saleh's assumption that the distortion spectrum is within the signal band to be satisfactory.

We will now verify the assumption with respect to the Gaussian distribution. The power of a Gaussian random variable is obtained by applying the definition of power for a random variable, and we obtain:

$$\overline{I_{NLD}^2} \approx \frac{1}{\sqrt{2\pi\sigma_I}} \int_{-\infty}^{0} I^2 exp[-(I - I_0)^2/2\sigma_I^2] dI \tag{3.17}$$

where I_0 is the mean received current, and σ_I^2 is the variance. This integral can be approximated by[21]:

$$\overline{I_{NLD}^2} \approx \sqrt{2/\pi} I_0^2 \mu^5 exp(-1/2\mu^2) \tag{3.18}$$

where μ is the total RMS modulation index, which is given by:

$$\mu = \sqrt{Nm^2/2} \tag{3.19}$$

Per channel, this reduces to a CNR given by[21]:

$$CNR = \sqrt{\pi/2}\mu^{-3} exp(1/2\mu^2) \tag{3.20}$$

With our example, assuming an optical modulation index $m = 0.091$, thus $\mu = 0.5572$, this expression predicts a CNR of 15.6 dB, which is within 3.5 dB of the result from our simulation. This is an acceptable margin of error for this work. Recall that for the Monte Carlo computer simulations, we allow for an error margin of 3 dB as well.

3.5 Relative Intensity Noise

We will now discuss the laser relative intensity noise (RIN), which by definition is given by:

$$RIN = \frac{< \Delta S >^2}{< S >^2} \tag{3.21}$$

where $< S >$ is the average laser light intensity and $< \Delta S >$ is the mean-square intensity fluctuations of the light output. It is due to the stochastic nature of light emission and absorption. As described in Chapter 1, each term in the rate equation represents a

physical process. Recalling, I/V' is the carrier injection, N/τ_n is the spontaneous emission, $g_0 N[1-\epsilon S]S$ is the stimulated emission, $g_0 N_{om}[1-\epsilon S]S$ is the stimulated absorption, and S/τ_p is the photon radiation from the active region. Each of these physical processes are stochastic and independent, and can be modeled as shot noise. Therefore, the spectrum is taken to be white and the power level to be equal to the average of the process. Each of the processes are independent and therefore the total noise power is the sum of the power of each term. To write down the total noise power of the photon and electron number, we consider the arrows that enter and leave the reservoirs, as given in Figure 26. The cross-spectrum is the sum of processes that go from one reservoir to the other.

We can lump the random fluctuations into single terms and place them into modified rate equations, where this time N' and S' relate to electron and photon number respectively, as opposed to densities. The modified equations now become:

$$\frac{dN'(t)}{dt} = \frac{I_A}{q} - \frac{N'}{\tau_n} - g_0'(N' - N_{om}')[1-\epsilon S']S' + F_n(t) \tag{3.22}$$

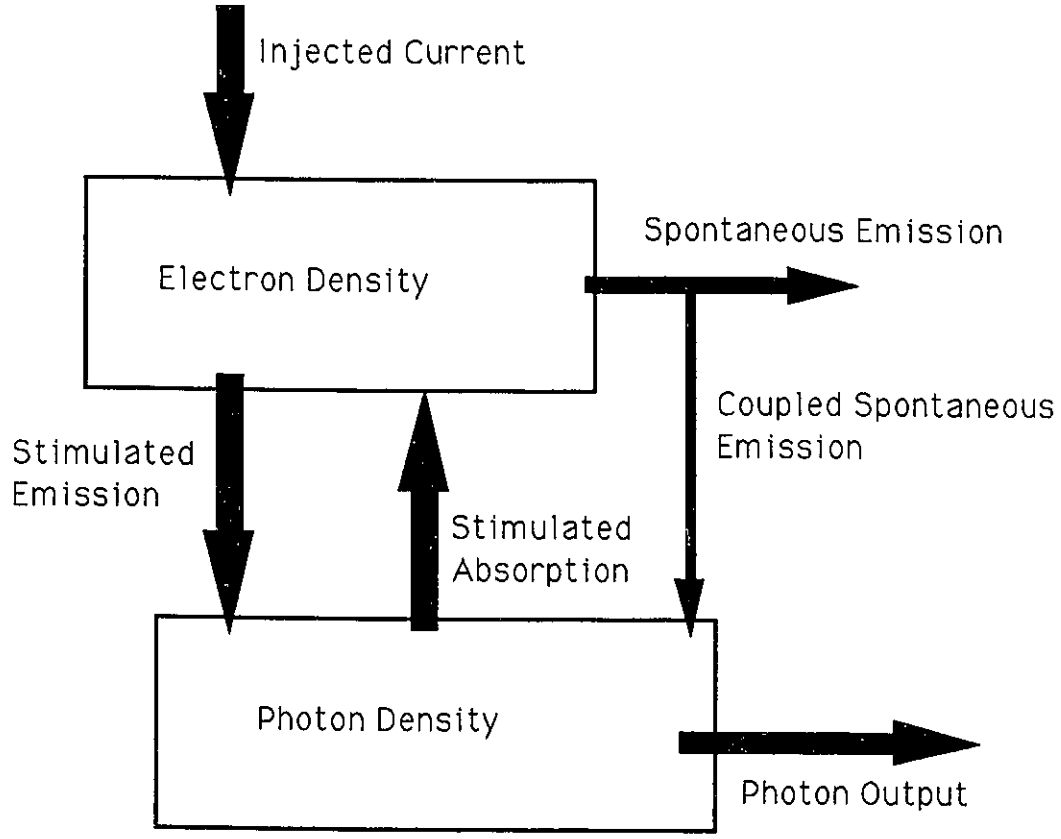

Fig. 26. Shot Noise processes that give rise to RIN.[22]

$$\frac{dS'(t)}{dt} = \Gamma g_0'(N' - N_{om}')[1 - \epsilon S']S' - \frac{S'}{\tau_p} + \Gamma\beta\frac{N'}{\tau_n} + F_s(t) \tag{3.23}$$

where all the terms have the same meaning as in the previous rate equations except that here N' is the number of carriers, S' is the number of photons, q is the electron charge, $F_n(t)$ is the carrier random fluctuations, and $F_s(t)$ is the photon random fluctuations, which are the Langevin noise terms. N_{om}' is the electron number for transparency and g_0' is the optical gain with respect to photon number.

We can write down the spectral densities as follows:

$$< F_n^2(f) >= \frac{I_A}{q} + \frac{N'}{\tau_n} + g_0'N'[1 - \epsilon S']S' + g_0'N_{om}'[1 - \epsilon S']S' \tag{3.24}$$

$$< F_s^2(f) >= \Gamma g_0'N'[1 - \epsilon S']S' + \Gamma g_0'N_{om}'[1 - \epsilon S']S' + \frac{S'}{\tau_p} + \Gamma\beta\frac{N'}{\tau_n} \tag{3.25}$$

$$< F_s(f)F_n(f) >= \Gamma g_0'N_{om}'[1 - \epsilon S']S' + \Gamma g_0'N'[1 - \epsilon S']S' + \Gamma\beta\frac{N'}{\tau_n} \tag{3.26}$$

Our interest here is to find the RIN spectrum from the modified rate equations, which is by definition given by:

$$RIN(w) = \frac{< \Delta S(\omega) >^2}{< S(\omega) >^2} \tag{3.27}$$

There are several approaches to obtain this spectrum. We will discuss two approaches: one is analytical and the other uses time domain simulation with BOSS. The analytical approach is to linearize the rate equations, as done in Section 1, and obtain the spectrum by taking the Fourier Transform[6]. We will detail this approach. This is an extension of previous work, as it includes the term ϵ, which is the gain compression. We will also give results obtained with BOSS and compare.

Applying perturbation analysis, we write down for the electron number and photon number a term for the steady state and a term that represents fluctuations about the steady state, as follows:

$$\begin{aligned} N(t) &= \overline{N'} + \Delta N \\ S(t) &= \overline{S'} + \Delta S \end{aligned} \tag{3.28}$$

Substituting these into the rate equations, we obtain the following second order set of differential equations:

$$\frac{d\Delta N}{dt} = C_1\Delta N + C_2\Delta S + F_n(t) \tag{3.29}$$

$$\frac{d\Delta S}{dt} = C_3\Delta N + C_4\Delta S + F_s(t) \tag{3.30}$$

where:

$$\begin{aligned} C_1 &= -g_0'[1-\epsilon\overline{S'}]\overline{S'} - \frac{1}{\tau_n} \\ C_2 &= -g_0'(\overline{N'} - N_{om}')[1-2\epsilon\overline{S'}] \\ C_3 &= \Gamma g_0'[1-\epsilon\overline{S'}]\overline{S'} + \Gamma\beta\frac{1}{\tau_n} \\ C_4 &= \Gamma g_0'(\overline{N'} - N_{om}')[1-2\epsilon\overline{S'}] - \frac{1}{\tau_p} \end{aligned} \tag{3.31}$$

Note that the C_i's are not the same as the A_i's derived for the linear transfer function of the laser as $\overline{N'}$ and $\overline{S'}$ refer to the steady state electron number and photon number, respectively.

We have a linear system that is driven by random noise fluctuations rather than a current as in Section 1. We can apply the Fourier Transform, and obtain the spectrum of photon fluctuations, given by:

$$\Delta S(\omega) = \frac{C_3F_c(\omega) + (j\omega - A_1)F_n(\omega)}{(C_1C_4 - C_2C_3 - \omega^2) - j\omega(C_1 + C_4)} \tag{3.32}$$

Applying the definition for RIN spectrum, one obtains the following[6]:

$$RIN(\omega) = \frac{1}{\overline{S'}^2}\frac{C_3^2 < F_c(\omega)^2 > + (\omega^2 + C_1^2) < F_n(\omega)^2 > -2C_1C_3 < F_c(\omega)F_n(\omega) >}{(C_1C_4 - C_2C_3 - \omega^2)^2 + \omega^2(C_1 + C_4)^2} \tag{3.33}$$

First, a few remarks are in order. The denominator is that of a second order system and the numerator has real zeros. We will therefore expect a similar response as for the small signal response for the laser, except that the A_i's and C_i's are not the same and there is the effect of the zeros. Indeed, we have computed the RIN spectrum for the laser at two bias points, 50mA and 75mA, as given in Figures 27 and 28. We see that in both cases there is peaking in the spectrum, but that in the case of the 75mA bias, the peaking is pushed out of the 6 GHz signal band. We again see the importance of the proper operating point for the laser in system design. In the case of the 50 mA bias, there is CNR degradation due to the peaking of the RIN at 6 GHz.

We can also use BOSS to generate the RIN spectrum. This will enhance our confidence in our understanding of the process, as well as the capabilities of BOSS and computer

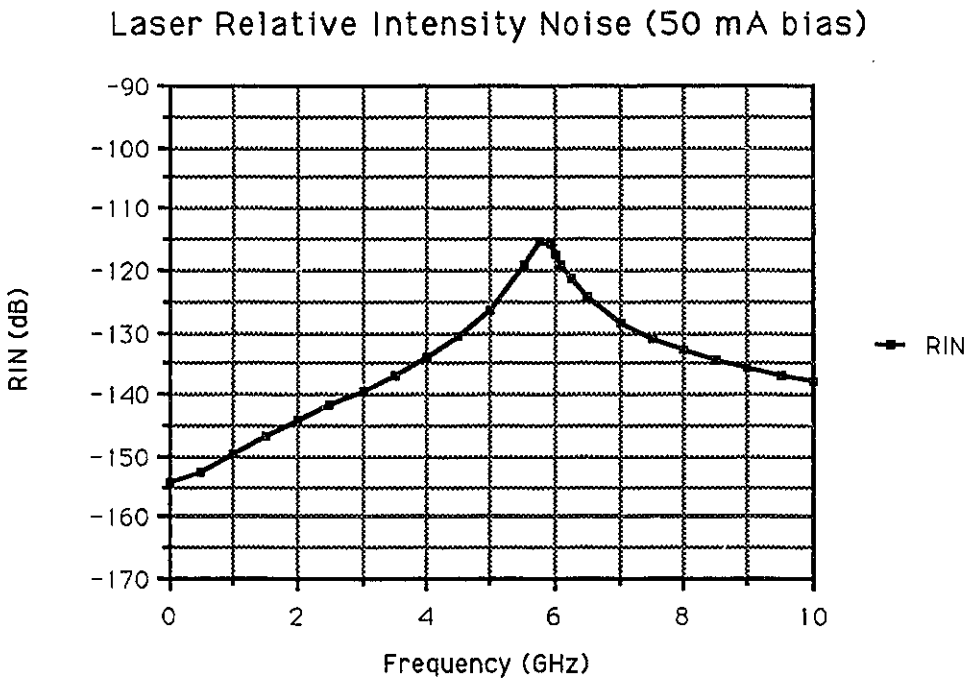

Fig. 27. Calculated RIN for 50 mA bias.

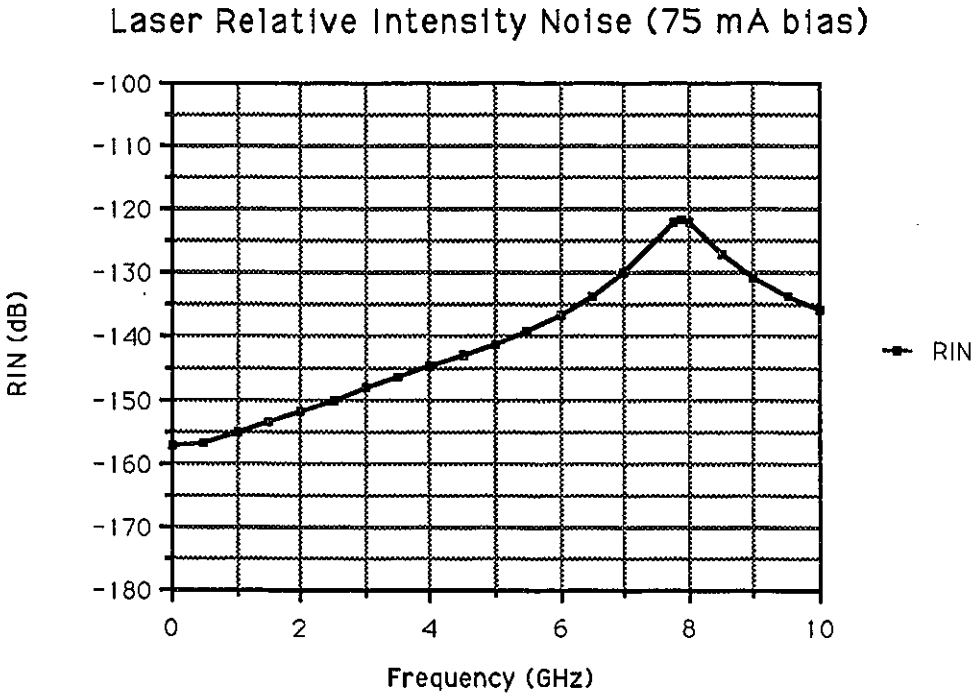

Fig. 28. Calculated RIN for 75 mA bias.

simulations in general. In this case, we use our laser module, previously developed, but we treat each term to be the mean value of a random variable, to which we add a noise component. As discussed in Chapter 2, we can use an arbitrary probability density function for each noise term. We will use a uniform distribution. The required block was constructed with BOSS, and used for each random process.

In Figures 29 and 30, we give the resultant spectrum for the usual bias currents of 50 mA and 75 mA. To get the RIN in units of $\sqrt{W}/Hz$, we must take the simulation results and add -67 dB (-70+3). The 70 dB factor is because the FFT interval is 10MHz, and the 3 dB factor is because the plot is double-sided. The resultant spectrum exhibits fluctuations, as expected. To compare our results from the simulation with our analytical results, we average over 16 runs and plot them with the previous results, as given in Figure 31. The results are very similar. The RIN level for this laser is common, if one

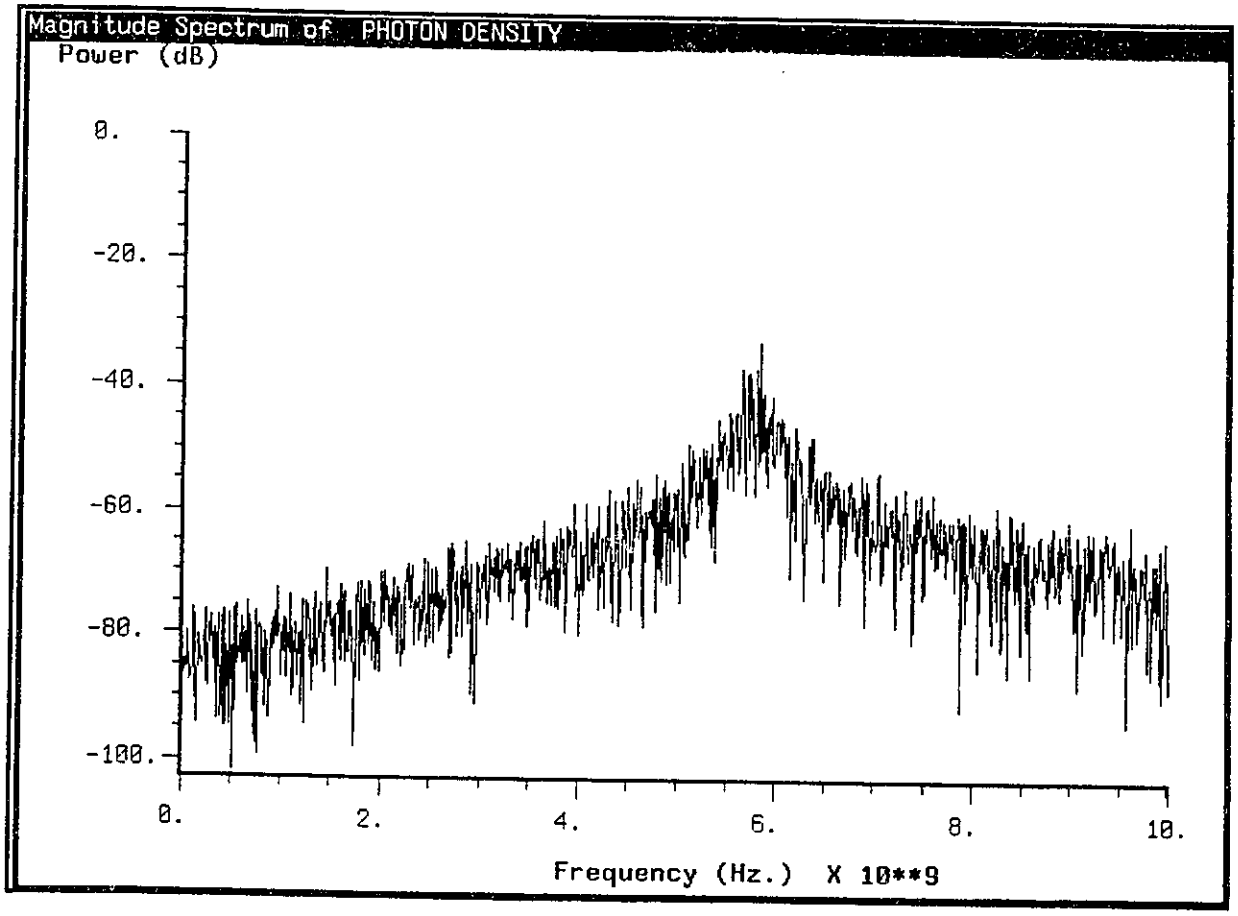

Fig. 29. RIN for 50 mA bias from BOSS.

compares with reported measurements in the literature. See, for example, Olshansky[23].

It should be pointed out that the RIN is dependent only on the bias and is independent of the received current. In system design, if the received current is high, which implies that the CNR from thermal noise and shot noise is high, RIN may be a significant noise source with respect to total system CNR.

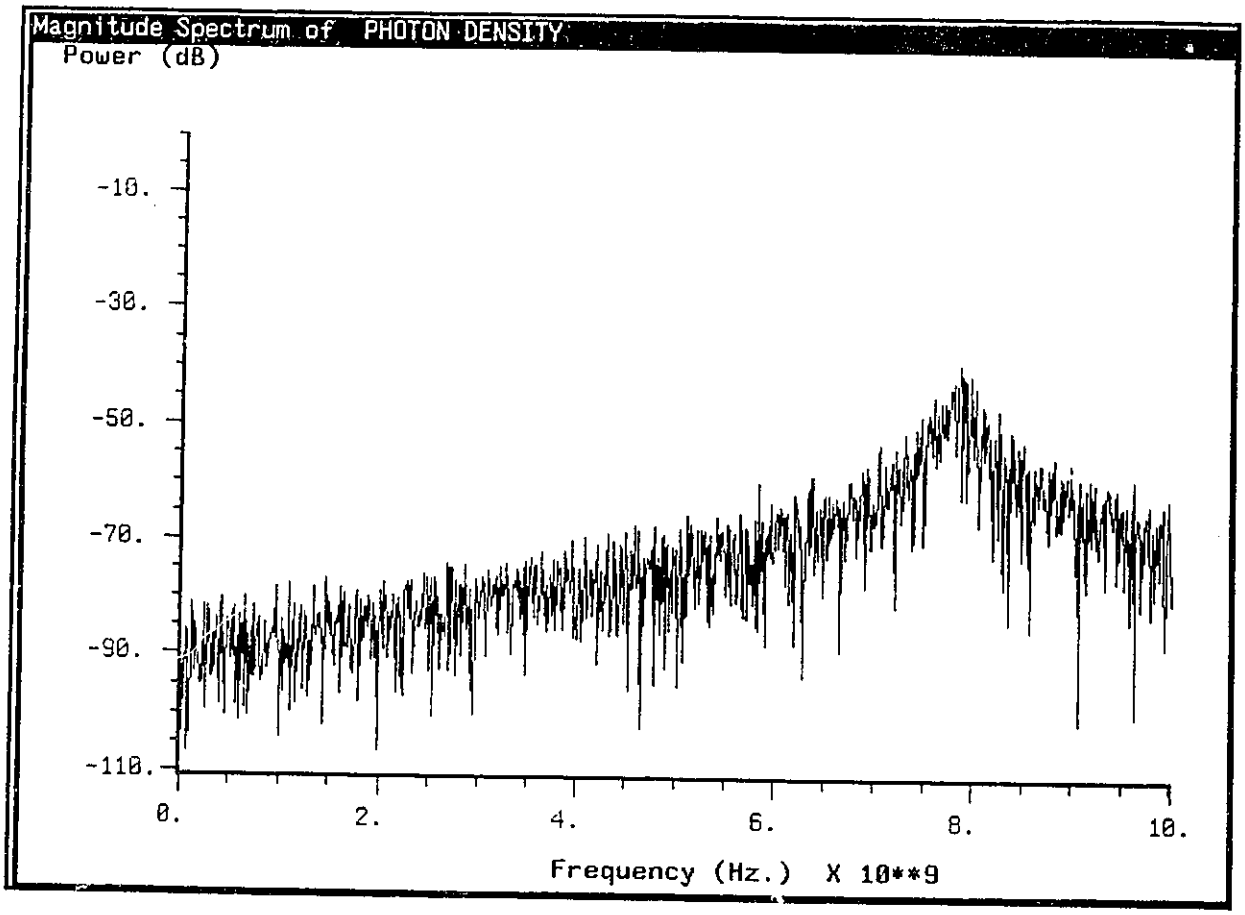

Fig. 30. RIN for 75 mA bias from BOSS

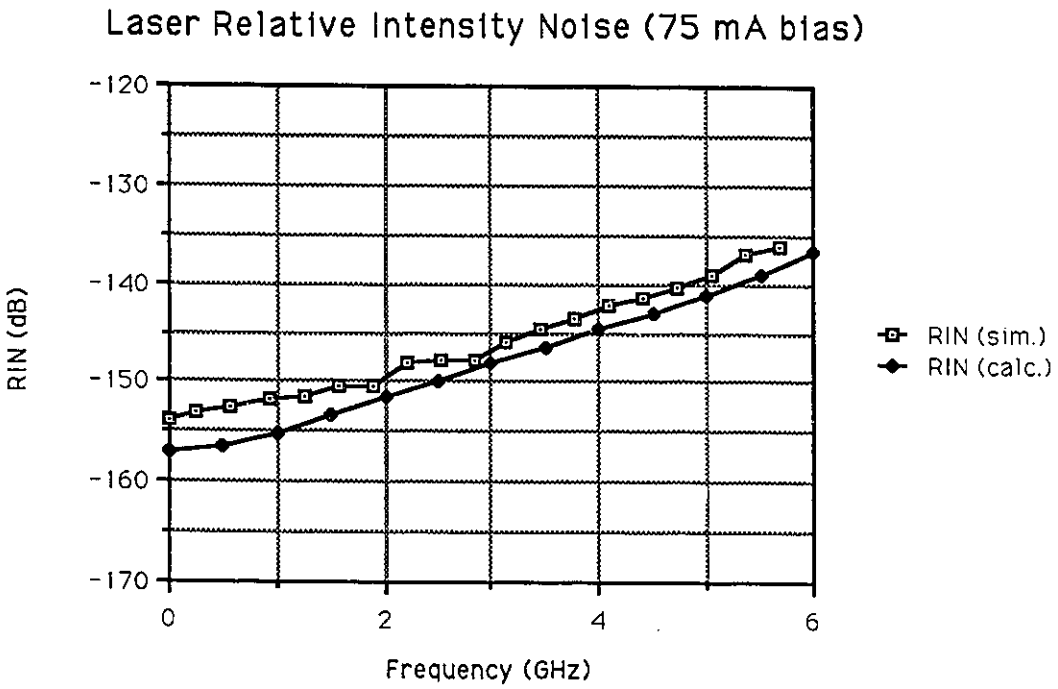

Fig. 31. Comparison of RIN levels for a 75 mA bias.

Chapter 4

Optical Amplifier

4.1 Introduction

In this chapter we will discuss modeling of the semiconductor optical amplifier. An optical amplifier essentially has the same structure as the semiconductor laser. However, the injected current is not modulated, but is kept at a constant level. The signal waveform is incident on one side of the amplifier and it is amplified as it goes through the active region of the amplifier. We can distinguish two types of semiconductor amplifiers, the Fabry-Perot (FP) amplifier and the traveling wave (TW) amplifier. The essential difference is that the FP amplifier has feedback, i.e. at the other side of the amplifier, some of the optical signal is reflected back into the medium. In the case of the TW, the sides of the amplifier are covered with anti-reflecting coating, so that upon going through the active region once, the signal is not reflected back (see Figure 32). Our primary interest is the TW amplifiers, as they have the bandwidth required for broadband applications such as subcarrier multiplexing. Bandwidths of $40 - 50nm$ are given in the literature[12]. The feedback cavity of the Fabry-Perot acts as a filter, and so we have a small usable signal spectrum. The disadvantage of the TW amplifier is the spontaneous noise sources of the amplifier, as we shall discuss later.

4.2 Nonlinear Model

In this section, we will discuss the set of equations used for the optical amplifier model. Though they appear different from the set of rate equations we had for the laser, they are essentially the same, although they have been reduced to different forms. The simplified

forms of the equations used here are as given by Saleh[8]. In the case of the wave equation, the derivation is from Maxwell's equations, and it is given in Appendix B, since it is not given in [8].

We first obtain the equation for carrier density, which we obtain from an equation of charge conservation, as follows:

$$\frac{dN(z,t)}{dt} = \frac{I}{V'} - \frac{N(z,t)}{\tau_n} - a\Gamma\frac{(N(z,t)-N_0)}{h\nu}\frac{\partial}{\partial z}\|E(z,t)\|^2 \tag{4.1}$$

where $N(z,t)$ is the carrier density, τ_n is the carrier lifetime, a is the optical gain, Γ is the optical confinement, $h\nu$ is the photon energy, and $E(z,t)$ is the optical field. This is very similar to the laser rate equations that we had previously. Here, the first term is due to the injected current, the second term is due to spontaneous emission, and the last term

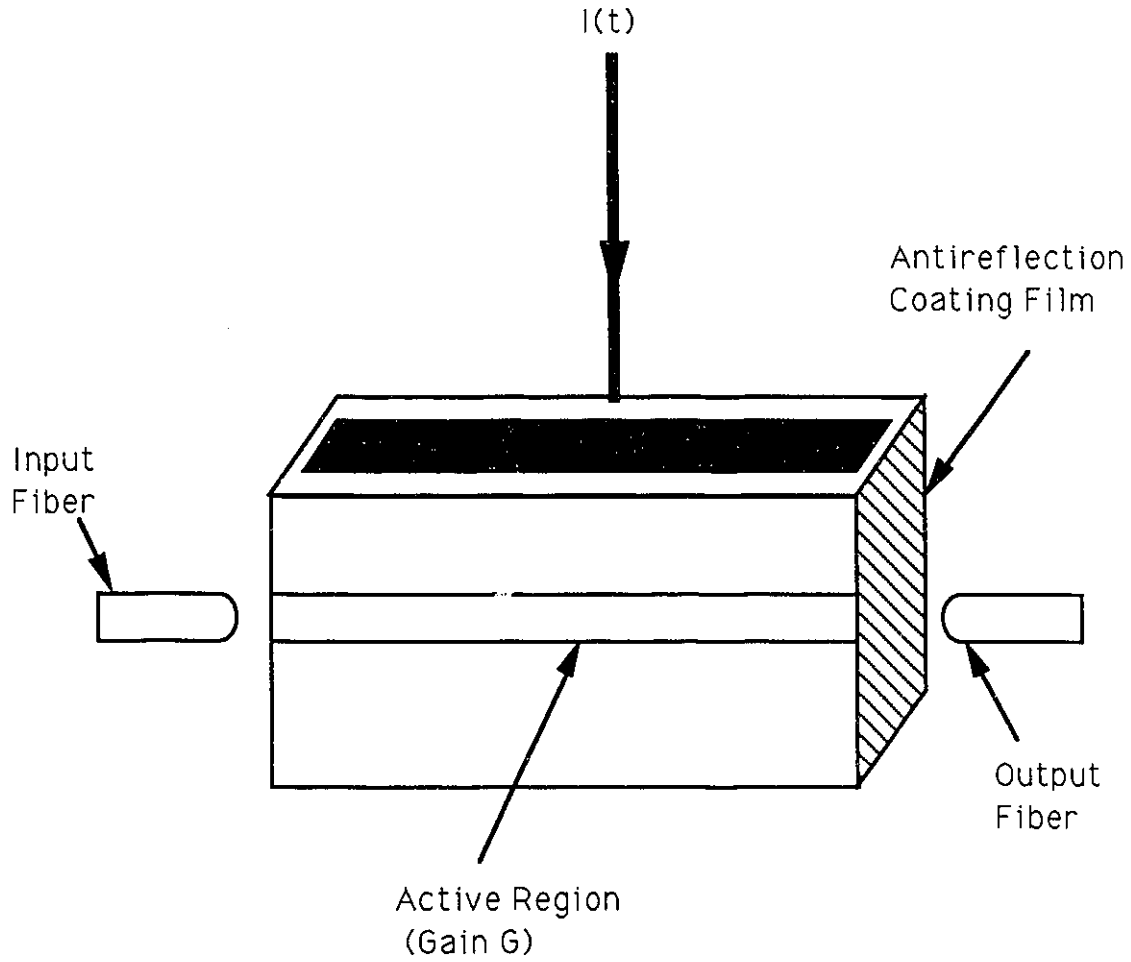

Fig. 32. The TW semiconductor optical amplifier structure.[24]

is due to stimulated emission. We will now recast this equation in terms of the incremental gain, $g(z,t) = \Gamma a[N(z,t) - N_0]$ which is the gain due to the injected current by stimulated emission.

We then obtain:

$$\tau_n \frac{\partial}{\partial t} g(z,t) = -[g(z,t) - g_0] - \frac{1}{P_{SAT}} \frac{\partial}{\partial z} \|E(z,t)\|^2 \tag{4.2}$$

where $g_0 = \Gamma a[\overline{N_0} - N_0]$ is the small-signal gain, $\overline{N_0}$ is the carrier density due to the d.c. bias. $E(z,t)$ is normalized such that $\|E(z,t)\|^2$ has units of watts. P_{SAT} is the amplifier saturation power. Integrating with respect to z, one obtains the final result[8]:

$$\left[1 + \tau_n \frac{d}{dt}\right] [G(t) - G_0] \approx -\|E_{out}(t)\|^2 / P_{sat} \tag{4.3}$$

where $G_0 = g_0 L$.

The second equation, with respect to the photon density, can be derived from Maxwell's equations (Appendix B). The resultant equation appears different from the laser rate equation for the photon density because here we use electric field instead and, once again, we use gain instead of electron density. In the case of the laser rate equation, we integrate over the whole active region and keep the time dependence[25]. In the case of the amplifier, we average over time and keep the dependence on the spatial coordinate z to obtain the so called travelling-wave equation. We also ignore spontaneous emission.

The equation reduces to the following[8]:

$$\|E_{out}(t)\| \approx \|E_{in}(t)\| exp[G(t)/2] \tag{4.4}$$

Using forward Euler integration, just as for the laser rate equations, one can solve for $G(nT + T)$ from the previous values for $G(nT)$ and $E_{out}(nT)$ with equation (4.3) and obtain directly $E_{out}(nT + T)$ from $G(nT + T)$ and $E_{in}(nT + T)$ with equation (4.4). The only required parameters are τ_n, for which we assume a typical value of $30ns$, and G_0, which is the gain from the injected current. Assuming $\|E_{out}(t)\|^2 \approx P_{sat}$, which is the usual level of operation, equation (4.3) reduces to $G_0 = G(t) + 1$ at steady state. With a 22dB amplifier gain (typical), we get $G(t) = 5.065$ from equation (4.4), which then gives us $G_0 = 6.065$. Assuming a fiber-to-amplifier and an amplifier-to-fiber coupling loss of 5dB, this gives us a fiber-to-fiber gain of 12 dB. We can therefore compensate for a 12 dB

system loss. A typical amplifier saturation power is 2 mW, and with $P_{out} \approx P_{sat}$, 0.663 mW is coupled into the fiber. Assuming that we require a $60\mu A$ received current, and that we have a detector responsivity of 0.87, we can allow another 10 dB of system loss before detection.

If the amplifier is not operated with $P_{out} \approx P_{sat}$, the amplifier will not be useful for our application. It would be useful to amplify a low-level signal, as part of a receiver structure, but upon amplification, we could not allow for further system margin before detection. In video distribution, where receiver cost is important, if the amplifier will be used, its cost must be shared by many users. Therefore, we must be able to further split the signal before detection. This is only possible if the amplifier is used around saturation.

Using the amplifier module, one can predict the distortion level for the various systems of interest. We will expand on how this is done in Chapter 5, but typical simulation results for the NTSC spectrum are given in Figure 33. We see that the CNR from nonlinear distortion is poor (about 12 dB at around 100 MHz). We can compare this result with an analytical expression given by Saleh[26]. Assuming that we are operating in the MHz range, the following expression has been derived for the CNR for the

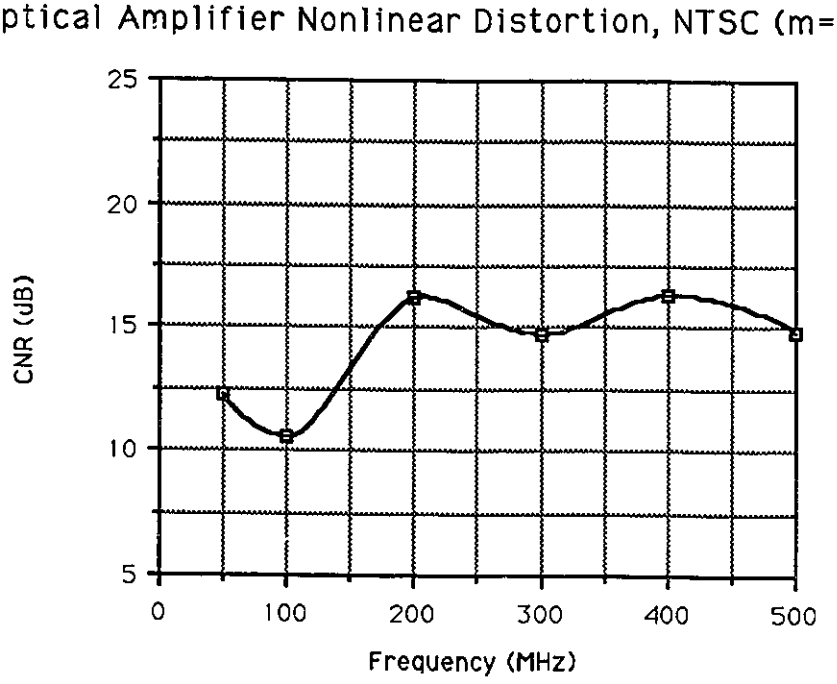

Fig. 33. The nonlinear distortion level for the optical amplifier with the NTSC spectrum.

optical amplifier:

$$CNR \leq (\frac{P_{cout}}{P_{sat}})^2 m^2 N \tag{4.5}$$

where m is the optical modulation index and N is the number of channels. Assuming a 75 channel system, with $P_{cout} \approx P_{sat}$, and with an optical modulation index $m = 0.03328$, the formula predicts a 10.8 dB CNR. This is similar to results given in Figure 33.

4.3 Amplifier Noise

We will now consider the various noise sources of the optical amplifier. Upon application of the photon master equation, the photon number appearing at the output of the amplifier is given by[27]:

$$\begin{aligned}\sigma_{out}^2 = G < n_{in} > &+(G-1)n_{sp}m_t\Delta f_1 + 2G(G-1)n_{sp}\chi < n_{in} > \\ &+(G-1)^2 n_{sp}^2 m_t \Delta f_2 + G^2(< n_{in}^2 > - < n_{in} >^2 - < n_{in} >)\end{aligned} \tag{4.6}$$

where σ_{out}^2 is the variance in the photon number per second at the amplifier, $< n_{in} >$ is the mean value of the input photon number per second incident on the amplifier, n_{sp} is the population inversion parameter of the amplifier medium, χ is the excess noise coefficient for the signal-spontaneous beat noise, Δf_1 and Δf_2 are the equivalent noise bandwidth for the spontaneous emission shot noise and the spontaneous-spontaneous beat noise, respectively, and m_t is the effective mode number of transverse modes. The five terms of the equation refer to, respectively, amplified shot noise, spontaneous emission shot noise,signal-spontaneous beat noise,spontaneous-spontaneous beat noise, and signal excess noise.

It should be noted that the beat noise terms are predominant over the shot noise terms because they are G times larger. The spontaneous-spontaneous noise spectrum is spread over a very large band, whereas the signal-spontaneous noise spectrum is in the signal band. Therefore, for CNR calculations, only the signal-spontaneous noise needs to be considered. Defining the noise figure F_o for the optical amplifier as the degradation in S/N ratio before and after amplification, and assuming only signal-spontaneous noise, the noise figure of the amplifier can be reduced to the following[27]:

$$F_o = 2n_{sp}\chi \tag{4.7}$$

Typically, n_{sp}=2.5 dB, χ=.5dB, giving a noise figure of 6 dB. We can relate the noise figure of the amplifier to the detected CNR with the following expression given by Way[12]:

$$CNR = \frac{m^2 I_0 C_1}{4e\eta_D F_o} \tag{4.8}$$

where m is the modulation index, I_0 is the received current, C_1 is the coupling efficiency from the amplifier to the fiber, e is the electron charge, η_D is the product of the p.i.n. diode quantum efficiency and the coupling efficiency from the single mode fiber into the diode. We will use this formula in Chapter 5.

Chapter 5

System Design

5.1 CNR Requirement

In system design, we must have a common basis to compare system performance. For video distribution systems, the measuring stick is the signal-to-noise ratio (SNR) of the modulated video signal. We will consider two levels of SNR, a 40 dB SNR which is referred to as CATV quality, and a 56 dB SNR which is referred to as studio quality reception. We will apply the CATV SNR requirement to the AM-VSB system and the studio quality SNR requirement to the FM and digital systems. This is commonly done in the literature[28]. With the additional cost of FM and digital systems, better performance is expected. In system design, one does not deal with modulated video signals, but with an unmodulated carrier. This makes analytical and simulation work practically feasible and instead of considering SNR, our measuring stick becomes the carrier-to-noise ratio (CNR). For each modulation scheme, one must meet a particular CNR in order to meet the same SNR. Essentially, for AM-VSB, the carrier is directly modulated, so that the SNR is the same as the CNR. For FM, using a high modulation index, i.e. a large frequency deviation, it is possible to get a substantial improvement in SNR over the input CNR. As given by Way, a 39.5 dB[28] improvement is possible. Assuming studio quality reception, a 56 dB SNR is required, and therefore a 16.5 dB CNR is required at the receiver. The cost associated with high index FM is that it requires a large signal bandwidth. In our work, we will assume a 40 MHz channel spacing.

An alternative approach, which also results in an improvement in CNR requirements is the use of digital QAM modulation schemes[11]. As for any digital transmission system,

we must establish a bit-error-rate (BER) requirement. For an equivalent studio quality SNR reception, we require a BER of $1E-9$[23]. We will consider a 4-level QAM signal constellation. Assuming additive white Gaussian noise, and using available charts for the P(e) performance of M-ary QAM systems[29], we obtain a 15.6 dB CNR requirement for the 4-level QAM to achieve a P(e) of $1E-9$. Going to a large M, we have more stringent CNR requirements, but we gain by having a reduced signal bandwidth. With a 90 Mb/s digital video signal, we assume a nominal RF modulation bandwidth of 120MHz. For an M-level system, the bandwidth reduction is by the factor $log_2 M$. Thus for M=4, the bandwidth is 60MHz. Note that the key assumption made here has been that all interferences, including nonlinear distortion, are independent and Gaussian.

We will also consider HDTV signaling. In particular, we shall consider the format proposed by Zenith. It uses the same signal spectrum as NTSC AM-VSB (i.e. 6MHz per channel), but has been designed so that it can be transmitted in today's unusable portions of the VHF and UHF spectrum, which are referred to as taboo channels. Taboo channels are not used with AM-VSB because the distortion from other channels is too severe. Conversely, if signals were placed in the taboo channels, they would interfere with signals in the allowed channels. Therefore, we must maintain the 6MHz bandwidth and reduce the CNR requirements significantly. From a report compiled by Sablatash[30], a 27 dB CNR improvement is claimed. The CNR requirement becomes 18 dB . This is based on a HDTV SNR requirement of 45 dB.

The improvement of 27 dB is an estimated lower bound. It is based on a 27 dB improvement of interference of NTSC into HDTV (which arises when we use HDTV in taboo channels and NTSC in the allowed channels). In the case of HDTV into HDTV, which is our current interest, the CNR improvement would be even better since HDTV gives rise to less intermodulation distortion. This is because in the Zenith scheme, low frequencies are removed and digitized, which reduces the peak power. We will now consider the estimated 27 dB improvement. It is due to the many stages of signal processing. They are: the use of precise offset: a 6 dB gain; temporal filtering: a 10 dB gain; companding: a 3 dB gain; time dispersion: a 5 dB gain; using the carrier at the center of the band: a 3 dB gain; giving a total gain of 27 dB. We will briefly describe each processing steps, as follows. In precise offset, a 1Hz accuracy is used to offset the carriers so that the inter-

Modulation	Channel Spacing	CNR Requirements	Bandwidth
AM-VSB	6 MHz	40 dB	50-500 MHz
FM	40 MHz	16.5 dB	3.0-6.0 GHz
4-level QAM	60 MHz	15.6 dB	1.5-6.0 GHz
HDTV (Zenith)	6 MHz	18 dB	50-500 MHz

Table 5.1: System Requirement

modulation products fall where they are least harmful. Temporal pre-emphasis results in a signal where there are pulses only from moving edges. After temporal filtering, peaks do remain, but they can then be further reduced by amplitude companding. This is followed by a chirp filter that stretches out the signal in time. In doing so, the amplitude of the signal is decreased as it is stretched over time. The net effect of all this is to whiten the signal and reduce the peak signal power.

We will now discuss the signal spectrum used with each system. It is generally advantageous to use the lower portion of the laser spectrum since the intermodulation distortion spectrum, as well as the RIN spectrum is lowest under 500MHz. With AM-VSB and HDTV (Zenith) we can space 75 channels in the NTSC 50-500MHz spectrum. For the other systems, that require greater channel spacing, one attempts to confine the channels to one octave, to avoid second order distortion. For the FM system, we can confine the channels to 3-6 GHz, assuming again 75 video channels. For the 4-level QAM system we must contend with second order distortion, as the spectrum is from 1.5 to 6.0 GHz. We summarized the system parameters in Table 5.1. In all these systems, we must consider receiver complexity. In this regard, the AM-VSB requires no conversion at the receiver. The FM system requires FM/AM conversion. The digital schemes require A/D convertors. The HDTV (Zenith) not only digitizes the low frequency part of the video signal, but also uses various signal processing techniques.

5.2 CNR Calculation

We will now calculate the total system CNR for each of the proposed systems. We will proceed by writing down the CNR of each source of degradation. We will assume that these degradations are independent and therefore, we can find the total distortion by adding the individual components. The CNR from the laser distortion is obtained

directly from the simulations, which we shall consider last.

The arrival of the optical signal is stochastic, which we model as shot noise. It is similar to laser RIN. It is a fundamental limit on system performance. Being proportional to the signal, it cannot be eliminated. Writing down the CNR[9]:

$$CNR_{shot-noise} = \frac{I_0 m^2}{4eB} \tag{5.1}$$

where I_0 is the received current and m is the optical modulation index, e is the electron charge and B is the equivalent noise bandwidth.

At the preamplifier, there is thermal noise due to the preamplifier resistor, for which we get the following expression for CNR[9]:

$$CNR_{thermal-noise} = \frac{I_0^2 m^2}{2n^2 B} \tag{5.2}$$

where n is the effective noise current, for which we shall assume a typical value of $10pA/\sqrt{Hz}$.

For laser RIN, the CNR can be shown to be[9]:

$$CNR_{RIN} = \frac{\frac{1}{2}m^2}{RINB} \tag{5.3}$$

Note that in all these expressions, the CNR is proportional to the square of the optical modulation m. The CNR for the shot noise and thermal noise also depend on I_0, the received photocurrent, but for RIN, it does not. In cases where I_0 is large, i.e. with little signal attenuation, RIN may be the dominant noise source. In our particular work, RIN is not very significant because we assume a 12 dB system margin. Also, thermal noise is more severe than shot noise, due to the value of n assumed. In [31], Figure 5, Darcie illustrates graphically the dependence of RIN, shot noise and thermal noise on system margin. The system design procedure becomes one of finding the optimal m such that the thermal noise and intermodulation distortion combine to give a minimum total CNR. The equivalent noise bandwidth, B, is smaller than the channel spacing, because we assume the use of realizable filters that have some roll-off. The equivalent bandwidths assumed are 4MHz for AM-VSB, 25MHz for 4-level QAM and 36MHz for FM.

5.3 Nonlinear Distortion

As we have seen in Chapter 2, the intermodulation distortion level in a multi-channel system is dependent on the phases of all the carriers. In a video transmission system, we assume that the phases of the carriers are independent. The intermodulation distortion level is therefore random. We therefore use Monte Carlo computer simulation, as proposed by Medhurst[1]. We have carried out the simulations by removing 4 adjacent carriers and averaging over 2 simulation runs, in which case we are accurate within 3 dB, 94 times out of 100.

Running these simulations are costly. However, we will show that the distortion level from a laser is only dependent on the signal level. Therefore, once we have results for a laser with particular channel spacing, we need not repeat the work to consider a system with a different number of channels. The distortion level is independent of the number of channels because, with an increase of N, the number of distortion components increase, but the power of each component decreases by the same factor. For example the number of second order products increases with the square of N, but the power of each component is reduced by the square of N. Likewise, the number of third order intermodulation components increases with the cube of N, but the power of each component is reduced by the same factor[28]. The total signal power of N channels is given as follows:

$$SignalPower = \frac{1}{2}(mI_{d.c.})^2 NR \tag{5.4}$$

where m is the optical modulation index and $I_{d.c.}$ is the injected current bias and R is taken to be 50Ω. Therefore, to obtain the same distortion level, we can trade N, the number of channels with m, the optical modulation index.

Medhurst's procedure was followed to obtain the distortion level for the four system configurations under consideration. 71 carriers where used. Each simulation was run at two signal levels: at 11dBm and at 1dBm. These levels were chosen such that little clipping occurs. In this case, we expect to have essentially a second or third order system. Clipping is then treated separately. In Figures 34 and 35 we present the results for the NTSC AM-VSB and FM systems. As expected, the AM-VSB system is essentially a second order system, whereas, the FM system, where the signal band is within an octave, is a third order system. The distortion level is frequency dependent, as was the case

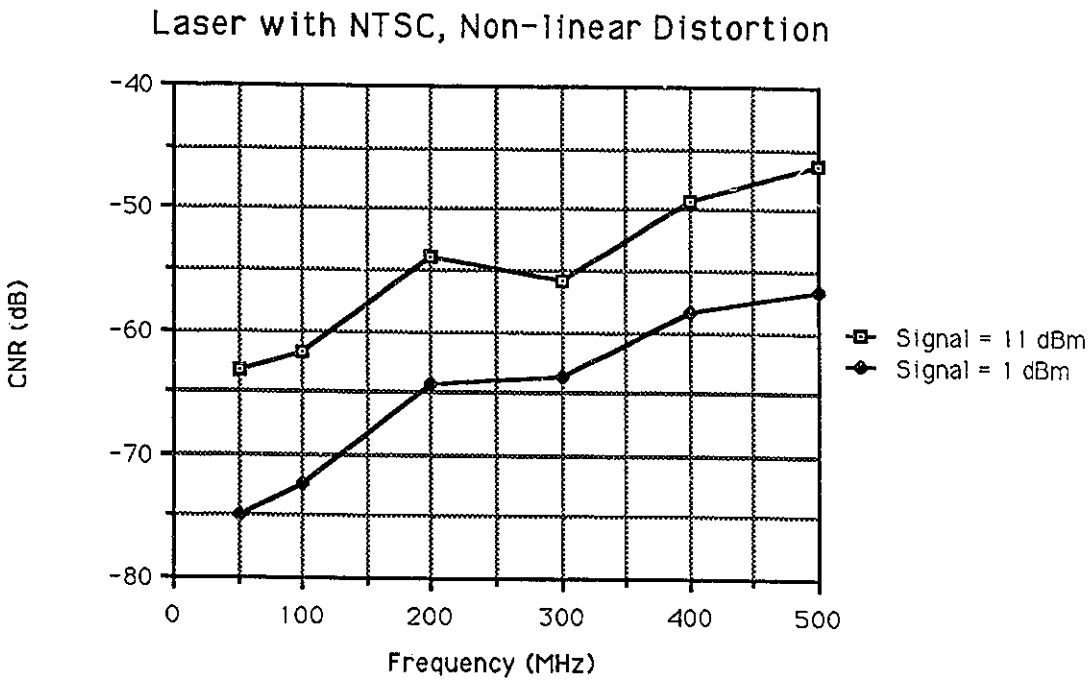

Fig. 34. Simulation Results averaged over 8 points, for NTSC.

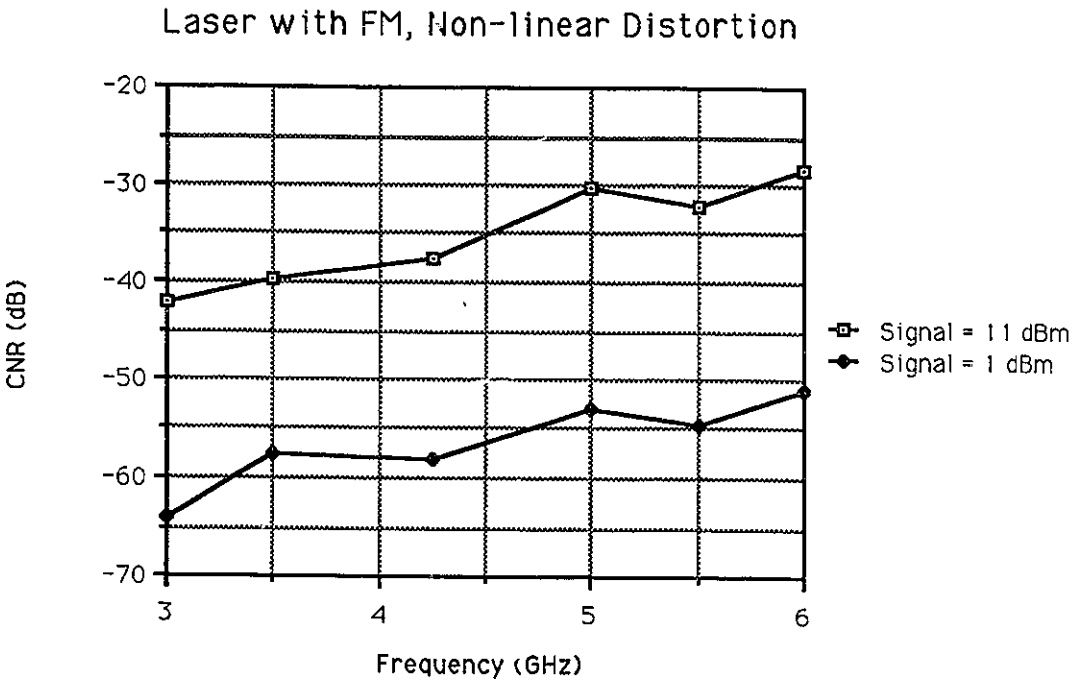

Fig. 35. Simulation Results averaged over 8 points, for FM.

for RIN. However, for the sake of system design, we consider the average distortion level over the spectrum. If, for example, the total CNR is frequency dependent, then some kind of pre-emphasis can be used on the transmitted signal to keep a constant CNR spectrum at the receiver.

5.4 System Design

System design proceeds as follows. First we must ensure that we have sufficient bandwidth for our signal spectrum, which, in our case is 6GHz. For the fiber and the detector, such bandwidth is readily available. Lasers with a 6 GHz bandwidth are also available, but it does represent more of a constraint. In Chapter 3 we have shown that with a 75 mA bias, our laser has the required bandwidth. In setting our bias, we must also consider the intermodulation distortion spectrum and the RIN spectrum. With our laser biased at 75 mA, as we have seen in Chapter 3, RIN peaks at roughly 8 GHz and intermodulation at about 8 GHz. For the 50 mA bias, we would have severe CNR degradation, since RIN peaks at 5.75GHz and the intermodulation distortion at 3 GHz. Also, with a higher bias, we are transmitting more power, so that, for the same optical modulation index, we receive a larger photocurrent. Therefore a 75 mA bias is used.

We then consider which optical modulation index to use. To find the optimal modulation index, we must compute the total CNR for various m and find the one where the CNR is maximal. This is the optimal m. One helpful tool is to use the so-called Λ-curve, where one plots the CNR from the different sources of degradation against optical modulation index. The Λ-shape results because noise term CNRs increase with increasing m and nonlinear distortion term CNRs decrease with increasing m. We can determine the range of m that should be considered when searching for the optimal m. The minimal m that should be considered is determined by including only noise terms in meeting the CNR requirement. The maximum value of m that should be considered is determined by including only nonlinear distortion terms in meeting the CNR requirement. The optimal m, if it exists, will be in this range.

We will now outline the set of parameters and assumptions made in our CNR calculations. We assume a 75 channel system. We assume that the laser outputs 3.46 mW of

optical power and with 5 dB coupling loss, 1.09 mW is coupled into the fiber. The system margin for fiber attenuation, splicing, and splitting, we assume to be 12 dB, to give a received photo current (assuming a detector responsivity of 0.87 A/W) of $60\mu A$.

The optical amplifier can be used to further extend the system margin. This applies only to systems operating in the microwave range. As we saw in Chapter 4, for the NTSC spectrum, the distortion is too high. We operate the amplifier such that the average output optical signal is 2 mW. Assuming a 5 dB fiber-to-amplifier and 5 dB amplifier-to-fiber coupling loss, and a 22 dB overall gain, we have a 12 dB fiber-to-fiber gain. We can therefore compensate for the 12 dB system loss from the laser to the amplifier with the 12 dB fiber-to-fiber gain. In addition, we can allow for a further 2 dB system margin before amplification. At the output of the amplifier, we couple 0.63 mW into the fiber, and again assuming a detector responsivity of 0.87 A/W we can allow for a further 10 dB system margin and still receive a photo-current of $60\mu A$. See Figure 36 for a schematic of the complete system. In Figure 37 we show the signal and noise levels for the FM system with an optical modulation index of $m = 0.0089$.

We have applied the same procedure to the optical amplifier as we did for the laser to determine the distortion level for each of the systems. To determine the total CNR, we must also consider the noise from the amplifier. Recall the following formula from Chapter 4[12]:

$$CNR_{sig.-sp.} = \frac{m^2 I_0 C_1}{4e\eta_D F_o} \tag{5.5}$$

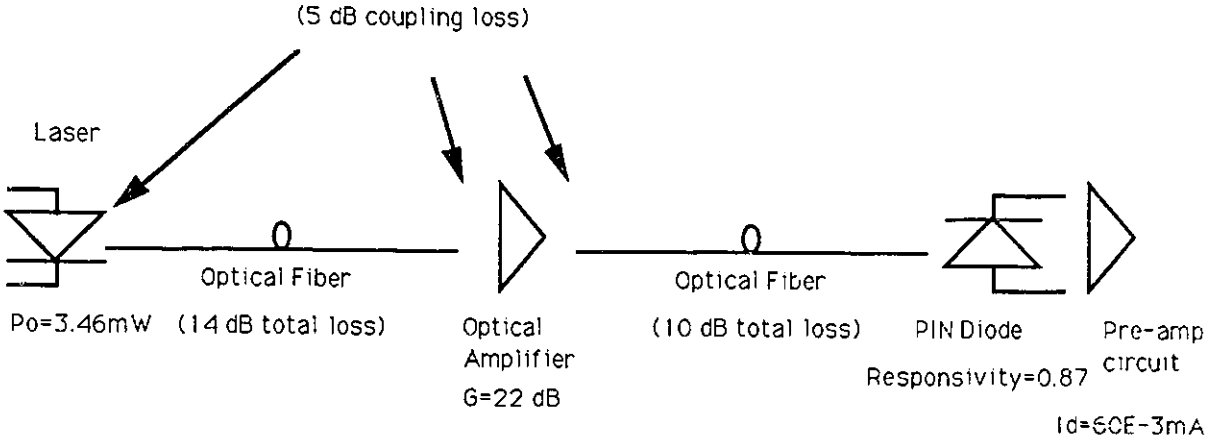

Fig. 36. Assumptions for CNR calculations

where m is the optical modulation index, I_0 is the received current, C_1 is the coupling efficiency which we take to be 5dB, η_D is the product of the p.i.n. diode quantum efficiency and the coupling efficiency from the single mode fiber into the diode, which we take to be 0.7. F_o, the noise figure for the amplifier, we take to be 6 dB.

We present in Figures 38, 41, 42, and 43 the Λ-curves for the four systems under consideration. The digital QAM and FM systems include an optical amplifier in the system configuration, giving a total system margin of 24 dB margin. With HDTV (Zenith) we cannot use an optical amplifier, but we allow a system margin of 22 dB, as we have assumed a received photo-current of only 6 μA (10 dB down from the other systems).

Clearly, from Figure 38, the AM-VSB does not meet the 40 dB CNR requirement for a 75 channel system, regardless of the setting of the optical modulation index. In Figure 39, we give the Λ-curve for AM-VSB with 20 channels, which illustrates that by reducing the number of channels we can achieve the required CNR. In Figure 40 we give the Λ-curve for AM-VSB, where we have reduced the system margin to 6.5 dB. This result has been previously reported in the literature[32]. One possible solution suggested[32] is to use the same quality of lasers and to use erbium-doped fiber amplifiers, which can increase the

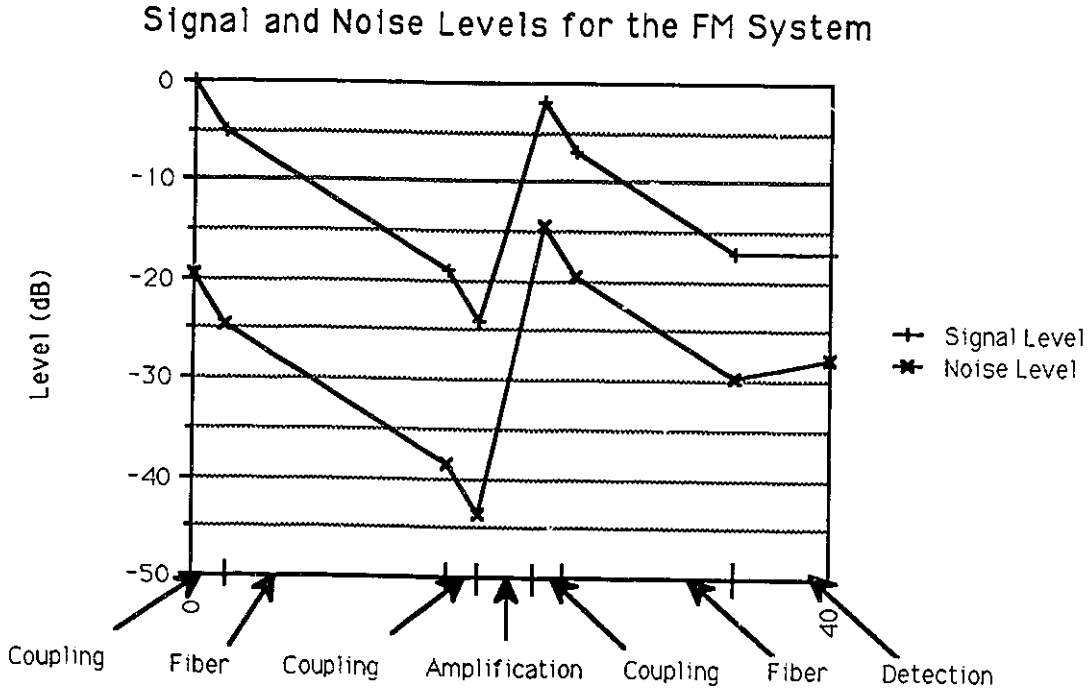

Fig. 37. Signal and noise level for FM system, $m = 0.0089$.

System	Channels	Margin	CNR Req.	CNR Ach .	m	Ampl.
AM-VSB (BOSS)	75	12 dB	40 dB	36.3 dB	0.047	0
AM-VSB (BOSS)	75	6.5 dB	40 dB	38.8 dB	0.033	0
AM-VSB (BOSS)	20	12 dB	40 dB	39.6 dB	0.075	0
AM-VSB (Darcie[9])	42	13 dB	40 dB	42 dB	0.02	0
FM (BOSS)	75	24 dB	16.5 dB	15 dB	0.018	1
FM (Olshansky[10])	60	12 dB	16.5 dB	16.5 dB	0.02	0
FM (Way[12])	90	22 dB	16.5 dB	16.5 dB	0.03	1
4-level QAM (BOSS)	75	24 dB	15.6 dB	16.48 dB	0.045	1
HDTV-Zenith (BOSS)	75	22 dB	18 dB	17.6 dB	0.082	0

Table 5.2: Summary

system margin to 15 dB, without introducing nonlinear distortion. This suggests how we can meet the required CNR and still transmit 75 channels.

Both the FM system and 4-level QAM system meet the system requirements. In fact, the FM system barely meets the 16.5 db requirement, with a 15 dB CNR at an optimal modulation index of 0.018. The most significant degradation sources are the signal-spontaneous beat noise and the laser nonlinearity. The 4-level QAM gives the most margin over the required CNR of 15.6 dB, with a CNR of 16.48 dB at $m = 0.045$. In this case, clipping and signal-spontaneous beat noise are the most severe sources of degradation. In either case, amplifier distortion is not very significant. It should be noted that going to a higher level QAM would not result in better system performance, since we would be trading readily available bandwidth for a higher CNR requirement.

For HDTV, at an optimal modulation index of 0.082, the CNR is 17.55 dB, just barely reaching the required CNR of 18 dB. The significant contributions are thermal noise and clipping. Note that this is achieved without the added cost of the optical amplifiers. Of course, the hidden cost is in all the processing circuitry required at the end terminal.

In conclusion, FM is the best system solution, as it requires a simple FM/AM conversion and we can use optical amplifiers. If digital signaling is required, we should use a signal constellation with the fewest number of levels. The proposal from Zenith, which uses extensive signal processing so that it can be used in the present taboo channels can offer significant system margin without optical amplifiers. If the AM-VSB NTSC scheme must be used, we can transmit fewer channels or operate with a smaller system margin.

Bandwidth Utilization	50-500 MHz
Channel Spacing	6 MHz
Noise Equivalent Bandwidth	4 MHz
Number of Channels	75
CNR Requirement	40 dB
CNR Achieved	36.3 dB
Optical Modulation Index	0.047
System Margin	12 dB
Number of Amplifier Stages	0

Table 5.3: System Parameters for NTSC

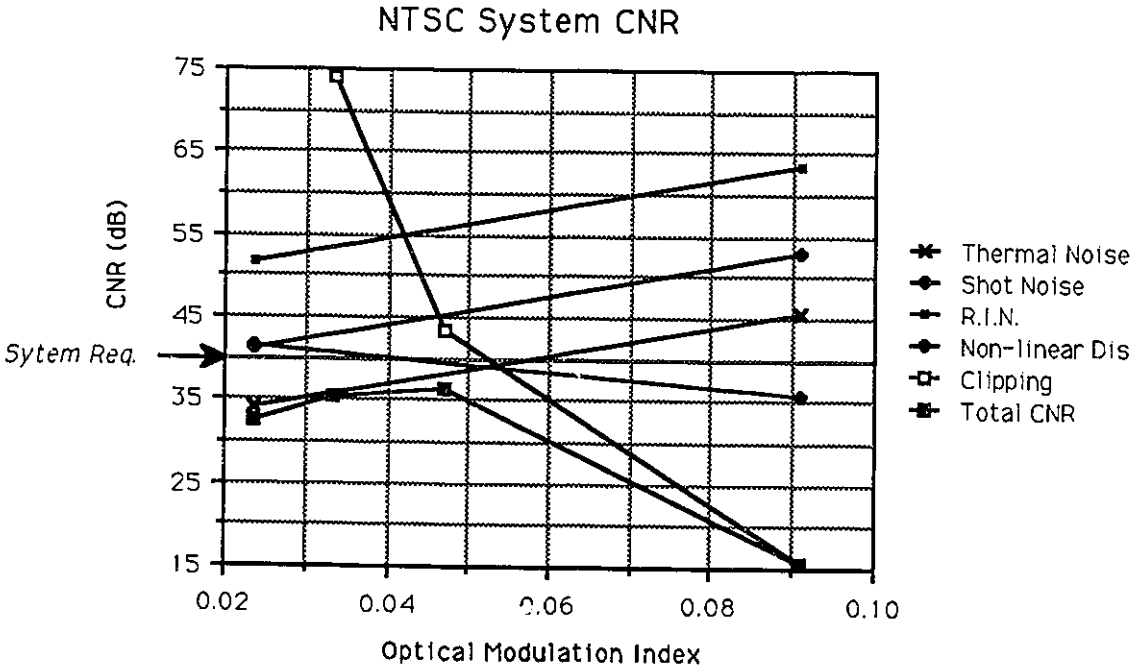

Fig. 38. Λ-curve for AM-VSB system

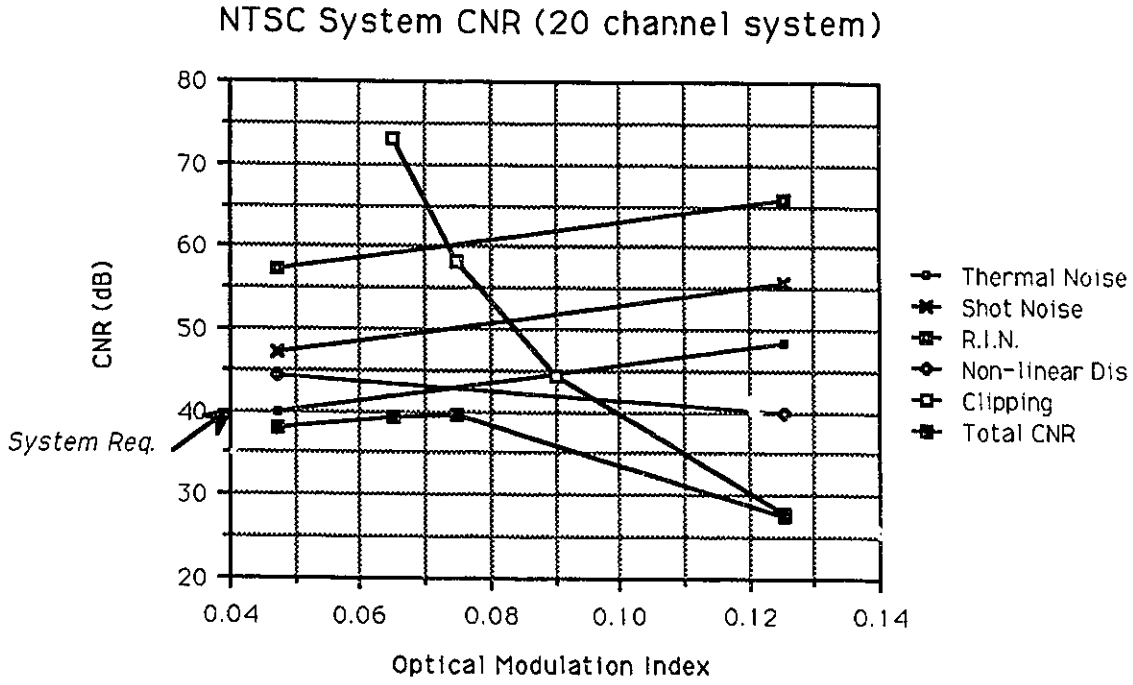

Fig. 39. Λ-curve for a 20 channel system, NTSC.

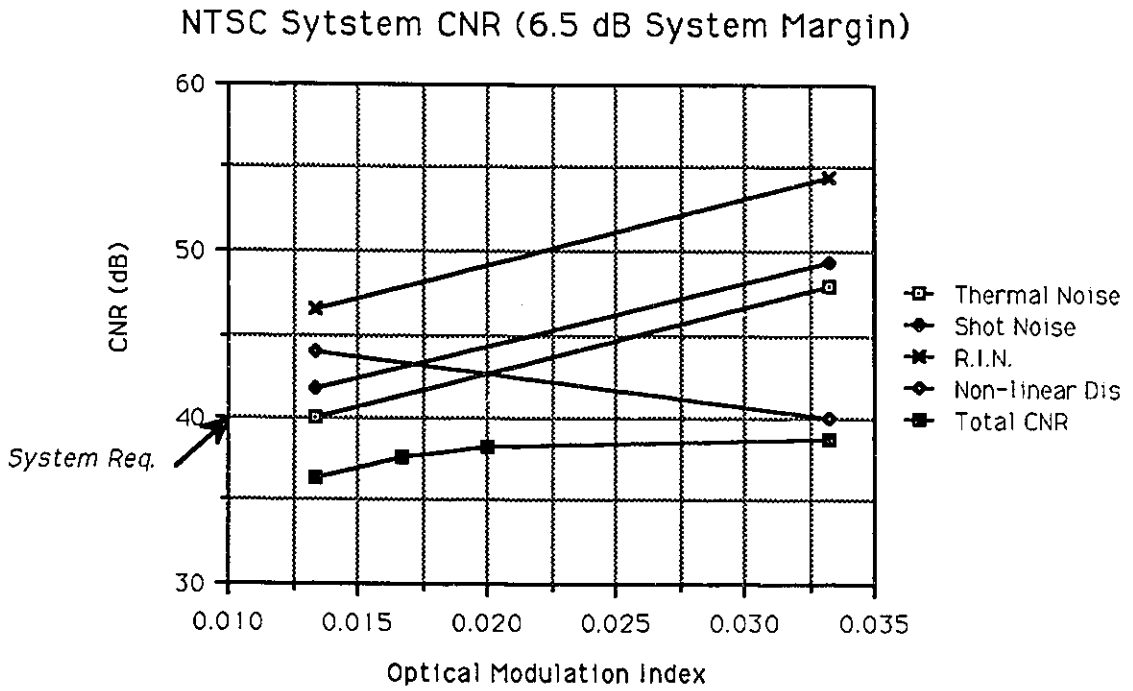

Fig. 40. Λ-curve for a 6.5 dB system margin, NTSC.

Bandwidth Utilization	3.0-6.0 GHz
Channel Spacing	40 MHz
Noise Equivalent Bandwidth	36 MHz
Number of Channels	75
CNR Requirement	16.5 dB
CNR Achieved	15 dB
Optical Modulation Index	0.018
System Margin	24 dB
Number of Amplifier Stages	1

Table 5.4: System Parameters for FM

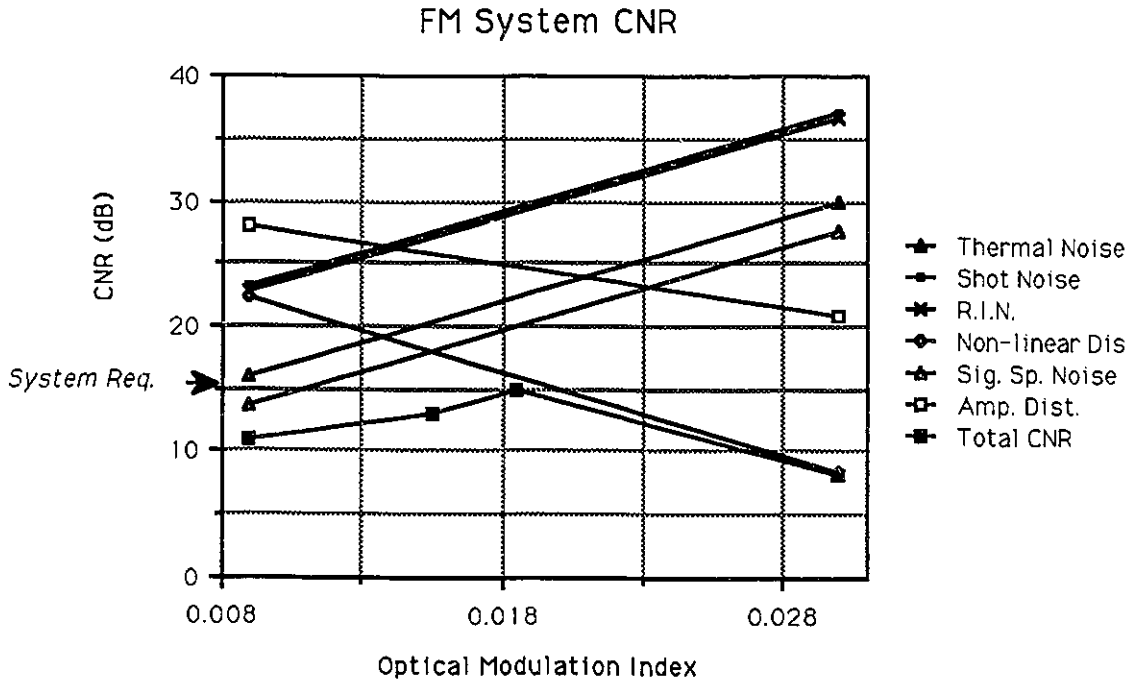

Fig. 41. Λ-curve for FM system

Bandwidth Utilization	1.5-6.0 GHz
Channel Spacing	60 MHz
Noise Equivalent Bandwidth	50 MHz
Number of Channels	75
CNR Requirement	15.6 dB
CNR Achieved	16.48 dB
Optical Modulation Index	0.045
System Margin	24 dB
Number of Amplifier Stages	1

Table 5.5: System Parameters for 4-level QAM

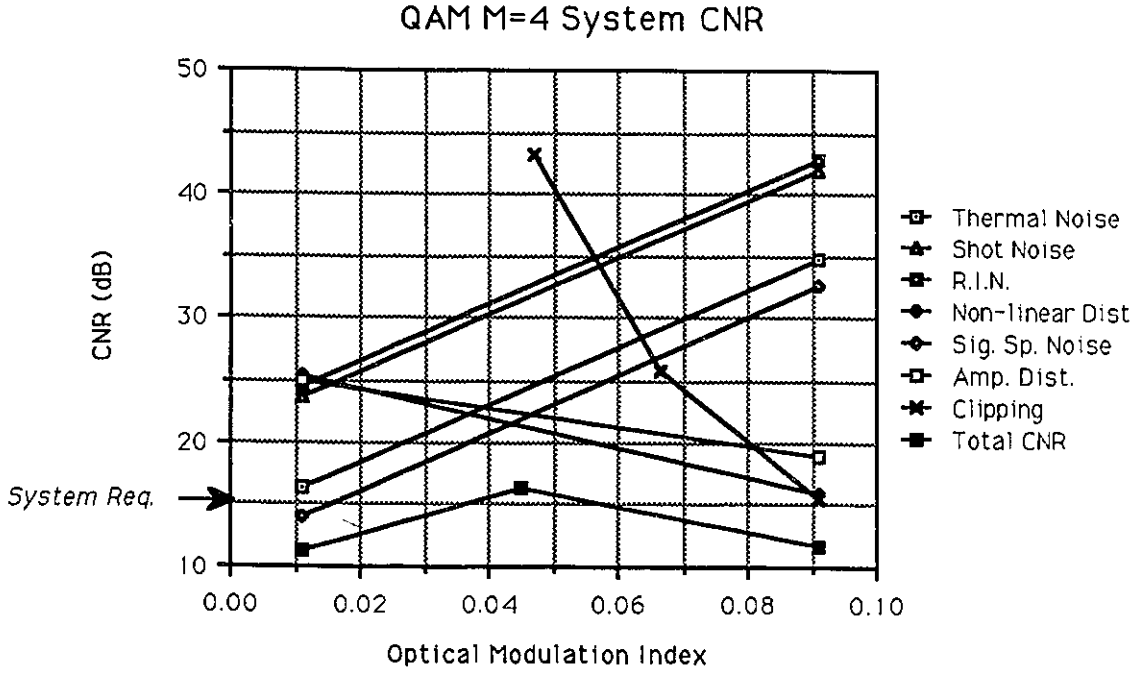

Fig. 42. Λ-curve for 4-level QAM system

Bandwidth Utilization	50-500 MHz
Channel Spacing	6 MHz
Noise Equivalent Bandwidth	4 MHz
Number of Channels	75
CNR Requirement	18 dB
CNR Achieved	17.6 dB
Optical Modulation Index	0.082
System Margin	22 dB
Number of Amplifier Stage	0

Table 5.6: System Parameters for HDTV (Zenith)

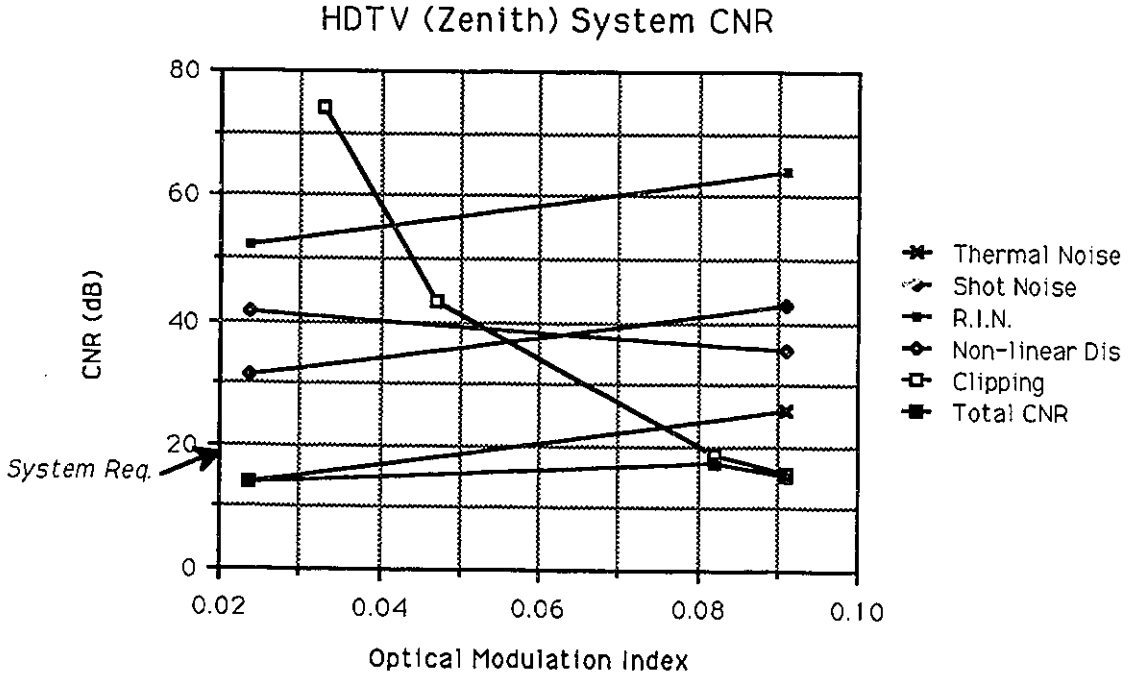

Fig. 43. Λ-curve for HDTV system

Chapter 6

Summary and Research Suggestions

6.1 Summary

In this thesis, we have considered fiber-based subcarrier multiplexed system design for video distribution. Such a design is performed by determining if we have the required CNR at the receiver such that the SNR at the output of the demodulator is sufficient. In a fiber-based system, the main sources of degradation are due to the laser nonlinearity and relative intensity noise, and signal shot noise and preamplifier thermal noise at the receiver. If optical amplifiers are used, we must also include terms for amplifier nonlinear distortion and signal-spontaneous beat noise.

The initial stage of the work was to develop an accurate model for the laser and optical amplifier with BOSS. The laser model is based on the classic rate equations, which couple the injected current to the output photonic signal through a pair of differential equations. These rate equations can be treated analytically, but, since they are not linear, we cannot apply ordinary linear system theory. We can apply perturbation analysis and obtain expressions for the nonlinear distortion spectrum. However, it is difficult to extend this to system design. We can, nonetheless, solve the rate equations numerically using Euler forward integration.

The laser clips the input signal whenever it drops below the threshold. Clipping is a highly nonlinear function of signal level. We can however deal with clipping separately from laser intrinsic nonlinearities, which are generally a second or third order function of the signal level. The clipping penalty is approximated with an expression given by Saleh.

Laser relative intensity noise can be dealt with analytically by adding Langevin noise

terms to the rate equations . The rate equations are linearized and the spectrum is obtained. Also, we have demonstrated how a time-domain computer simulation can be used to obtain the RIN spectrum.

Semiconductor optical amplifiers are readily applicable to subcarrier systems operating in the microwave range. It is therefore useful to develop a good model for the nonlinear distortion of the amplifier. Again, this was done by using a numerical model, based on a reduced form of the amplifier rate and wave equations.

System design proceeds by calculating the CNR for each degradation source. We have simple expressions for shot noise, thermal noise and laser RIN. The intermodulation distortion level is stochastic. We can find an accurate estimate of the distortion level by averaging over 8 simulation runs. We can find the optimal modulation index by using Λ-curves, where one plots the CNR for each degradation source verses the optical modulation index. This was performed for AM-VSB, FM, 4-level QAM and HDTV (Zenith).

The conclusion of this study will now be repeated. Although highly desirable because of its compatibility with existing CATV distribution systems, AM-VSB CNR requirements are too high for use with available lasers to transmit 75 video channels. We can transmit up to 20 channels or reduce the system margin. FM systems are highly desirable, as they only require FM/AM conversion, and they can be used with optical amplifiers. If digital signaling is to be used, we should employ the signal constellation with the smallest number of levels, as we have readily available bandwidth and can more easily meet the CNR requirements. HDTV (Zenith) is also promising, as it can be used with almost the same system margin as other systems with optical amplifiers. However, we must account for the added cost of the processing circuitry.

6.2 Suggestions for Further Research

In our study, we have included many distortion and noise sources. We have been consistent in that we have included them for all systems. For lasers, we have considered nonlinear distortion, as predicted by the laser classic rate equation, which describes the behavior in the active region. As indicated by Olshansky[23], there are further static nonlinearities caused by leakage currents and effects outside the active region which we

have not considered. These effects can be modeled with a power series expansion.

We have considered direct intensity modulation of the laser, which can be used with FM and the QAM modulation. For AM-VSB, an alternative technique would be to use external modulators[33], which may result in an acceptable distortion level.

With respect to laser noise, we have not considered back reflections from waves reflected back into the active region. A model for this effect has been proposed by Way[5], where back reflections are modeled by a light-dependent FM source, which he could not implement because he was using SPICE. This could be attempted with BOSS.

We have only considered the RIN spectrum of an unmodulated laser. Experimental results indicated that when it is modulated, the spectrum is flattened out[31]. This effect could be investigated with a computer simulation. Note that it would be harder to attempt this analytically.

Appendix A

A Carrier Frequency Assignment for Nonlinear Distortion

We include the source code for a program that generates a carrier frequency assignment for nonlinear distortion.

The problem can be stated as being one of choosing a set of integers (frequencies) which, when passed through a nonlinear system, give rise to second and third order distortion components, which do not occur at any of the original frequencies.

As given by Simons[34], assuming we have three input carriers with frequencies ω_1, ω_2, and ω_3, with $\omega_1 > \omega_2 > \omega_3$, we have second order distortion at the following frequencies:

$$2\omega_1, 2\omega_2, 2\omega_3 \tag{A.1}$$

$$\omega_1 \pm \omega_2, \omega_1 \pm \omega_3, \omega_2 \pm \omega_3 \tag{A.2}$$

We have third order distortion at the following frequencies:

$$3\omega_1, 3\omega_2, 3\omega_3 \tag{A.3}$$

$$2\omega_1 \pm \omega_2, 2\omega_1 \pm \omega_3, 2\omega_2 \pm \omega_1, 2\omega_2 \pm \omega_3, 2\omega_3 \pm \omega_1, 2\omega_3 \pm \omega_2 \tag{A.4}$$

$$\omega_1 \pm \omega_2 \pm \omega_3 \tag{A.5}$$

We now give the program code that generates the set of integers with the required properties. We also give the set of the first 35 integers with this property.

```
PROGRAM intermod;
uses printer;
const maxnum=10000;

var i,j,k,l,m,n:integer;
    freq:array[1..100]of integer;
    numfreq:integer;
    a:array[0..maxnum]of boolean;

procedure marka(i:integer);
begin
  a[i]:=true;
end;

{This procedure marks second order distortion}
procedure marksecond(i,j:integer);
begin
  marka(abs(i+j));
  if i<>j then marka(abs(i-j));
end;

{This procedure marks third order distortion}
procedure markthird(i,j,k:integer);
begin
  marka(abs(i+j+k));
  if (j<>k) and (i<>k) then marka(abs(i+j-k));
  if (i<>j) and (k<>j) then marka(abs(i-j+k));
  if (i<>j) and (i<>k) then marka(abs(i-j-k));
end;

function checkfreq:boolean;
var i,j,k,l:integer;
    ok:boolean;
begin
  ok:=true;
  for i:=1 to 3*numfreq do a[i]:=false;
  for l:=1 to numfreq do
  begin
    for i:=1 to numfreq do if i<>l then
    begin
      for j:=1 to numfreq do
      begin
        marksecond(freq[i],freq[j]);
        for k:=1 to numfreq do markthird(freq[i],freq[j],freq[k]);
      end
    end;
    ok:=true;
    for i:=1 to numfreq do ok:=ok and (not a[freq[i]]);
  end;
  checkfreq:=ok;
end;

function checkall:boolean;
var i,j,k,l:integer;
    ok:boolean;
begin
```

```
    writeln('checking   ');
    ok:=true;
    for i:=1 to 3*freq[numfreq] do a[i]:=false;
    for i:=1 to numfreq do
    begin
      a[freq[i]]:=true;
      for j:=1 to numfreq do
      begin
        marksecond(freq[i],freq[j]);
        for k:=1 to numfreq do markthird(freq[i],freq[j],freq[k]);
      end
    end;
    checkall:=ok;
  end;

  BEGIN
    numfreq:=1;
    freq[numfreq]:=1;
    for i:=1 to maxnum do a[i]:=false;
    writeln(lst,'1---1');
    n:=2;
    repeat
      for i:=1 to numfreq do writeln('freq ',freq[i]:5);
      if checkall then;
      writeln('...');
      repeat
        i:=1;
        while a[i] do inc(i);
        writeln(lst,n,'---',i);
        inc(numfreq);
        freq[numfreq]:=i;
      until checkall;
      n:=n+1;
      writeln(numfreq:5,freq[numfreq]:5,(freq[numfreq] div numfreq):5);
    until (numfreq>=100) or (freq[numfreq]>maxnum-100);
    readln;
  END.
```

We give here the set of the first 35 integers with the required property, as follows.

1---1
2---4
3---10
4---17
5---29
6---52
7---67
8---89
9---132
10---164
11---205
12---259
13---303
14---350
15---405
16---505
17---529
18---588
19---680
20---903
21---1016
22---1061
23---1248
24---1358
25---1445
26---1838
27---1878
28---2086
29---2117
30---2195
31---2613
32---2840
33---3060
34---3314
35---3422

Appendix B

Traveling Wave Equation for Optical Amplifier

Saleh[8] gives a reduced form for the optical amplifier traveling wave equation. He gives only a partial derivation. We give here the derivation, starting from Maxwell's equations.

Starting with Maxwell's equation:

$$\nabla \times \vec{E} = -\frac{\partial \vec{B}}{\partial t} \tag{B.1}$$

Taking the curl of the L.H.S. and applying a vector identity, we obtain:

$$\nabla \times \nabla \times \vec{E} = \nabla(\nabla \cdot \vec{E}) - \nabla^2 \vec{E} = -\nabla^2 \vec{E} \tag{B.2}$$

where we have assumed $\nabla \cdot \vec{D} = 0$. Taking the curl of the R.H.S. of equation B.1, we obtain:

$$\nabla \times \frac{\partial \vec{B}}{\partial t} = \mu \nabla \times \frac{\partial \vec{H}}{\partial t} = \mu \frac{\partial^2 \vec{D}}{\partial t^2} + \mu \frac{\partial \vec{J}}{\partial t} = \mu \frac{\partial^2 \vec{D}}{\partial t^2} \tag{B.3}$$

where we have assumed $\frac{\partial \vec{J}}{\partial t} = 0$ and used Maxwell's equation $\nabla \times \vec{H} = \frac{\partial \vec{D}}{\partial t} + \vec{J}$.

Substituting for $\vec{D} = \epsilon_0 \vec{E} + \vec{P}$ and using the fact that $\mu = 1/\epsilon_0 c^2$, we obtain:

$$\nabla \times \frac{\partial \vec{B}}{\partial t} = \mu \epsilon_0 \frac{\partial^2 \vec{E}}{\partial t^2} + \mu \frac{\partial^2 \vec{P}}{\partial t^2} = \frac{1}{c^2} \frac{\partial^2 \vec{E}}{\partial t^2} + \frac{1}{\epsilon_0 c^2} \frac{\partial^2 \vec{P}}{\partial t^2} \tag{B.4}$$

Equating the L.H.S. and R.H.S. of equation (B.1), we obtain:

$$\nabla^2 \vec{E} - \frac{1}{c^2} \frac{\partial^2 \vec{E}}{\partial t^2} = \frac{1}{\epsilon_0 c^2} \frac{\partial^2 \vec{P}}{\partial t^2} \tag{B.5}$$

We will now distinguish between two sources of polarization: polarization induced by the material and polarization induced by the injected current for which we shall keep the

variable $\vec{P}$. With $\vec{P}_{material} = \epsilon_0 \chi \vec{E}$ we obtain:

$$\frac{1}{c^2}\frac{\partial^2 \vec{E}}{\partial t^2} + \frac{1}{\epsilon_0 c^2}\frac{\partial^2 \vec{P}}{\partial t^2} = \frac{1}{c^2}n^2\frac{\partial^2 \vec{E}}{\partial t^2} + \frac{1}{\epsilon_0 c^2}\frac{\partial^2 \vec{P}}{\partial t^2} \tag{B.6}$$

where we have set $n = \sqrt{1+\chi}$, which is defined as the refractive index of the medium. Now, with regards to the carrier induced polarization we have:

$$\vec{P} = \epsilon_0 \frac{nc}{w}(1 + j\alpha)g(z,t)\vec{E} \tag{B.7}$$

where α is the linewidth enhancement factor and $g(z,t)$ is the incremental gain from the current. Substituting the above equation into (B.6) one gets the following:

$$\nabla^2 \vec{E} = \frac{\partial^2}{\partial t^2}\left[\frac{n^2}{c^2} + \frac{n}{c\omega}(1 + j\alpha)g(z,t)\right]\vec{E} \tag{B.8}$$

We now assume that the electric field is propagating in the z-direction, for which we can substitute $\vec{E} = E(z,t)exp[j(\omega t - kz)]$ where $k = \omega n/c$ is the propagation constant. With this substitution and making the assumption that the time scale of the gain and envelope variations are much smaller than the electric field variations, i.e. that $\frac{\partial}{\partial t}exp[j(\omega t - kz)] \gg \frac{\partial}{\partial t}E(z,t)$ and likewise for $g(z,t)$, we can substitute as well $\frac{\partial^2}{\partial t^2} \rightarrow (j\omega)^2$ and $\frac{\partial^2}{\partial z^2} \rightarrow (-jk)^2 - j2k\frac{\partial}{\partial z}$ and then obtain the following simplified scaler differential equation:

$$\frac{\partial}{\partial t}E(z,t) = \left[\frac{1 + j\alpha}{2}\right]E(z,t)g(z,t) \tag{B.9}$$

The solution is that of a first order linear differential equation given as:

$$E(z,t) = Cexp\left(\frac{1 + j\alpha}{2}\int_0^L g(z,t)dt\right) \tag{B.10}$$

Now $E(0,t) = E_{in}(t)$ and $E(L,t) = E_{out}(t)$ where L is the cavity length. With $G(t) = \int_0^L g(z,t)dt$, and taking the magnitude, we have the following result, as given by Saleh[8]:

$$\|E_{out}(t)\| \approx \|E_{in}(t)\|exp[G(t)/2] \tag{B.11}$$

Appendix C

BOSS Modules

The first four modules were used for laser intermodulation distortion. We also give the initialization code for the module 20SINEGRP. The next nine modules were used for laser relative intensity noise simulation. We then give the module used for clipping. The next two modules were used for the optical amplifier. The final two modules were used for phase plane generation.

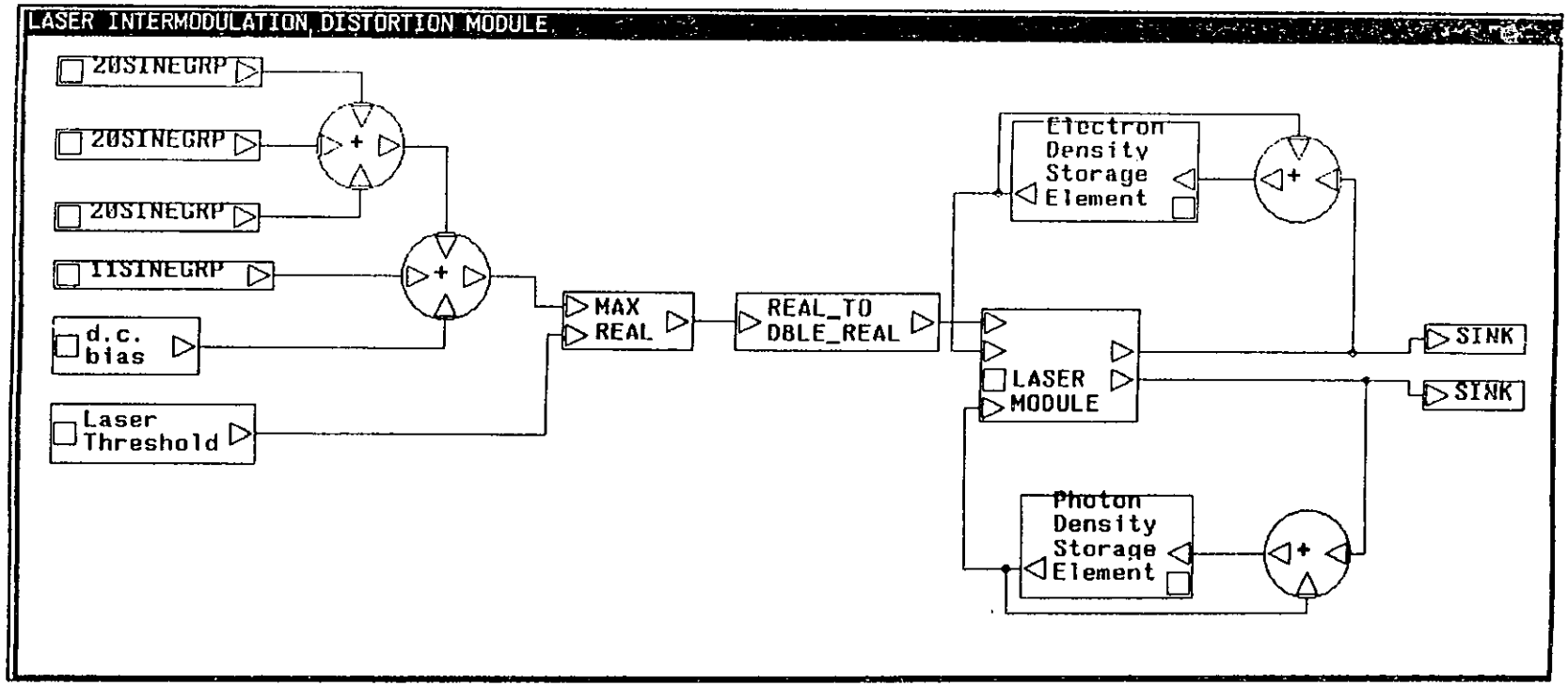
LASER INTERMODULATION DISTORTION MODULE
20SINEGRP
20SINEGRP
20SINEGRP
11SINEGRP
d.c. bias
Laser Threshold
+
+
MAX REAL
REAL_TO DBLE_REAL
Electron Density Storage Element
+
LASER MODULE
SINK
SINK
Photon Density Storage Element
+

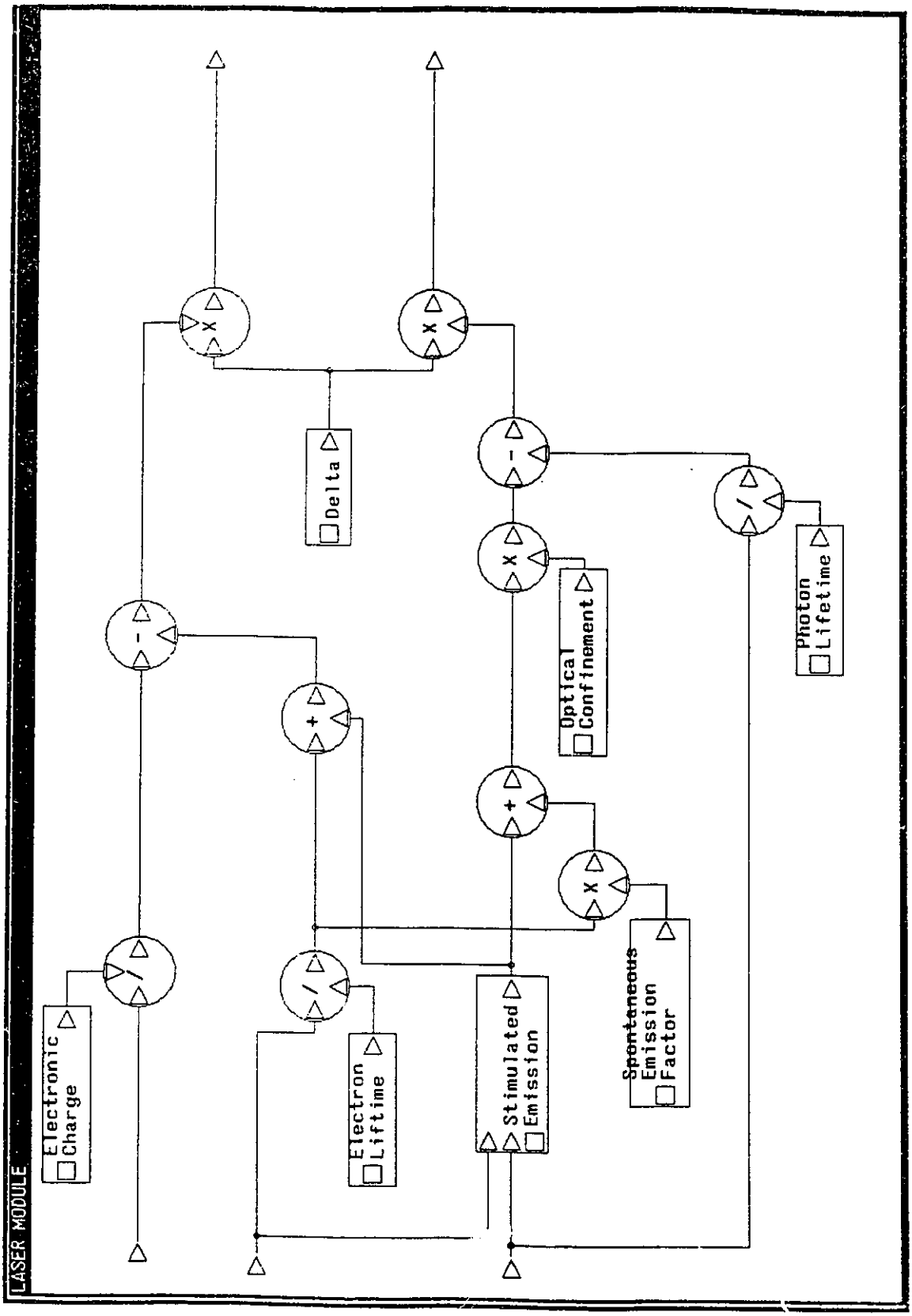
LASER MODULE
Electronic Charge
Electron Liftime
Stimulated Emission
Spontaneous Emission Factor
Optical Confinement
Photon Lifetime
Delta

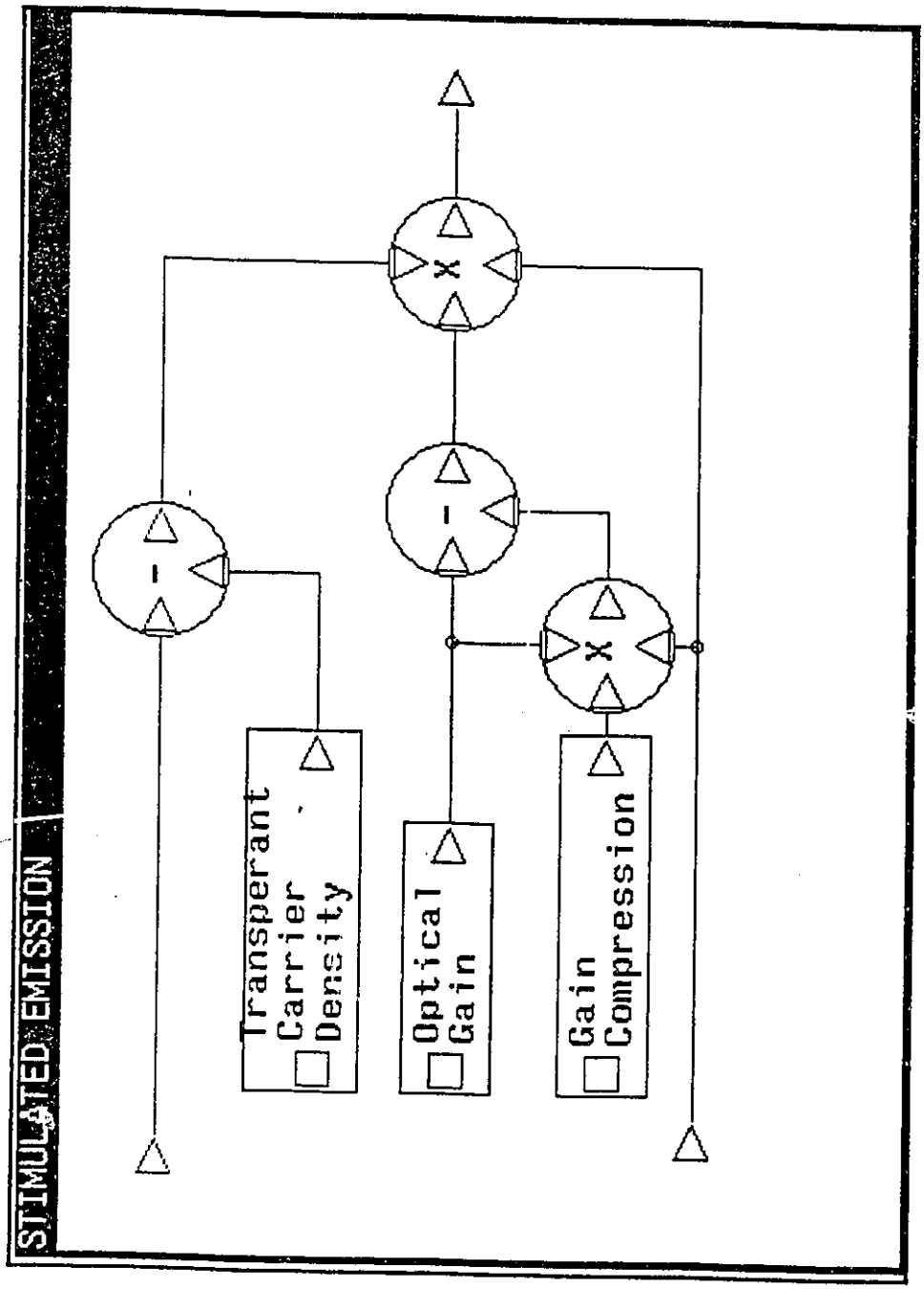
STIMULATED EMISSION
Transperant Carrier Density
Optical Gain
Gain Compression

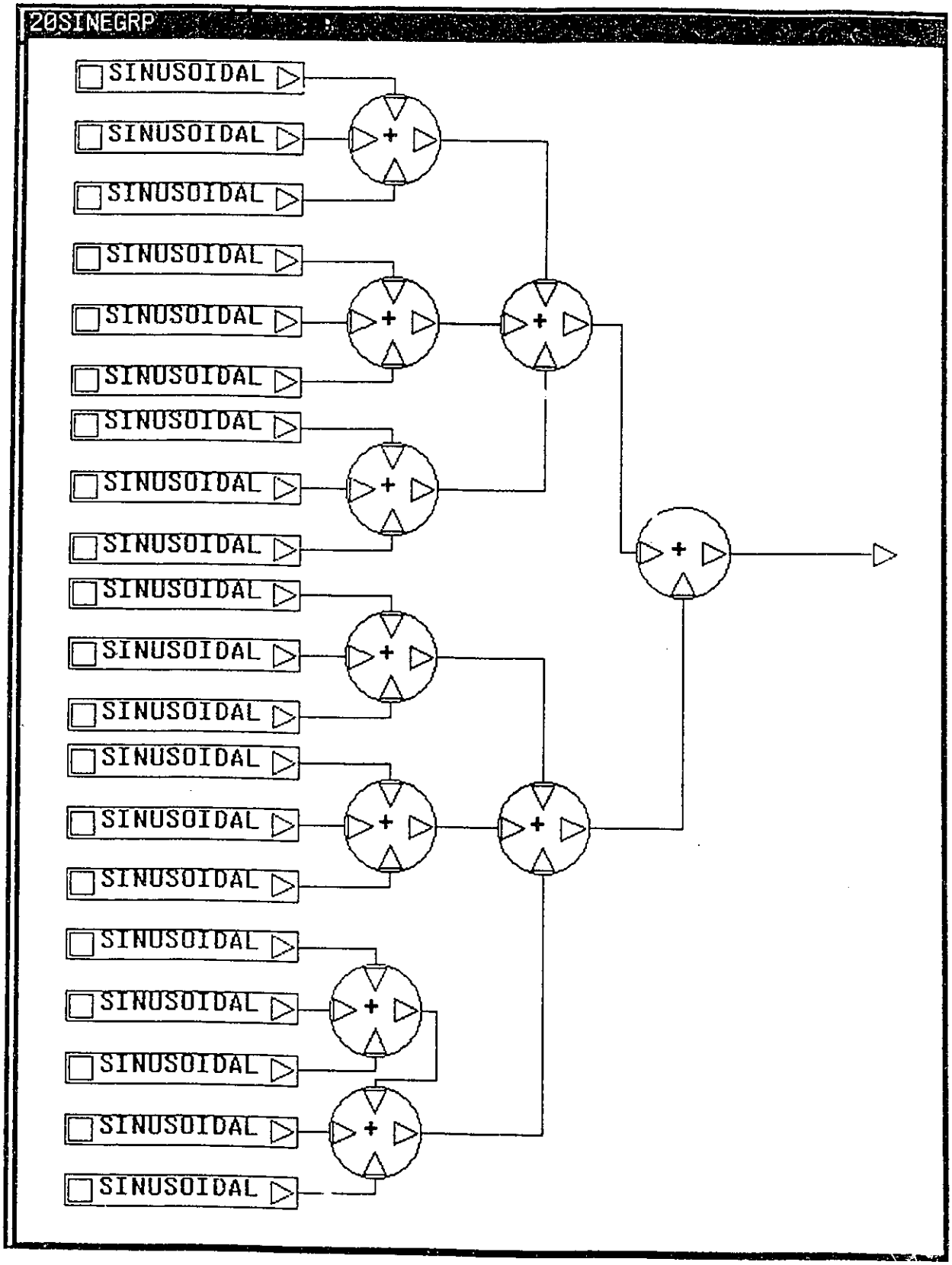
20SINEGRP
SINUSOIDAL
SINUSOIDAL
SINUSOIDAL
SINUSOIDAL
SINUSOIDAL
SINUSOIDAL
SINUSOIDAL
SINUSOIDAL
SINUSOIDAL
SINUSOIDAL
SINUSOIDAL
SINUSOIDAL
SINUSOIDAL
SINUSOIDAL
SINUSOIDAL
SINUSOIDAL
SINUSOIDAL
SINUSOIDAL
SINUSOIDAL
SINUSOIDAL
SINUSOIDAL

This is the initialization code for the BOSS module 20SINEGRP. The phase for each of the sinusoids is set by the random number generator.

```
      subroutine rd (p1,p2,p3,p4,p5,p6,p7,p8,
     &  p9,pa,pb,pc,pd,pe,pf,pg,ph,pi,pj,pk,iseed)
      implicit undefined (a-z)
      integer iseed
      real p1,p2,p3,p4,p5,p6,p7,p8,p9,pa,pb,
     &  pc,pd,pe,pf,pg,ph,pi,pj,pk,ran
      p1 = ran(iseed)*6.2383185307179586e+0
      p2 = ran(0)*6.2383185307179586e+0
      p3 = ran(0)*6.2383185307179586e+0
      p4 = ran(0)*6.2383185307179586e+0
      p5 = ran(0)*6.2383185307179586e+0
      p6 = ran(0)*6.2383185307179586e+0
      p7 = ran(0)*6.2383185307179586e+0
      p8 = ran(0)*6.2383185307179586e+0
      p9 = ran(0)*6.2383185307179586e+0
      pa = ran(0)*6.2383185307179586e+0
      pb = ran(0)*6.2383185307179586e+0
      pc = ran(0)*6.2383185307179586e+0
      pd = ran(0)*6.2383185307179586e+0
      pe = ran(0)*6.2383185307179586e+0
      pf = ran(0)*6.2383185307179586e+0
      pg = ran(0)*6.2383185307179586e+0
      ph = ran(0)*6.2383185307179586e+0
      pi = ran(0)*6.2383185307179586e+0
      pj = ran(0)*6.2383185307179586e+0
      pk = ran(0)*6.2383185307179586e+0
      return
      end
```

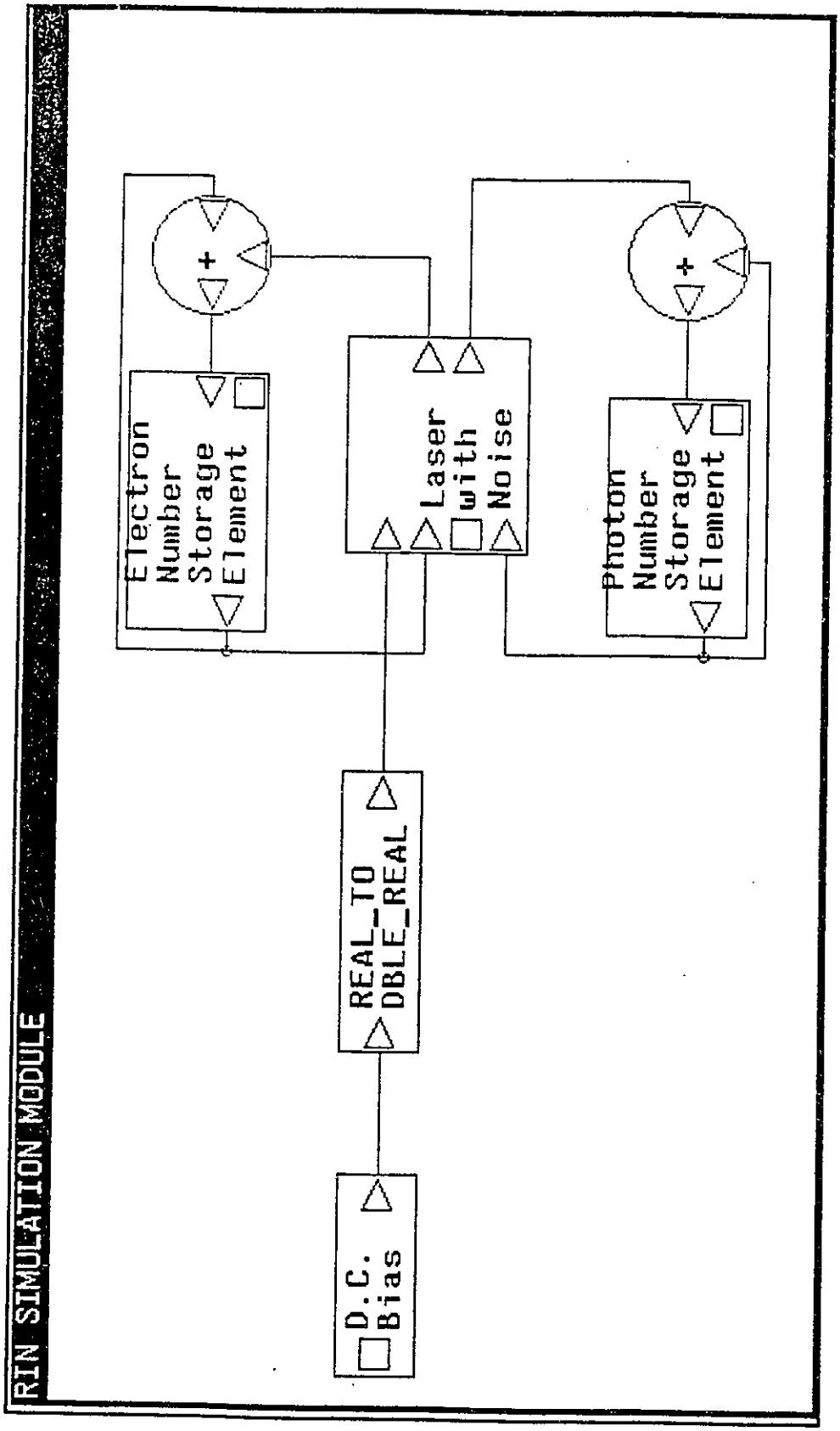
RIN SIMULATION MODULE
+
+
Electron Number Storage Element
Laser with Noise
Photon Number Storage Element
REAL_TO DBLE_REAL
D.C. Bias

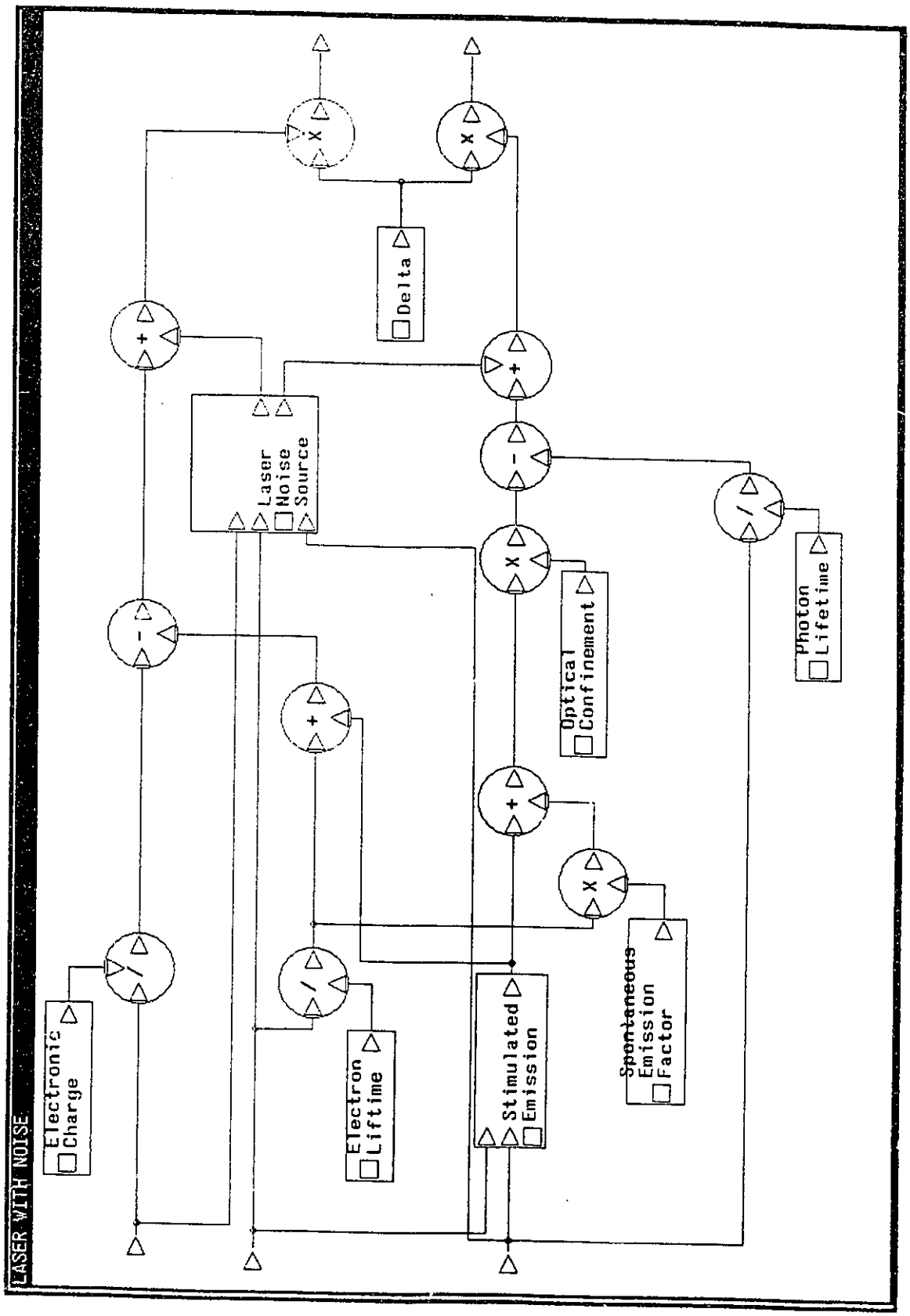
LASER WITH NOISE
Electronic Charge
Electron Liftime
Stimulated Emission
Spontaneous Emission Factor
Optical Confinement
Photon Lifetime
Laser Noise Source
Delta

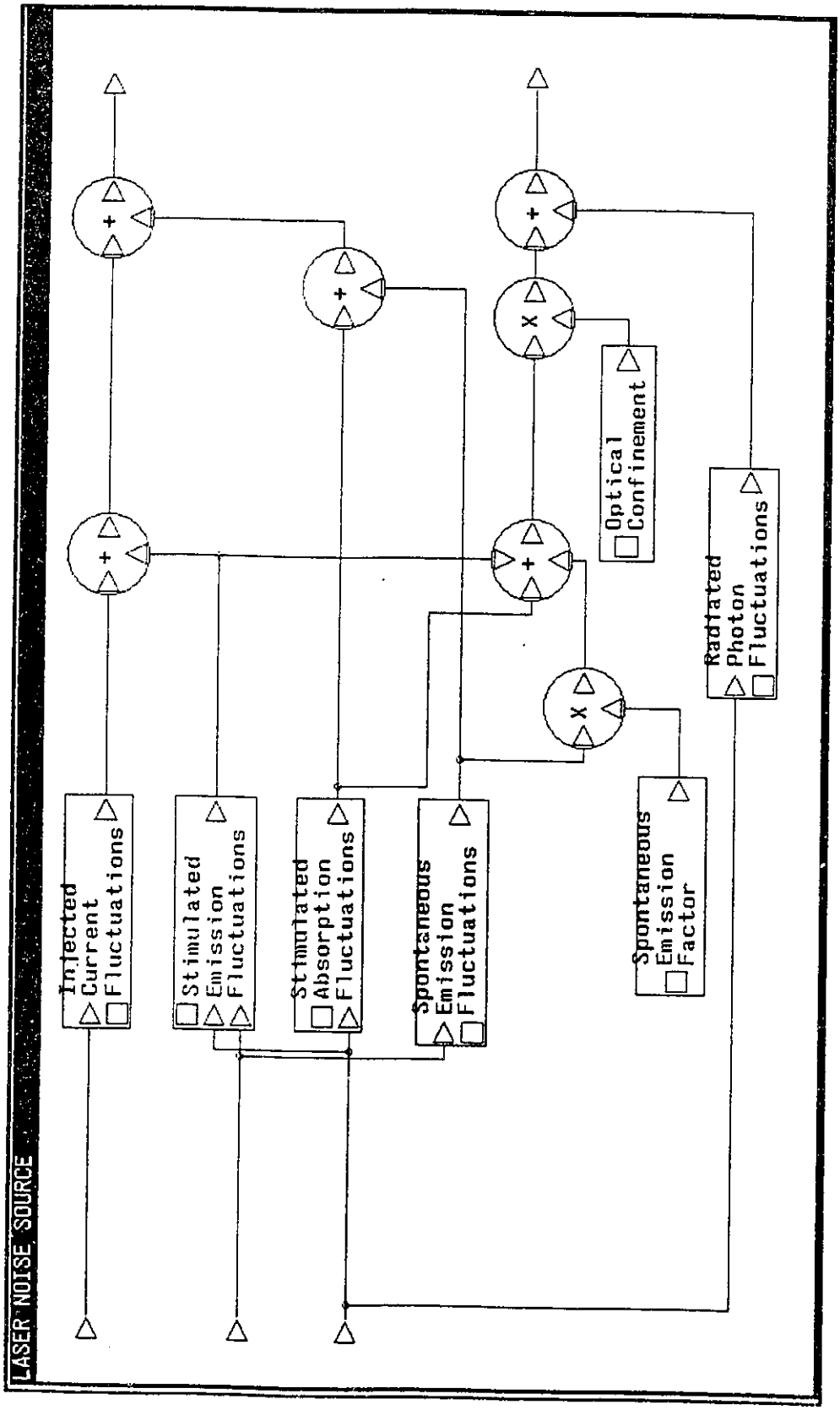
LASER NOISE SOURCE
Injected Current Fluctuations
Stimulated Emission Fluctuations
Stimulated Absorption Fluctuations
Spontaneous Emission Fluctuations
Spontaneous Emission Factor
Optical Confinement
Radiated Photon Fluctuations
+
+
+
+
+
x
x

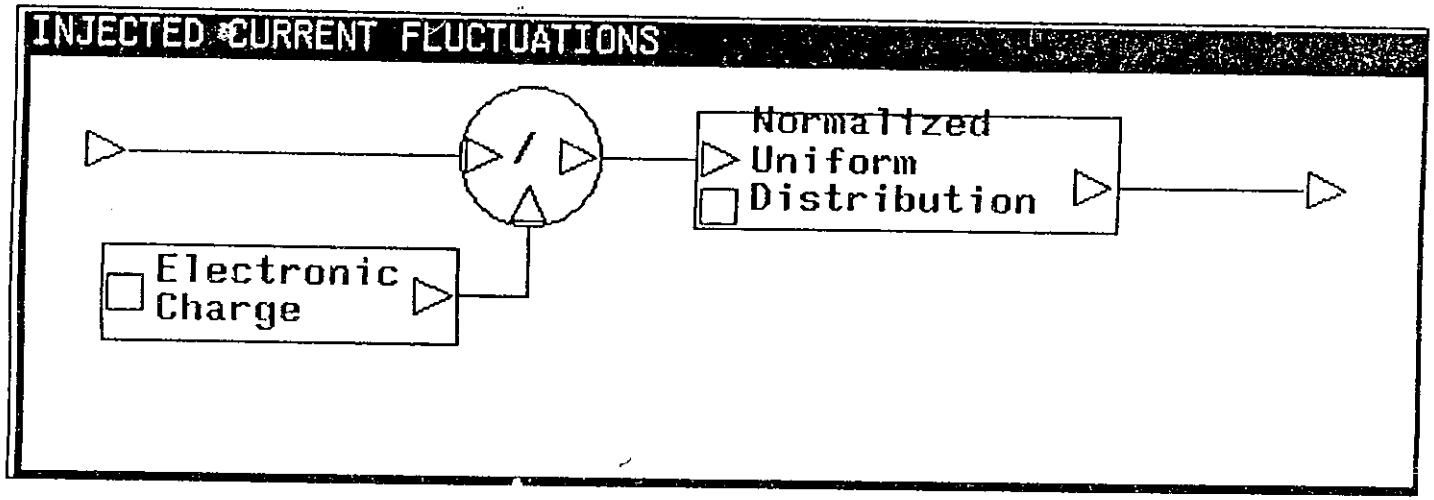
INJECTED CURRENT FLUCTUATIONS
/
Normalized
Uniform
Distribution
Electronic
Charge

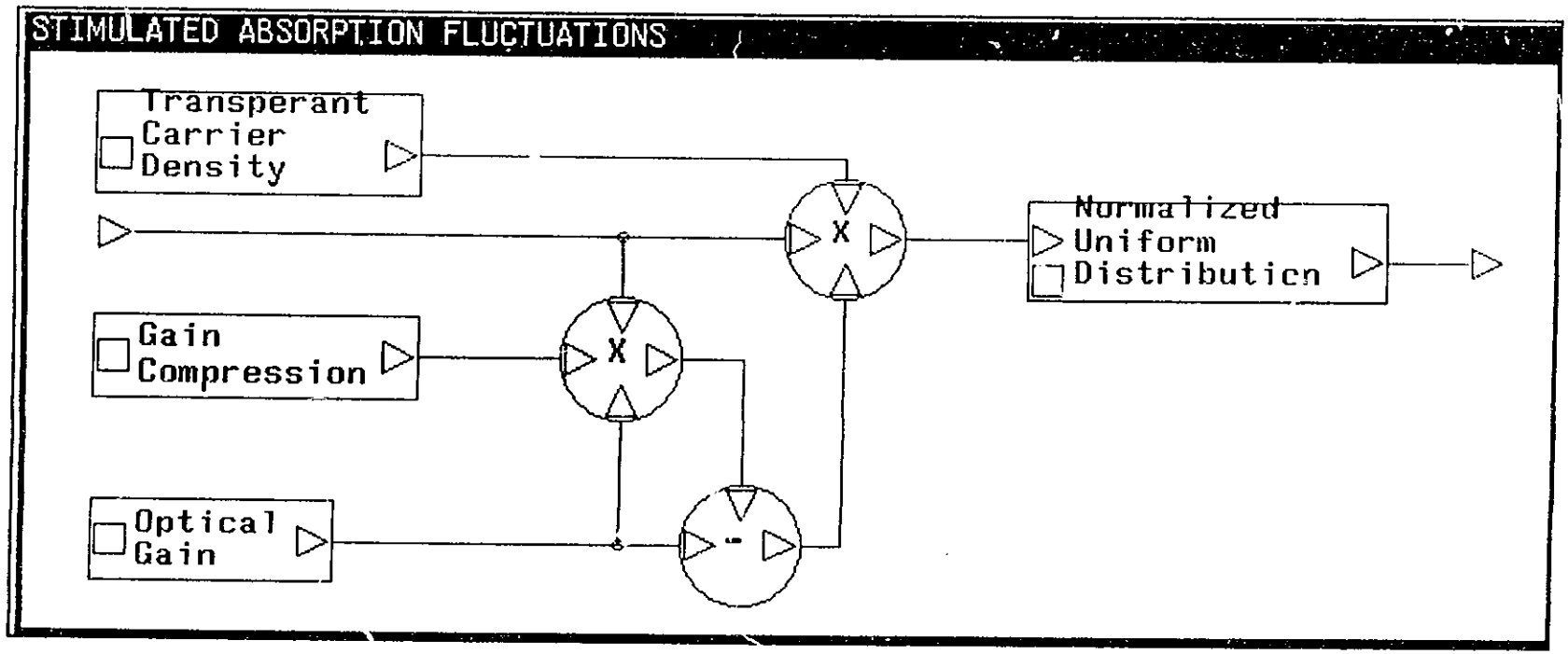
STIMULATED ABSORPTION FLUCTUATIONS
Transperant Carrier Density
Gain Compression
Optical Gain
X
X
-
Normalized Uniform Distribution

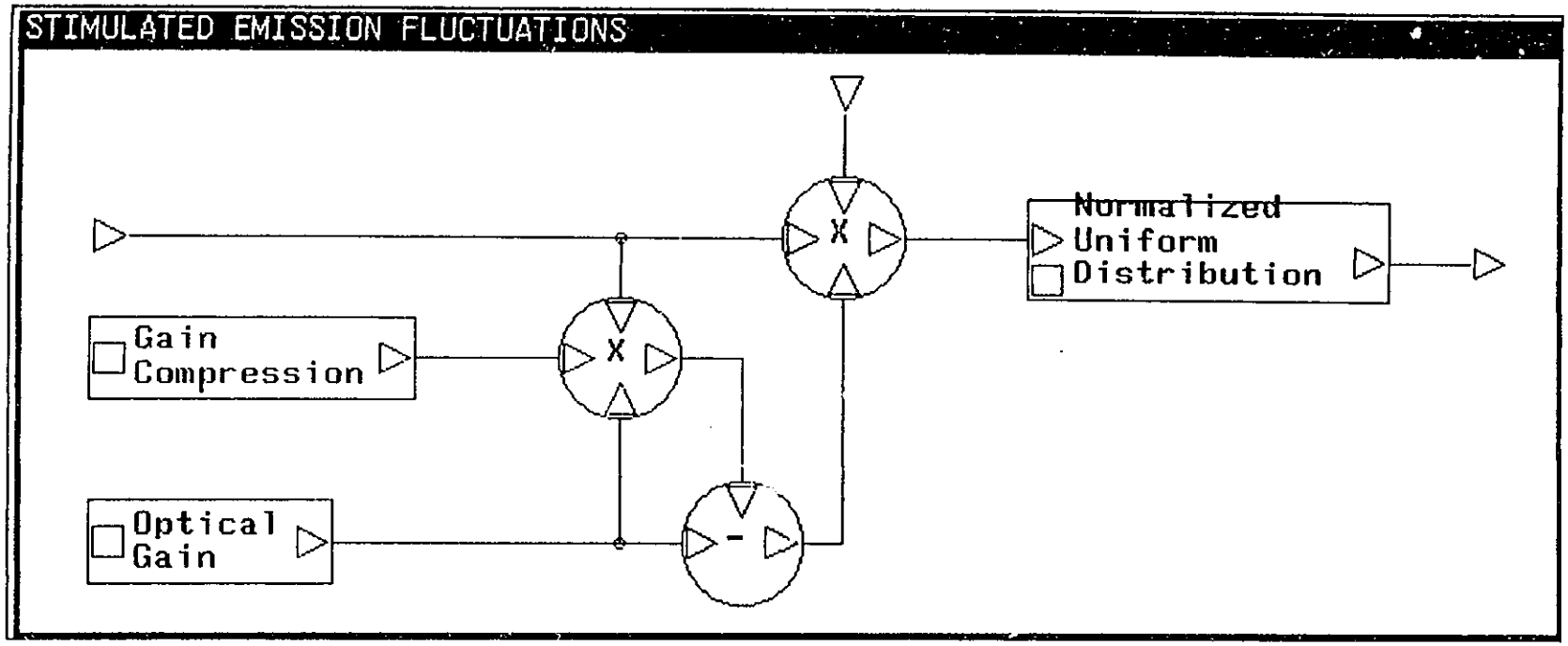
STIMULATED EMISSION FLUCTUATIONS
X
Normalized
Uniform
Distribution
Gain
Compression
X
Optical
Gain
-

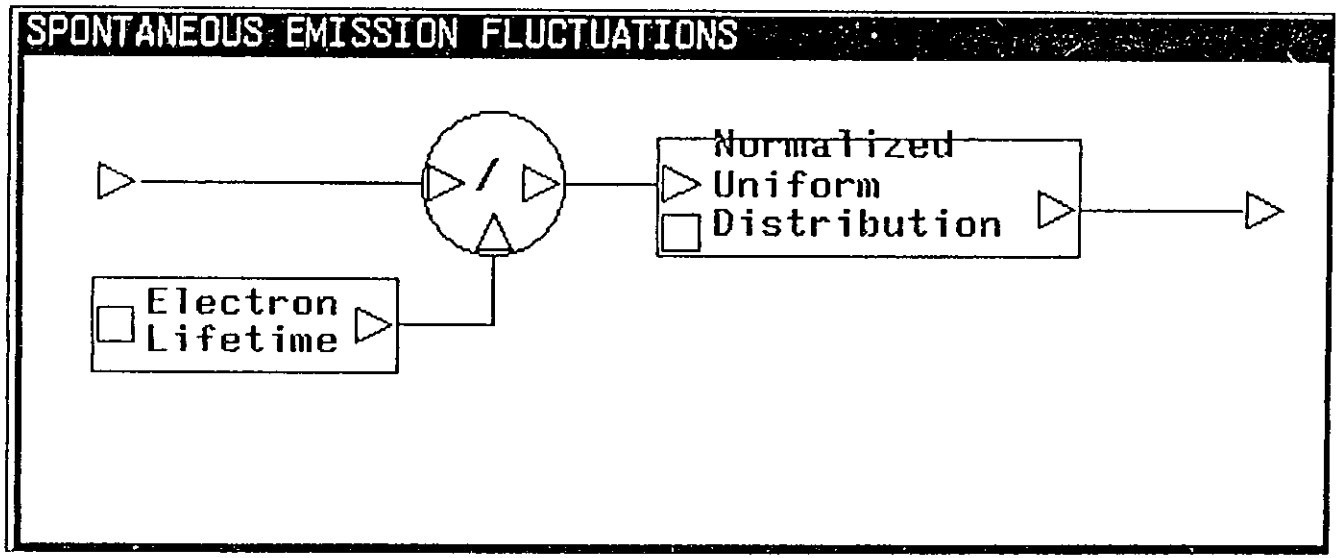
SPONTANEOUS EMISSION FLUCTUATIONS
/
Normalized
Uniform
Distribution
Electron
Lifetime

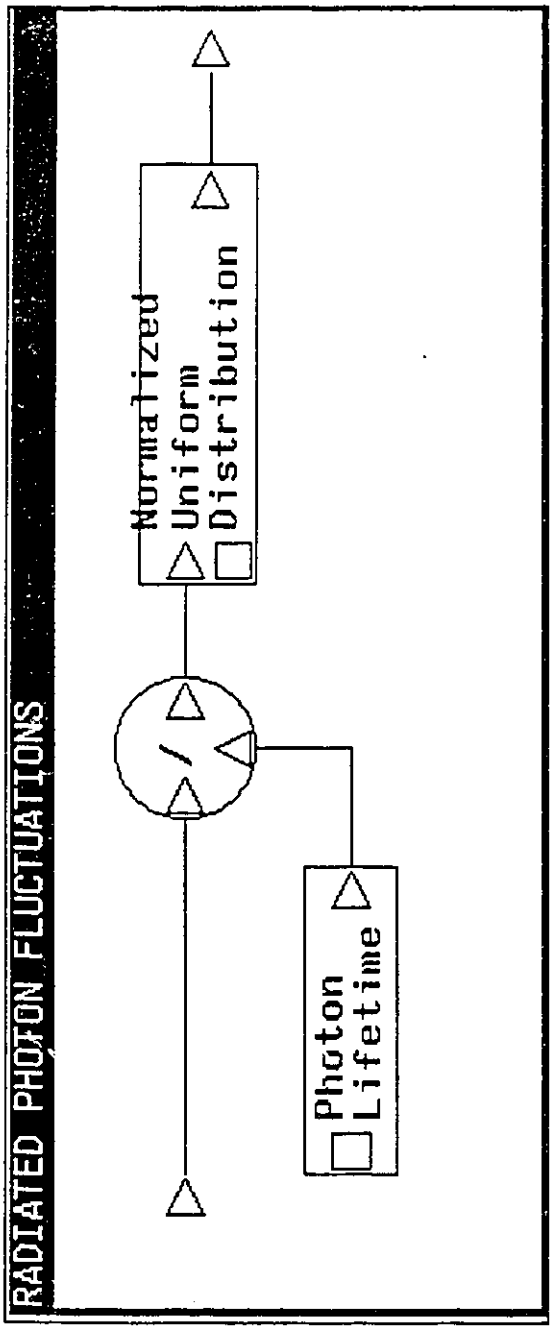
RADIATED PHOTON FLUCTUATIONS
Normalized
Uniform
Distribution
/
Photon
Lifetime

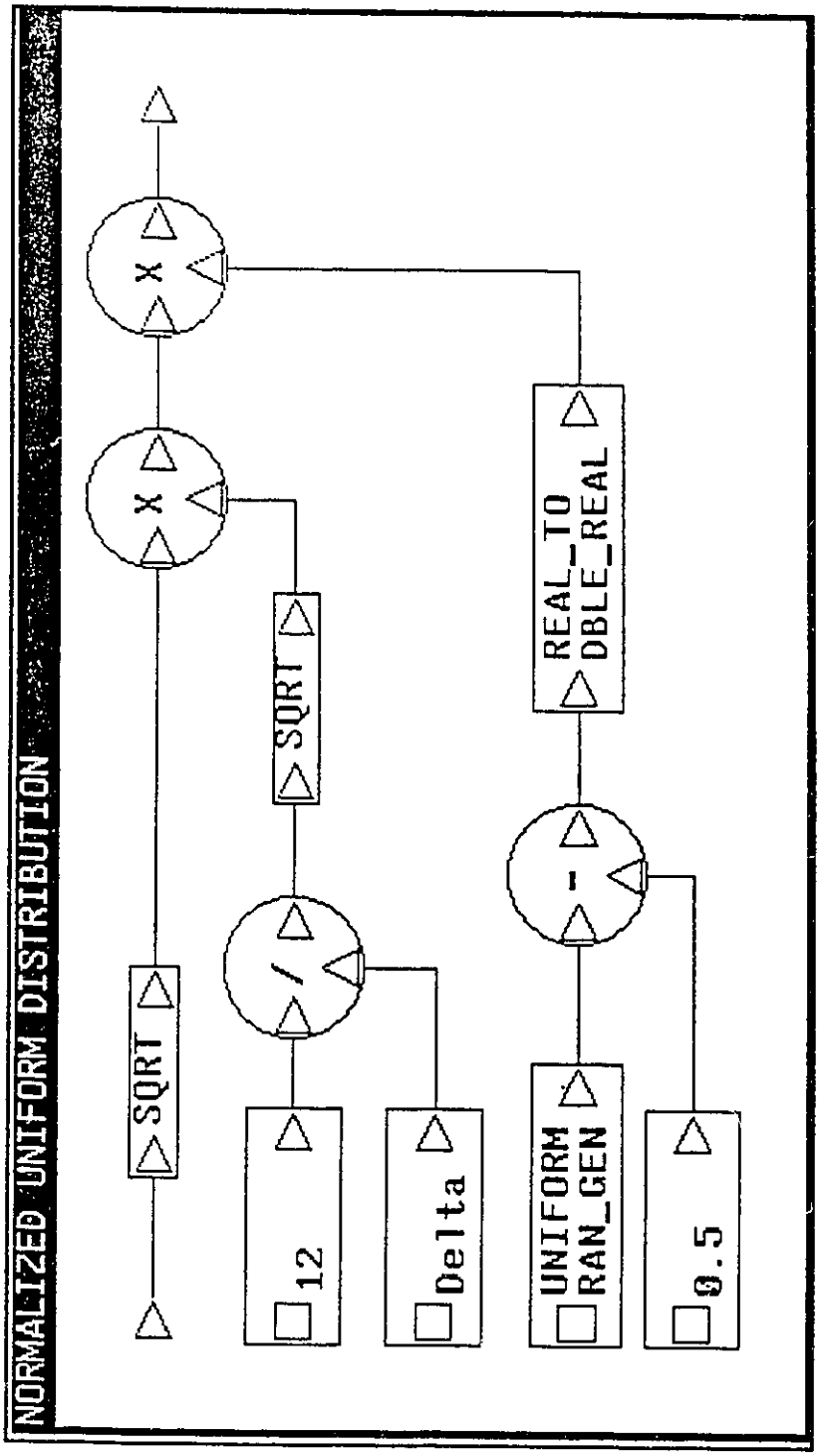
NORMALIZED UNIFORM DISTRIBUTION
X
X
SQRT
SQRT
/
-
REAL_TO
DBLE_REAL
12
Delta
UNIFORM
RAN_GEN
0.5

CLIPPING SIMULATION
20SINEGRP
20SINEGRP
20SINEGRP
15SINEGRP
d.c.
bias
Laser
Threshold
+
+
-
MAX
REAL
SINK

OPTICAL AMPLIFIER INTERMODULATION DISTORTION
29SINEGRP
20SINEGRP
29SINEGRP
11SINEGRP
d.c.
bias
+
+
Optical
Amplifier
Module
SINK

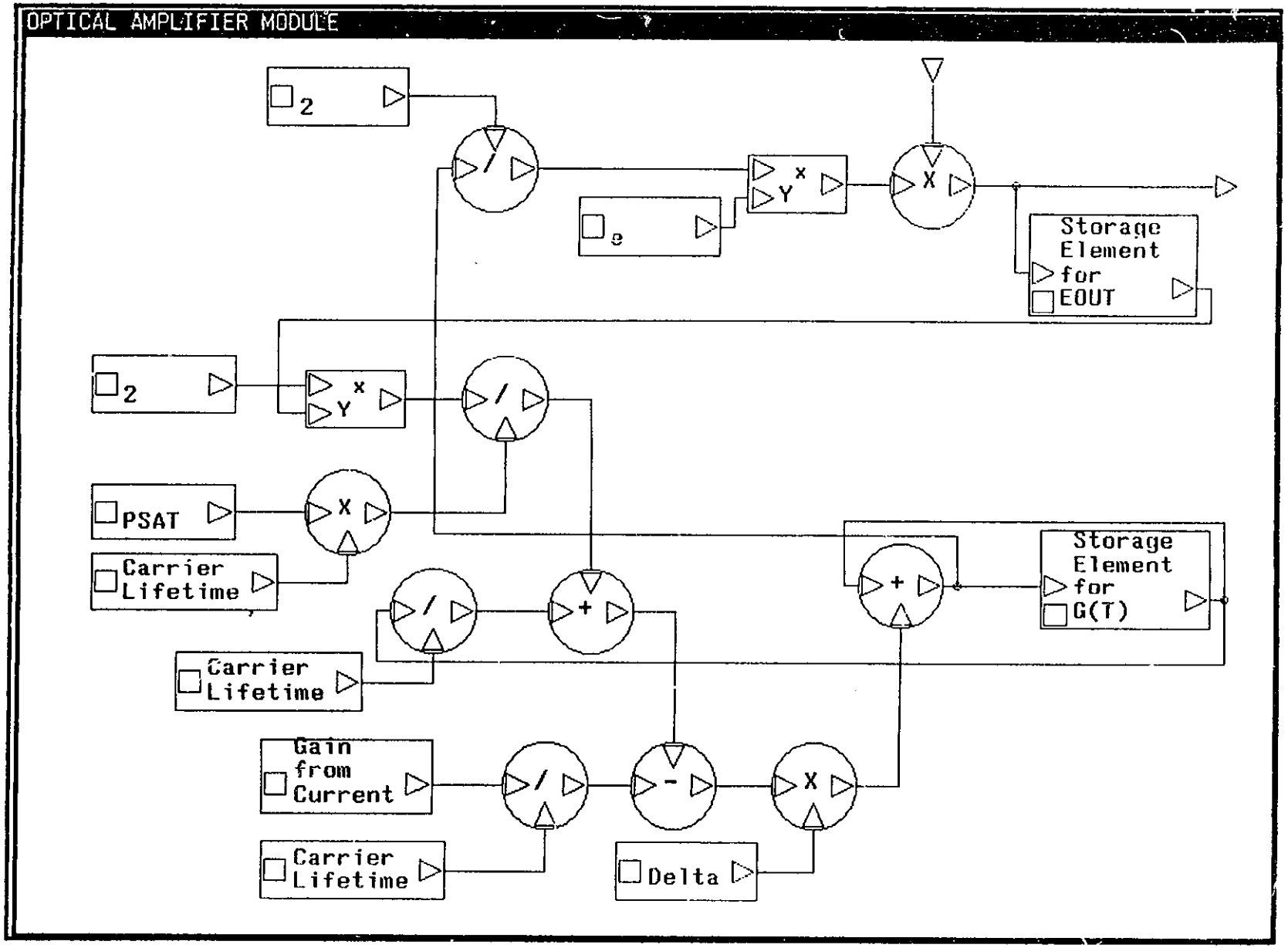
OPTICAL AMPLIFIER MODULE
2
/
e
Y^x
X
Storage Element for EOUT
2
Y^x
/
PSAT
X
Carrier Lifetime
/
+
+
Storage Element for G(T)
Carrier Lifetime
Gain from Current
/
-
X
Carrier Lifetime
Delta

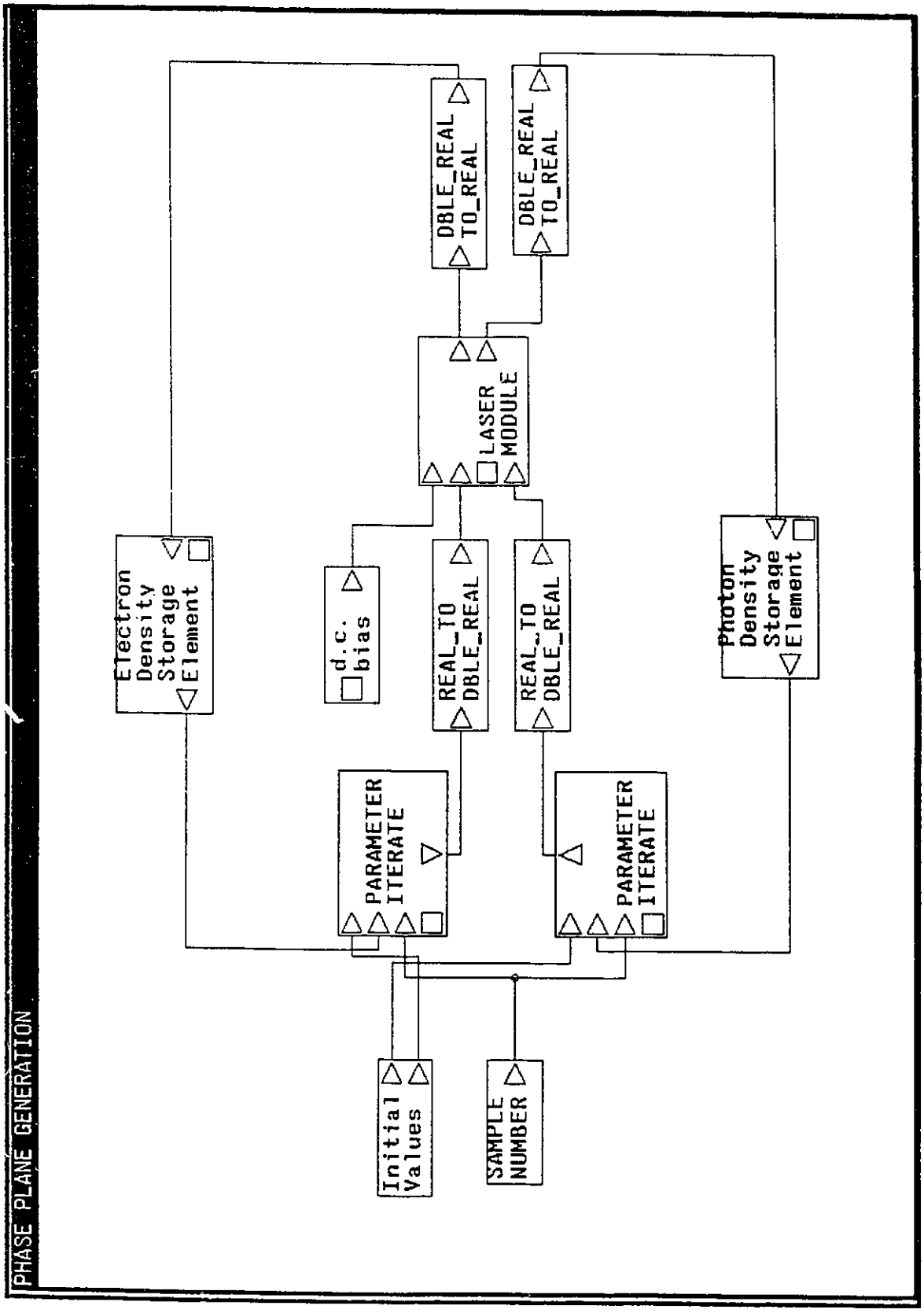
PHASE PLANE GENERATION
DBLE_REAL TO_REAL
DBLE_REAL TO_REAL
LASER MODULE
Electron Density Storage Element
d.c. bias
REAL_TO DBLE_REAL
REAL_TO DBLE_REAL
Photon Density Storage Element
PARAMETER ITERATE
PARAMETER ITERATE
Initial Values
SAMPLE NUMBER

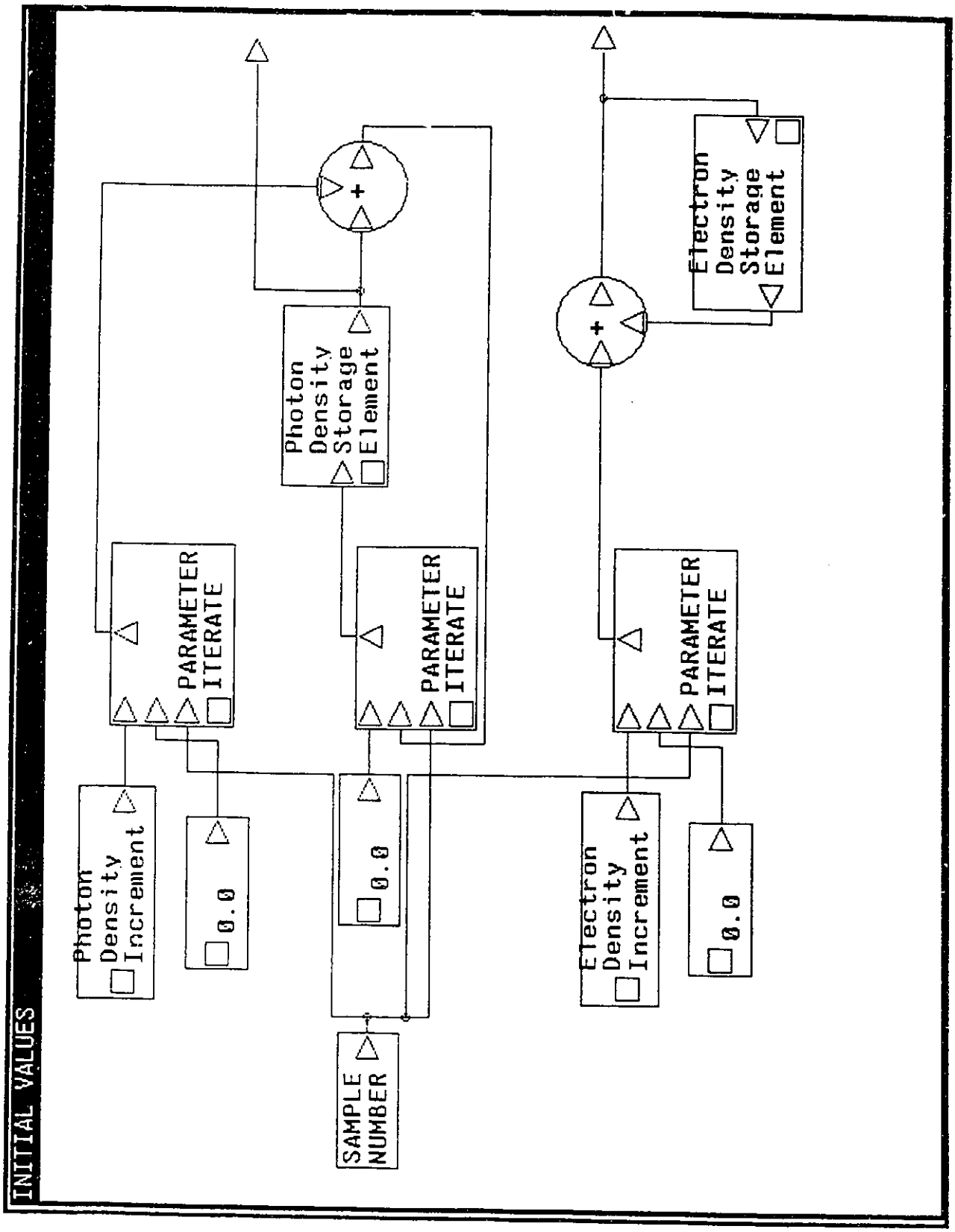
INITIAL VALUES
Photon Density Increment
0.0
SAMPLE NUMBER
PARAMETER ITERATE
Photon Density Storage Element
+
PARAMETER ITERATE
0.0
Electron Density Increment
0.0
PARAMETER ITERATE
+
Electron Density Storage Element

Bibliography

[1] R.G. Medhurst, J. H. Roberts,"Evaluation of distortion in f.m. trunk radio systems by a Monte Carlo method", *Proc. IEE*, Vol. 113, No. 4 pp.570-580, April 1966.

[2] R.S. Tucker, D.J. Pope, "Circuit Modeling of the Effect of Diffusion on Damping in a Narrow-Stripe Semiconductor Laser", *IEEE J. Quantum Electron.*, Vol. QE-19. No. 7, pp. 1179-1183, July 1983.

[3] K.Y. Lau, A. Yariv, "Intermodulation distortion in a directly modulated semiconductor injection laser", *Appl. Phys. Lett.*, Vol. 45, No. 10, pp. 1034-1036, November 1984.

[4] P. Neusy, W.F. McGee, "Effects of Laser Nonlinearities on TV Distribution using Subcarrier Multiplexing", presented at Canadian Conference on Electrical and Computer Engineering, Montreal, PQ, September 1989, pp. 883-836.

[5] W.I. Way, "Large Signal Nonlinear Distortion Prediction for a Single-Mode Laser Diode Under Microwave Intensity Modulation", *J. Lightwave Technol.*, Vol. LT-5, No. 3, pp.305-315, March 1987.

[6] Y. Yamamoto, "AM and FM Quantum Noise in Semiconductor Lasers-Part1: Theoretical Analysis", *IEEE J. Quantum Electron.*, Vol. QE-19, No. 1, pp.34-46, January 1983.

[7] G.P. Agrawal, "Four-wave mixing and phase conjugation in semiconductor laser media", *Optics Letters*, Vol. 12, No. 4, pp. 260-262, April 1987.

[8] A. A. M. Saleh, "Nonlinear Models of Traveling-wave Optical Amplifiers", *Electron. Lett.*, Vol. 24, No. 14, pp. 835-837, July 1988

[9] T. E. Darcie, G. E. Bodeep, "Lightwave Multi-channel Analog AM Video Distribution Systems", *ICC'89*, 32.4.1-32.4.4, June 1989

[10] R. Olshansky, V. A. Lanzisera, "60-Channel FM Video Subcarrier Multiplexed Optical Communication System", *Electron. Lett.*, Vol. 23, No. 22, pp. 1196-1198, October 1987

[11] N. Kanno, K. Ito, "Fiber Optic Subcarrier Multiplexing Transport for Broadband Subscriber Distribution Network",*ICC'89* 32.3.1-32.3.8, June 1989

[12] W. I. Way, et. al.,"Applications of Traveling-Wave Laser Amplifiers in Subcarrier Multiplexed Lightwave Systems", *ICC'89*, 32.2.1-32.2.9, June 1989

[13] M. D. Atkinson, et. al.,"Integer Sets with Distinct Sums and Differences and Carrier Frequency Assignments for Nonlinear Repeaters", *IEEE Trans. on Com.*, Vol. COM-34, No. 6, pp. 614-617, June 1986

[14] R. Gregorian, G. C. Temes, *Analog MOS Integrated Circuits for Signal Processing*, John Wiley and Sons, New York, N.Y., 1986

[15] D. Marcuse, "Computer Simulation of Laser Photon Fluctuations: Theory of Single-Cavity Laser", *IEEE J. Quantum Electron.*, Vol. QE-20, No. 10,pp. 1139-1147, October 1984

[16] D. Marcuse, "Computer Simulation of Laser Photon Fluctuations: Single-Cavity Laser Results", *IEEE J. Quantum Electron.*, Vol. QE-20, No. 10,pp. 1148-1155, October 1984

[17] M.D. Atkinson, A. Hassenklover, "Sets of integers with distinct differences", Sch. Comput. Sci., Carleton Univ., Ottawa, Ont., Canda, Rep. SCS-TR-63, Aug. 1984

[18] B. C. Kuo, *Automatic Control Systems*, Fifth Edition, Prentice-Hall, Englewood Cliffs, N.J. 1987

[19] E. Kreyszig, *Advanced Engineering Mathematics*, Fifth Edition, John Wiley and Sons, New York, N.Y., 1983

[20] T.E. Darcie, R.S. Tucker,"Intermodulation and harmonic distortion in InGaAsP lasers", *Electron. Lett.*, vol. 21, pp.665-666,1985.

[21] A. A. Saleh, "Fundamental Limit on Number of Channels in Subcarrier Multiplexed Lightwave CATV System", *Electron. Lett.*, vol.25, pp.776-777, 1989

[22] C. Harder, et. al., "Noise Equivalent Circuit of a Semiconductor Laser Diode", *IEEE J. Quantum Electron.*, vol. QE-18, No. 3, pp. 333-337, March 1982

[23] R. Olshansky, et. al.,"Subcarrier Multiplexed Lightwave System for Broadband Distribution", *J. Lightwave Technol.*, vol LT-7, No. 9, pp. 1329-1342, September 1989.

[24] G. Eisenstein,"Semiconductor Optical Amplifiers",*IEEE Circuits and Devices Magazine*,pp. 25-30, July 1989

[25] R. Baets, et. al., "The modelling of semiconductor laser diodes", *Ann. Telecommun.*, Vol. 43, No. 7-8, pp. 423-433, 1988

[26] A. A. Saleh, et. al., "Nonlinear Distortion due to Optical Amplifiers in Subcarrier Multiplexed Lightwave Communications Systems", *Electron. Lett.*, vol. 25, pp. 79-80, 1988

[27] T. Saitoh, T. Mukai, "1.5 μm GaInAsP Traveling-Wave Semiconductor Laser Amplifier", *IEEE J. Quantum Electron.*, Vol. QE-25, No. 6, pp. 1010-1020, June 1987

[28] W. I. Way, "Subcarrier Multiplexed Lightwave System Design Considerations for Subscriber Loop Applications", *J. Lightwave Technol.*, vol LT-7, No. 11, pp. 1806-1818, November 1989

[29] K. Feher, *Digital Communications: Microwave Applications*, Prentice-Hall, Englewood Cliffs, N.J., 1981

[30] M. Sablatash,"Evaluative Study of the Proposed Zenith Electronics Corporation High-Definition Television System: A Working Paper", C. R. C., Dept. of Comm., July 1989.

[31] T. E. Darcie, et. al.,"Fiber Optic Device Technology for Broadband Analog Video Systems", *IEEE LCS*, Vol. 1, No. 1, pp.46-52, February 1990.

[32] W. I. Way, et. al., "Multi-channel AM-VSB Television Signal Transmission Using an Erbium-Doped Optical Fiber Power Amplifier", *IEEE Photon. Technol. Lett.*, Vol. 1, No. 10, pp. 343-345, October 1989.

[33] G. E. Bodeep, T. E. Darcie,"Semiconductor Lasers Versus External Modulators: A Comparison of Nonlinear Distortion for Lightwave Subcarrier CATV Applications", *IEEE Photon. Technol. Lett.*, vol. 1, No. 11, pp.401-403, November 1989.

[34] K. A. Simons,"The Decibel Relationship between Amplifier Distortion Products",*Proceedings of the IEEE* Vol. 58, No. 7, pp. 1071-1086, July 1970